UNIVERSITAT POLITÈCNICA DE CATALUNYA
BARCELONATECH
Escola d'Enginyeria de Telecomunicació
i Aeroespacial de Castelldefels

TREBALL DE FI DE GRAU

TFG TITLE: Determination of drag coefficients in a free molecular flow

DEGREE: Grau en Enginyeria d'Aeronavegació

AUTHOR: Bernat Minguell Montes

ADVISORS: Jordi Gutiérrez Cabello
Pilar Gil Pons

DATE: July 17, 2018

Títol: Determinació del coeficient d'arrossegament en un flux molecular lliure

Autor: Bernat Minguell Montes

Directors: Jordi Gutiérrez Cabello
Pilar Gil Pons

Data: 17 de juliol de 2018

Resum

Aquest projecte té com a objectiu estudiar el coeficient d'arrossegament (C_D) dels satèl·lits en un flux molecular lliure. L'estudi està basat principalment en els models de Schaaf & Chambre i de Schamberg. Són models antics (de 1958), però encara són les grans referències utilitzades en l'actualitat. S'analitzaran els dos models per geometries planes i esfèriques, tenint en compte reflexió especular i difusa.
Per presentar l'escenari del nostre estudi es fa una descripció de la termosfera i de l'interès en l'estudi d'aquesta regió de l'atmosfera. Una vegada està definit l'escenari, es descriu el tipus de flux amb el que es tracta en aquest estudi. S'expliquen els paràmetres que divideixen els gasos en diferents règims, així com les característiques bàsiques del flux molecular lliure i la interacció entre aquest i la superfície del satèl·lit.
El primer model d'estudi és el de Schaaf i Chambre, amb el qual s'han estudiat els dos tipus de reflexió (especular i difús) per a cada geometria. Els nostres resultats per la placa plana-paral·lela mostren que el paràmetre més influent és l'angle d'atac. En el cas de l'esfera, la simetria fa que aquest paràmetre sigui irrellevant i, a més, la temperatura de la superfície del satèl·lit tampoc no provoca variacions significatives.
Amb el model de Schamberg també es poden veure grans variacions de C_D en funció de l'angle d'atac en el cas pla-paral·lel. El cas de l'esfera dóna també C_D constant pel cas especular. També hi ha una clara dependència amb la temperatura de la superfície als casos difús i entremig.
Els valors del C_D pel cas de reflexió difusa difereixen molt entre models. De fet, el model de Schamberg retorna uns valors que no concorden amb els valors empírics de satèl·lits reals en certes condicions. Per aquest motiu s'ha decidit finalment estudiar un tercer model, el model de Sentman per reflexió difusa. Aquest model dóna resultats molt semblants al model de Schaaf i Chambre. Addicionalment, els resultats de la bibliografia apunten a les greus limitacions del model de Schamberg per estudiar el cas difús i angles d'atac petits. Hem pogut comprovar la necessitat pràctica d'utilitzar combinacions de models, en funció de les condicions de la reflexió.
Hem pogut concloure que un primer estudi de C_D (i, eventualment, de la densitat a la termosfera), hauria de fer ús de satèl.lits amb simetria esfèrica, per tal de minimitzar el nombre de variables d'entrada i acotar millor els paràmetres influents ineludibles. La problemàtica tècnica del llançament de satèl·lits esfèrics es podria resoldre situant aquests satèl·lits esfèrics a dintre d'estructures de geometria CubeSat durant el llançament, i permetent que s'obrissin quan estiguessin en òrbita, o fent servir dispensadors d'uns quants satèl.lits esfèrics integrats en CubeSats.

Title : Determination of drag coefficients in a free molecular flow

Author: Bernat Minguell Montes

Advisors: Jordi Gutiérrez Cabello
Pilar Gil Pons

Date: July 17, 2018

Overview

This project aims to study the drag coefficient (C_D) for satellites in a free molecular flow. The study is mainly based on Schaaf & Chambre and Schamberg models. These are old models (from 1958), but still are the most widely used nowadays. The two models are analyzed for flat and spherical geometries, considering both specular and diffuse reflection. In order to set the scenario of our study, we describe the thermosphere and justify the interest of studying this region of the terrestrial atmosphere. Then, we describe the specific type of flux considered in this work. The parameters which divide the behaviour of the gases into different regimes, as well as the basic characteristics of the free molecular flow and the interaction between it and the surface of the satellite, are explained.
The first model studied is the one by Schaaf and Chambre, considering the two types of reflection for each geometry. We observe that, in the case of flat plate geometry, the angle of attack is the most important parameter for the determination of C_D. For the spherical case, we see that C_D adopts almost constant values, since the angle of attack is irrelevant due to the geometry, and the temperature does not cause great variations.
With respect to Schamberg model we obtain large variations of C_D due to variations in the angle of attack, as in the previous model. The case of the sphere also gives a constant C_D in the specular case. There is also a clear dependency on the wall temperature for the diffuse and intermediate cases.
The values obtained for C_D under the diffuse reflection show large discrepancies between models. In fact, Schamberg's model gives values that are at odds with empirical values under certain conditions. For this reason, we also analyze a third model: Sentman's model for diffuse reflection. This model gives results similar to those of Schaaf & Chambre. Additionally, the bibliography points to serious shortcomings of Schamberg's model in the diffuse reflection case and low angles of attack. We have checked the practical necessity of combining these models for different reflection conditions.
We have concluded that a first study of C_D (and, eventually, of the thermospheric density) should make use of spherical satellites in order to minimize the number of relevant variables, and to better identify the most influential parameters. The problem of launching spherical satellites could be solved by holding them inside a suitable satellite dispenser, perhaps with a CubeSat-like configuration, and release them once in orbit. These satellites dispensers could release either one or several spherical satellites.

CONTENTS

Acknowledgements 1

Introduction 3

CHAPTER 1. Theoretical foundations for the study of the thermosphere 5

1.1. The Thermosphere 6
1.1.1. Why study the thermosphere? 6
1.1.2. Structure and variability 8
1.1.3. Empirical density models 9

1.2. Gas dynamics 10
1.2.1. Mean free path 10
1.2.2. Knudsen number 11
1.2.3. Division of flow regimes 11

1.3. Free Molecular Flow 12

1.4. Gas-Surface Interactions 14

CHAPTER 2. Schaaf and Chambre model for drag coefficients . . 17

2.1. Model description 17
2.1.1. Energy considerations 17
2.1.2. Flux of momentum considerations 17

2.2. Flat plate 18
2.2.1. Completely specular reflection 19
2.2.2. Completely diffuse reflection 19
2.2.3. Specular - Diffuse reflection 21

2.3. Sphere 22
2.3.1. Completely specular reflection 22
2.3.2. Completely diffuse reflection 23
2.3.3. Transition Specular - Diffuse reflection 24

CHAPTER 3. Schamberg model for drag coefficients 25

3.1. Model description 25

3.1.1. Analytic representation of surface interaction . . . 26
3.1.2. Drag coefficient of flat plates and convex bodies . . . 27

3.2. Flat plate . . . 28
3.2.1. Completely specular reflection . . . 28
3.2.2. Completely diffuse reflection . . . 32
3.2.3. Specular - Diffuse reflection . . . 36

3.3. Sphere . . . 41
3.3.1. Completely specular reflection . . . 41
3.3.2. Completely diffuse reflection . . . 42
3.3.3. Specular - Diffuse reflection . . . 43

CHAPTER 4. Sentman model for drag coefficients . . . 45

4.1. Model Description . . . 45

CHAPTER 5. Conclusions . . . 49

Bibliography . . . 53

APPENDIX A. Typical Thermal Accommodation Coefficient values for air . . . 1

APPENDIX B. Extra Figures . . . 3

B.1. Schaaf and Chambre model . . . 3

B.2. Schamberg model . . . 3

APPENDIX C. Matlab code . . . 5

C.1. Schaaf and Chambre model . . . 5
C.1.1. Flat plate . . . 5
C.1.2. Sphere . . . 9

C.2. Schamberg model . . . 12
C.2.1. Flat plate . . . 12
C.2.2. Sphere . . . 29

C.3. Sentman model . . . 36

LIST OF FIGURES

1.1 Altitude profiles of atmospheric temperature (*left*) and density (*right*) according to NRLMSISE-00 model. . . . 6
1.2 *Left*: The changing shape of the orbit from its launch until re-entry. *Right*: Time evolution of the semi-major axis and its rate of change. Credit (1) . . . 7
1.3 *Left*: Graph of apogee and perigee heights during the final lifetime prior re-entry. *Right*: Map of the predicted orbital ground track. Last TLE is indicated by an open square and re-entry point is indicated by a triangle. Credit (1) . . . 8
1.4 Variation of the Earth's atmospheric composition with altitude as defined by NRLM-SISE00 model. . . . 9
1.5 Mean free path (λ). Credit (2) . . . 10
1.6 Different dynamic flow regimes in the Re-M diagram. Credit (3). . . . 12
1.7 Variation of the Knudsen number versus height in the Earth's atmosphere. Credit (2). . . . 13
1.8 Sketch depicting a hyperthermal (upper panel) and a normal velocity fluid (lower panel). Credit (2). . . . 13
1.9 Incident and reflected fluxes on a convex body. Credit (2). . . . 14
1.10 Incident normal and tangential momentum versus angle of attack. . . . 15

2.1 Analyzed Schaaf and Chambre models for flat plate and specular reflection. $\theta = [0,90]^{o}$ and $\sigma = 0$. . . . 19
2.2 Analyzed Schaaf and Chambre models for flat plate and diffuse reflection. $\theta = [0,90]^{o}$, $\sigma = 1$ and $T_w = [0\ 25\ 50\ 75\ 90]^{o}C$. . . . 20
2.3 Analyzed Schaaf and Chambre models for flat plate and diffuse reflection. $\theta = [0\ 15\ 30\ 45\ 60\ 75\ 90]^{o}$, $\sigma = 1$ and $T_w = [0,100]^{o}C$. . . . 21
2.4 Analyzed Schaaf and Chambre models for flat plate and transition from specular to diffuse reflection. $\theta = [0\ 15\ 30\ 45\ 60\ 75\ 90]^{o}$, $\sigma = [0,1]$ and $T_w = 50^{o}C$. . . . 22
2.5 Schaaf and Chambre models for sphere. Diffuse reflection. $T_w = [0,100]^{o}C$. . . 23
2.6 Schaaf and Chambre models for sphere. Transition specular-diffuse reflection. $T_w = [0\ 25\ 50\ 75\ 100]^{o}C$. . . . 24

3.1 Schamberg's GSIM. Credit (2) . . . 27
3.2 Analyzed Schamberg models for flat plate and specular reflection. $T_w = [0\ 50\ 100]^{o}C$, $\alpha = [0\ 0.5\ 1]$, $\theta = [0,90]^{o}$, $\phi = 1$ and $\frac{1}{\nu} = 1$. Note that solid lines correspond to $T_w = 0^{o}C$, dashed lines correspond to $T_w = 50^{o}C$ and dotted lines correspond to $T_w = 100^{o}C$. . . . 29
3.3 Analyzed Schamberg models for flat plate and specular reflection. $T_w = [0\ 25\ 50\ 75\ 100]^{o}C$, $\alpha = [0\ 0.5\ 1]$, $\theta = [0,90]^{o}$, $\phi = 1$ and $\frac{1}{\nu} = 1$. Note that solid lines correspond to $\alpha = 0$, dashed lines correspond to $\alpha = 0.5$ and dotted lines correspond to $\alpha = 1$. . . . 30
3.4 Analyzed Schamberg models for flat plate and specular reflection. $T_w = [0\ 25\ 50\ 75\ 100]^{o}C$, $\alpha = [0,1]$, $\theta = [0\ 15\ 30]^{o}$, $\phi = 1$ and $\frac{1}{\nu} = 1$. Note that solid lines correspond to $\theta = 0^{o}$, dashed lines correspond to $\theta = 15^{o}$ and dotted lines correspond to $\theta = 30^{o}$. . . . 31

3.5 Analyzed Schamberg models for flat plate and specular reflection. T_w = [0 25 50 75 100]$^o C$, α = [0,1], θ =[60 75 90]^o, $\phi = 1$ and $\frac{1}{\nu} = 1$. Note that solid lines correspond to $\theta = 60^o$, dashed lines correspond to $\theta = 75^o$ and dotted lines correspond to $\theta = 90^o$. 32
3.6 Analyzed Schamberg models for flat plate and diffuse reflection. T_w = [0 50 100]$^o C$, α = [0 0.25 0.5 0.75 1], θ =[0,90]^o, $\phi = \frac{2}{3}$ and $\frac{1}{\nu} = 0$. Note that solid lines correspond to $T_w = 0^o C$, dashed lines correspond to $T_w = 50^o C$ and dotted lines correspond to $T_w = 100^o C$. 33
3.7 Analyzed Schamberg models for flat plate and diffuse reflection. T_w = [0 25 50 75 100]$^o C$, α = [0 0.5 1], θ =[0,90]^o, $\phi = \frac{2}{3}$ and $\frac{1}{\nu} = 0$. Note that solid lines correspond to $\alpha = 0$, dashed lines correspond to $\alpha = 0.5$ and dotted lines correspond to $\alpha = 1$. 34
3.8 Analyzed Schamberg models for flat plate and diffuse reflection. T_w = [0 25 50 75 100]$^o C$, α = [0,1], $\theta = 0^o$, $\phi = \frac{2}{3}$ and $\frac{1}{\nu} = 0$. 35
3.9 Analyzed Schamberg models for flat plate and diffuse reflection. T_w = [0 25 50 75 100]$^o C$, α = [0,1], θ =[15 30 45]^o, $\phi = \frac{2}{3}$ and $\frac{1}{\nu} = 0$. Note that solid lines correspond to $\theta = 15^o$, dashed lines correspond to $\theta = 30^o$ and dotted lines correspond to $\theta = 45^o$. 36
3.10 Analyzed Schamberg models for flat plate and diffuse reflection. T_w = [0 25 50 75 100]$^o C$, α = [0,1], θ =[60 75 90]^o, $\phi = \frac{2}{3}$ and $\frac{1}{\nu} = 0$. Note that solid lines correspond to $\theta = 60^o$, dashed lines correspond to $\theta = 75^o$ and dotted lines correspond to $\theta = 90^o$. 36
3.11 (C_D *vs.* $\phi(\phi_0)$) - Analyzed Schamberg models for flat plate and transition from specular to diffuse reflection. T_w = [0 50 100]$^o C$, $\alpha = 0$, θ =[0 15 30 45 60 75 90]^o, $\phi = [1, \frac{2}{3}]$ and $\frac{1}{\nu} = [1, 0]$. 37
3.12 (C_D *vs.* $\frac{1}{\nu}$) - Analyzed Schamberg models for flat plate and transition from specular to diffuse reflection. T_w = [0 50 100]$^o C$, $\alpha = 0$, θ =[0 15 30 45 60 75 90]^o, $\phi = [1, \frac{2}{3}]$ and $\frac{1}{\nu} = [1, 0]$. 38
3.13 (C_D *vs.* $\phi(\phi_0)$) - Analyzed Schamberg models for flat plate and transition from specular to diffuse reflection. T_w = [0 50 100]$^o C$, $\alpha = 0.5$, θ =[0 15 30 45 60 75 90]^o, $\phi = [1, \frac{2}{3}]$ and $\frac{1}{\nu} = [1, 0]$. Note that solid lines correspond to $T_w = 0^o C$, dashed lines correspond to $T_w = 50^o C$ and dotted lines correspond to $T_w = 100^o C$. 39
3.14 (C_D *vs.* $\frac{1}{\nu}$) - Analyzed Schamberg models for flat plate and transition from specular to diffuse reflection. T_w = [0 50 100]$^o C$, $\alpha = 0.5$, θ =[0 15 30 45 60 75 90]^o, $\phi = [1, \frac{2}{3}]$ and $\frac{1}{\nu} = [1, 0]$. Note that solid lines correspond to $T_w = 0^o C$, dashed lines correspond to $T_w = 50^o C$ and dotted lines correspond to $T_w = 100^o C$. . . 39
3.15 (C_D *vs.* $\phi(\phi_0)$) - Analyzed Schamberg models for flat plate and transition from specular to diffuse reflection. T_w = [0 50 100]$^o C$, $\alpha = 1$, θ =[0 15 30 45 60 75 90]^o, $\phi = [1, \frac{2}{3}]$ and $\frac{1}{\nu} = [1, 0]$. Note that solid lines correspond to $T_w = 0^o C$, dashed lines correspond to $T_w = 50^o C$ and dotted lines correspond to $T_w = 100^o C$. 40
3.16 (C_D *vs.* $\frac{1}{\nu}$) - Analyzed Schamberg models for flat plate and transition from specular to diffuse reflection. T_w = [0 50 100]$^o C$, $\alpha = 1$, θ =[0 15 30 45 60 75 90]^o, $\phi = [1, \frac{2}{3}]$ and $\frac{1}{\nu} = [1, 0]$. Note that solid lines correspond to $T_w = 0^o C$, dashed lines correspond to $T_w = 50^o C$ and dotted lines correspond to $T_w = 100^o C$. . . 41
3.17 Analyzed Schamberg models for sphere and diffuse reflection. T_w = [0 50 100]$^o C$, $\alpha = [0, 1]$, $\phi = \frac{2}{3}$ and $\frac{1}{\nu} = 0$. 43
3.18 Analyzed Schamberg models for sphere and diffuse reflection. $T_w = [0, 100]^o C$, α = [0 0.5 1], $\phi = \frac{2}{3}$ and $\frac{1}{\nu} = 0$. 43

3.19 Schamberg models for sphere. Specular-Diffuse reflection. T_w = [0 50 100]°C, α = [0 0.5 1], $\phi = [1, \frac{2}{3}]$ and $\frac{1}{v} = [1, 0]$. Note that solid lines correspond to $\alpha = 0$, dashed lines to $\alpha = 0.5$ and dotted lines to $\alpha = 1$. 44
3.20 Schamberg models for sphere. Specular-Diffuse reflection. T_w = [0 50 100]°C, α = [0 0.5 1], $\phi = [1, \frac{2}{3}]$ and $\frac{1}{v} = [1, 0]$. Note that solid lines correspond to $T_w = 0°C$, dashed lines to $T_w = 50°C$ and dotted lines to $T_w = 100°C$. 44

4.1 Different cases of particle reflection. Credit (4). 45
4.2 Analyzed Sentman model for flat plate and diffuse reflection. $\theta = [0, 90]°$ and α = [0 0.25 0.5 0.75 1]. 47
4.3 Analyzed Sentman model for sphere and diffuse reflection. $\alpha = [0, 1]$. 47

5.1 Comparison between Schaaf and Chambre (3) and Schamberg (5) for flat plate and specular reflection. 49
5.2 Comparison between Schaaf and Chambre (3) and Schamberg (5) for (a) Flat plate and (b) Sphere and diffuse reflection. 50
5.3 Comparison between Schaaf and Chambre (3), Schamberg (5) and Sentman (6) for flat plate and diffuse reflection. 50

B.1 Analyzed Schaaf and Chambre models for sphere and specular reflection. $\sigma = 0$ and $T_w = [0, 100]°C$. 3
B.2 Analyzed Schamberg models for flat plate and specular reflection. T_w = [0 25 50 75 100]°C, α = [0,1], $\theta = 45°$, $\phi = 1$ and $\frac{1}{v} = 1$. 3
B.3 Analyzed Schamberg models for sphere and specular reflection. T_w = [0 50 100]°C and $\alpha = [0, 1]$ 4
B.4 Analyzed Schamberg models for sphere and specular reflection. $T_w = [0, 100]°C$ and α = [0 0.5 1] 4

LIST OF TABLES

1.1 The regimes of gas dynamics in terms of Kn. Credit (7) 11

2.1 Analyzed Schaaf and Chambre model for flat plate and specular reflection. $\theta = [0,90]^o$ and $\sigma = 0$. 19
2.2 Analyzed Schaaf and Chambre models for flat plate and diffuse reflection. $\theta = [0,90]^o$, $\sigma = 1$ and $T_w = [0\ 25\ 50\ 75\ 90]^oC$. 20
2.3 Analyzed Schaaf and Chambre models for flat plate and diffuse reflection. $\theta =$ [0 15 30 45 60 75 90]°, $\sigma = 1$ and $T_w = [0,100]^oC$. 20
2.4 Analyzed Schaaf and Chambre models for flat plate and transition from specular to diffuse reflection. $\theta =$ [0 15 30 45 60 75 90]°, $\sigma = [0,1]$ and $T_w = 50^oC$. . . . 21
2.5 Analyzed Schaaf and Chambre models for sphere and specular reflection. $\sigma = 0$ and $T_w = [0,100]^oC$. 23
2.6 Schaaf and Chambre models for sphere. Diffuse reflection. $T_w = [0,100]^oC$. . . 23
2.7 Schaaf and Chambre models for sphere. Transition specular-diffuse reflection. $T_w =$ [0 25 50 75 100]°C. 24

3.1 Analyzed Schamberg models for flat plate and specular reflection. $T_w =$ [0 50 100]°C, $\alpha =$ [0 0.5 1], $\theta = [0,90]^o$, $\phi = 1$ and $\frac{1}{\nu} = 1$. 29
3.2 Analyzed Schamberg models for flat plate and specular reflection. $T_w =$ [0 25 50 75 100]°C, $\alpha =$ [0,1], $\theta =$[0 15 30 45 60 75 90]°, $\phi = 1$ and $\frac{1}{\nu} = 1$. 31
3.3 Analyzed Schamberg models for flat plate and diffuse reflection. $T_w =$ [0 50 100]°C, $\alpha =$ [0 0.5 1], $\theta =$[0,90]°, $\phi = \frac{2}{3}$ and $\frac{1}{\nu} = 0$. 33
3.4 Analyzed Schamberg models for flat plate and diffuse reflection. $T_w =$ [0 25 50 75 100]°C, $\alpha =$ [0,1], $\theta =$[0 15 30 45 60 75 90]°, $\phi = \frac{2}{3}$ and $\frac{1}{\nu} = 0$. 35
3.5 Analyzed Schamberg models for flat plate and transition from specular to diffuse reflection. $T_w =$ [0 50 100]°C, $\alpha = 0$, $\theta =$[0 15 30 45 60 75 90]°, $\phi = [1, \frac{2}{3}]$ and $\frac{1}{\nu} = [1,0]$. 37
3.6 Analyzed Schamberg models for flat plate and transition from specular to diffuse reflection. $T_w =$ [0 50 100]°C, $\alpha = 0.5$, $\theta =$[0 15 30 45 60 75 90]°, $\phi = [1, \frac{2}{3}]$ and $\frac{1}{\nu} = [1,0]$. 38
3.7 Analyzed Schamberg models for flat plate and transition from specular to diffuse reflection. $T_w =$ [0 50 100]°C, $\alpha = 1$, $\theta =$[0 15 30 45 60 75 90]°, $\phi = [1, \frac{2}{3}]$ and $\frac{1}{\nu} = [1,0]$. 40
3.8 Analyzed Schamberg models for sphere and specular reflection. $T_w = [0,100]^oC$, $\alpha = [0,1]$, $\phi = 1$ and $\frac{1}{\nu} = 1$. 42
3.9 Analyzed Schamberg models for sphere and diffuse reflection. $T_w = [0,100]^oC$, $\alpha = [0,1]$, $\phi = \frac{2}{3}$ and $\frac{1}{\nu} = 0$. 42
3.10 Analyzed Schamberg models for sphere and transition from specular to diffuse reflection. $T_w =$ [0 50 100]°C, $\alpha =$ [0 0.5 1], $\phi = [1, \frac{2}{3}]$ and $\frac{1}{\nu} = [1,0]$. 44

A.1 Thermal accommodation coefficient α for air depending on the surface. 1

ACKNOWLEDGEMENTS

I would like to express my sincere gratitude to Jordi Gutiérrez and Pilar Gil, for giving me the opportunity to develop this project with them and supporting me during all these months in those moments when the project seemed to break into pieces due to the difficulty in finding information and its accessibility.

Moreover, I would like to thank my family, specially my mother Pilar, my father Silvestre and my sister Marta, for their support and advice during the progress of this project.

Finally, I would like to thank my friends for being by my side all this time and never stop trying to help me in everything I have needed.

INTRODUCTION

Is space overcrowded? In the last decades, the space competition has reached its limit, as it is reasonably easy and "Low-Cost" to send an object to the space. For that reason, space's population has increased a lot recently and therefore, space is overcrowded. That's why it is important to know and determine correctly the orbital trajectories of satellites in order to avoid collisions.

A correct assessment of spacecraft trajectories near the Earth requires a proper knowledge of the interactions between the Earth's atmosphere and the spacecrafts themselves. In spite of the great effort done in the last century, these interactions and, ultimately, their effects on the dynamics of spacecrafts is not well understood.

State-of-the-art

The atmosphere of the Earth extends to about a 1000 km in height, becoming less and less dense with increasing altitude, but not showing a physical clear-cut limit.

Legally, airspace is limited to a height of 100 km (the von Kármán line), but its effects on satellites are relevant up to altitudes in excess of 400–500 km. Its most important influence is the decrease in semi-major axis (orbital spiraling-in), leading to the re-entry of satellites in the atmosphere.

The atmospheric density varies in a very wide range, between values of the order of 1 kg/m^3 near the Earth's surface, and down to values of the order of 10^{-15} kg/m^3 at the uppermost layers of the atmosphere. As a consequence, a complete understanding of physics of the atmosphere involves a proper knowledge of fluid dynamics in very different regimes, ranging between the continuum (near the Earth's surface), and the rarefied fluid dynamics (at higher layers). Besides, it is important to realize, that atmospheric density values are not constant with time. In particular, density above a height $\sim$ 100 km strongly depends on the specific solar activity and geomagnetic conditions at a given time.

There are several mathematical models, such as NRMLSISE-00 developed by the US Naval Research Laboratory (8), or JB2006, by Jacchia and Bowman (9) which forecast the air's density at altitudes between 100 km and 1000 km, and which are used, for example, to predict the timing of satellite re-entries. However all their outputs are –to some point– uncertain, even when considering the varying effects of solar activity (through the so–called $F_{10.7}$ proxy), or the geomagnetic state (by means of the A_p parameter).

This poor knowledge of atmospheric density values is specially true in regions of low Earth orbit (hereafter referred to as LEO)[1] which are not densely populated by satellites. One of such regions, the lower thermosphere, is located between 100 and 300km, and is particularly important, because it dominates the last stages of satellite re-entries.

Most satellites found in the thermosphere are actually in their re-entry stage and lack a proper attitude control. This fact sets strong limitations on our knowledge of re-entry dynamics and, in particular, on the dynamics of drag. This problem is not solved by the existence of satellites orbiting at extremely low altitudes, like some of the Earth's gravitational field explorers (e.g. CHAMP, or GRACE), as well as some optical/IR intelligence

[1] LEO orbits typically correspond to heights between 200 m and 2000 m above the Earth's surface.

satellites. The reason is that these spacecrafts do not provide information on the drag they experience. As a consequence, one of the most important aspects of spacecraft dynamics, that is, drag dynamics, remains poorly constrained.

Scope

In this work we intend to improve the current knowledge of drag dynamics. This knowledge is expected to be used in the analysis of a specific space mission. The payload of this mission would be a swarm of very small, spherical satellites in the femtosatellite category (masses between 10 and 100 g).

These femtosatellites will carry a high-sensitivity, microelectromechanical system (MEMS) accelerometer, a MEMS Global Navigation Satellite System (MEMS GNSS) receiver, a transmitter, and a primary battery (as well as some other electronic devices required for the functioning of the satellite). The accelerometers will be able to measure accelerations as low as 1 μg caused by the drag with the residual atmosphere. This drag can be modelled by means of expressions whose validity is extended to the case found in space from the continuous case (see 1.1).

Methodology and structure of the project

This project will be based on a thorough research of articles, books and thesis about the study of the thermosphere and drag modelling, and, once understood the basic foundations, we will develop a Matlab code for each drag model to obtain several plots regarding different cases of study. Each model will have two Matlab codes; a main menu, in which the case of study will be chosen, and a function in which all the calculations will be done. All Matlab codes developed for this project can be found in Appendix C.

This work is structured as follows: in chapter 1, an introduction to the theoretical foundations for the study of the thermosphere is given in order to set the basis of the following drag characterization. chapter 2 develops the Schaaf and Chambre model for drag coefficients, where several cases are presented either for flat plate or sphere surfaces. chapter 3 develops the Schamberg model for drag coefficients, which adds more parameters to vary depending on the characteristics of the environment and several cases are presented as in the previous chapter. chapter 4 develops Sentman model for diffuse reflection, which gives more accurate values either for flat-plate or sphere when diffuse reflection occurs. Finally, chapter 5 draws our conclusions and possible future developments.

CHAPTER 1. THEORETICAL FOUNDATIONS FOR THE STUDY OF THE THERMOSPHERE

Aerodynamic drag is one of the most significant orbital perturbations in Low Earth Orbit (LEO) as it reduces the orbital energy by interchanging momentum between the upper atmosphere and the spacecraft, resulting in a change of the eccentricity towards a more circular orbit and a reduction of the semi-major axis until the eventual re-entry of the spacecraft. That is the reason why modelling this force and its variability is a key issue to determine and predict spacecraft trajectories as well as measure atmospheric density via satellite drag. A common approach to calculate the drag acceleration experienced by a body is:

$$\vec{a} = \frac{1}{2}\rho v_{\mathrm{rel}}^2 \frac{SC_{\mathrm{D}}}{m}\hat{v}_{\mathrm{rel}} \tag{1.1}$$

Where ρ represents the atmospheric neutral density, v_{rel} is the relative velocity of the vehicle with respect to the atmosphere, C_D is the drag coefficient, S is the reference surface area and m the mass of the body.

Despite the huge theoretical and experimental efforts done in the last decades (REFERENCES), three of the above parameters: ρ, v_{rel} and C_D remain highly uncertain.

- **Neutral density (ρ)** is the main source of error, as the atmosphere is a moving mass of air and its density varies with time, altitude and location. The solar extreme ultraviolet radiation is absorbed by the atmospheric constituents and hence causes the corresponding density variations. Geomagnetic fluctuations caused by solar storms, which occur more frequently during periods of peak solar activity, also increase thermospheric density.

- **Relative velocity** v_{rel}: when calculating the relative velocity of the spacecraft with respect to the atmosphere it is a common to assume that the atmosphere rotates integrally with the Earth. However, the existence of winds may cause a significant departure from the former hypothesis. Winds can increase or decrease the drag coefficient depending on their blowing direction. This fact is an important source of uncertainty as wind velocities can be as high as several hundred m/s, and the reliability of their predictions is very limited.

- **Drag coefficient** C_D: the traditional perspective assumes a constant C_D, because precise modeling of this parameter is lacking. However, it is well known that the drag coefficient is not constant and, in fact, it can vary in a wide range of values, mostly depending on the body shape and the atmospheric temperature, as well as on chemical composition of the surfaces and the remaining atmosphere.

In spite of all the difficulties which involve the computation of satellite drag, its importance has maintained and even increased the interest in spacecraft drag modelling in recent times. An improvement on the knowledge of this topic will significantly increase the accuracy of orbit determination and space objects tracking.

1.1. The Thermosphere

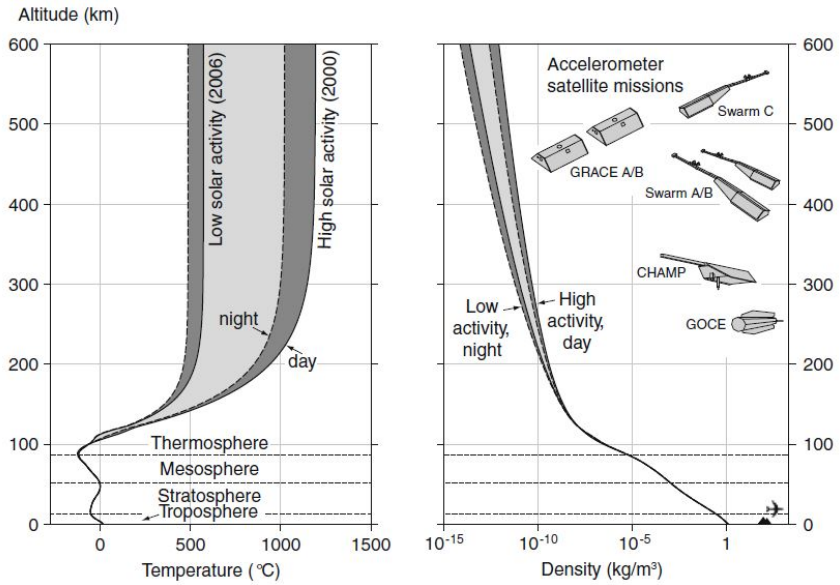

Figure 1.1: Altitude profiles of atmospheric temperature (*left*) and density (*right*) according to NRLMSISE-00 model.

The standard classification of the different parts of the Earth's atmosphere is shown in the left panel of Figure 1.1. The neutral atmospheric region of interest for satellite aerodynamics is the thermosphere, which is an atmospheric layer above an altitude of 85 km and about 500–600 km. This layer absorbs the extreme ultraviolet (EUV) energy from the Sun so the temperature profile of the thermosphere increases sharply with altitude at the lower part, while remaining almost constant with height at the upper part. This limit temperature is called exospheric temperature, and it may change with time, with values ranging, approximately, between 500°C and 2000°C.

Neutral density in the thermosphere is one of the most important variables to model for applications in solar-terrestrial physics and drag computations for satellite orbit determination. Both temperature and neutral density vary under the influence of complex interactions between the Earth system and solar processes, specifically on the amount of energy received by the thermosphere, mostly from from solar flux and geomagnetic activity.

1.1.1. Why study the thermosphere?

Thermosphere density models are applied in scientific investigations and in many types of satellite orbit computations. The accuracy of density models influences scientific results but it also affects requirements for space mission operations, tracking systems and propellant consumption. Some of the main reasons to study the thermosphere are summarized as follows.

1.1.1.1. Applications in Space Mission Analysis and Operations

The atmospheric drag force causes all LEO objects to spiral downward, so they may eventually re-enter the densest atmospheric layers. Since density and orbital velocity decrease with altitude, the drag force is stronger at the perigee of the orbit, and at this point the transformation of kinetic energy into heat is more efficient. The decrease in mechanical energy naturally leads to a circularization of the orbit. Figure 1.2 shows the change in shape of the PAM-D object with catalogue number 22659.

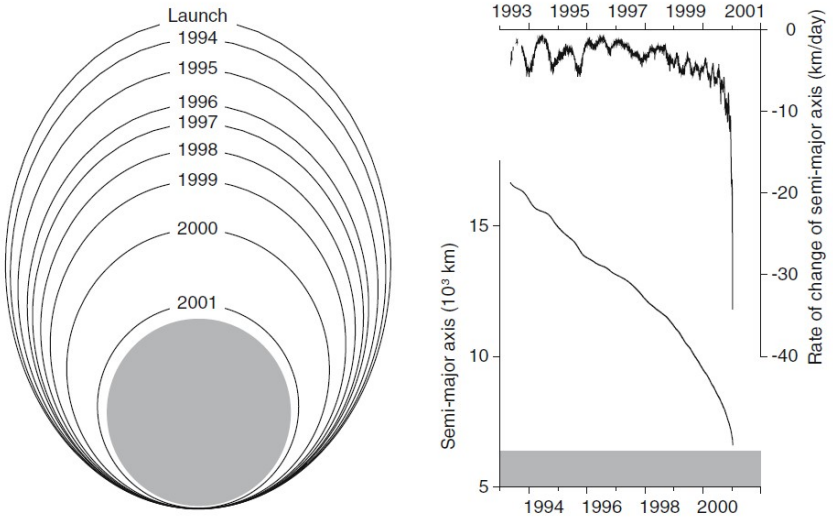

Figure 1.2: *Left*: The changing shape of the orbit from its launch until re-entry. *Right*: Time evolution of the semi-major axis and its rate of change. Credit (1)

1.1.1.2. Lifetime Analysis

As shown in Figure 1.2, there is a rate of decay of the semi-major axis of LEO orbiting objects. This variation is mainly caused by changes in atmospheric density. An accurate modelling of these variations is important for predicting the lifetime of satellite missions.

1.1.1.3. Re-Entry Operations

Most of the objects that re-enter into the denser layers of the atmosphere burn up and are disintegrated. Occasionally, though, some parts of these objects may reach the ground. Figure 1.3 shows what happened during the final week of the orbital lifetime of object 22659. Re-entry and collision events are rare and they normally occur over oceans or deserts, where there is not a high risk of damage. In some cases re-entries involve spacecrafts with large masses or carrying hazardous payloads, such as nuclear reactors. In such cases re-entry trajectories are as carefully controlled as possible, although density fluctuations may affect the accuracy of the control. It is also interesting to ponder that an uncertainty of just 15 minutes in the re-entry prediction, which is beyond our current capabilities, is equivalent to a displacement of about one sixth of the orbit, making the forecast of the re-entry region highly uncertain.

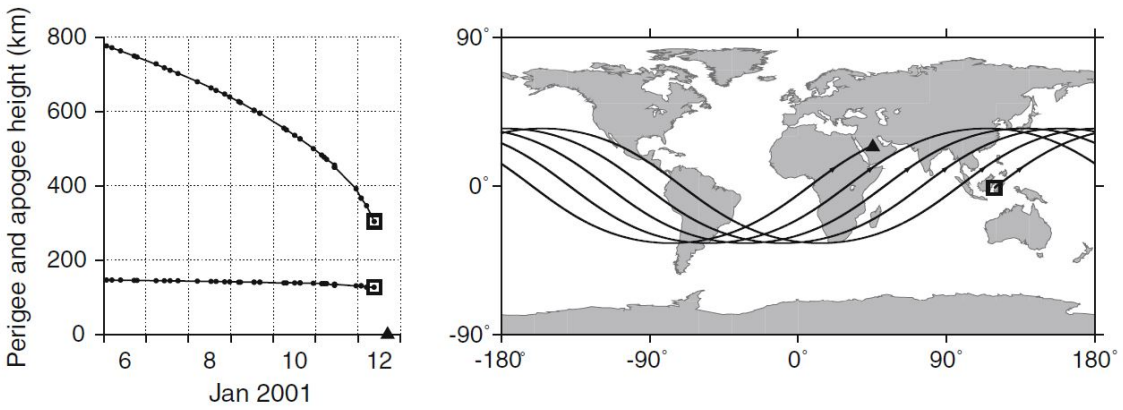

Figure 1.3: *Left*: Graph of apogee and perigee heights during the final lifetime prior re-entry. *Right*: Map of the predicted orbital ground track. Last TLE is indicated by an open square and re-entry point is indicated by a triangle. Credit (1)

1.1.1.4. Manoeuvre Planning for Orbit Maintenance

Some satellites are required to follow a specific ground track pattern or remain within a certain altitude. The orbit decay of these types of satellite is compensated using thrusters. At high latitudes, the drift is driven by luni-solar perturbations, while at equator is driven by aerodynamic drag.

1.1.2. Structure and variability

The atmosphere is usually defined as a fragile, finite and thin layer of gases that surrounds our planet, but since the numerical density of particles forming the atmosphere decreases exponentially with altitude there is not a clear boundary between the atmosphere and outer space. Although density at orbital altitudes is at least a billion times smaller than at sea level, there's still drag force due to high orbital velocities. Figure 1.1 shows the variations of both temperature and density due to solar activity as defined in (1). As explained before, there is a temperature maximum (exospheric temperature) that is reached at the thermosphere. Notice that variations in temperature lead to density variations.

1.1.2.1. Solar Activity Variation

One of the main factors that produce density and temperature variations is the solar activity. The thermosphere only absorbs extreme ultraviolet (EUV) and X-ray wavelengths, which can be extremely variable.

The amplitude of the density variation due to solar activity increases with altitude along the thermosphere, and it can vary up to a factor of 20. This density increase during peak solar activity periods is the dominant factor affecting spacecraft aerodynamic performances.

The index that measures the solar radiation is the $F_{10.7}$. It is a measure of the solar flux emitted at a wavelength of 10.7 cm measured in solar flux units (sfu), equivalent to 10^4 jansky (10^{-22} W/m·Hz).

1.1.2.2. Geomagnetic Activity Variation

Active regions are related to solar flares. which eject large amounts of charged particles into space. These particles are mostly deflected by the Earth's magnetic field, and only a fraction can enter the atmosphere through the polar cusps of the magnetosphere, causing geomagnetic storms usually accompanied by auroral displays. During these storms, vast amounts of energy are deposited in the polar regions of the thermosphere causing density variations up to one order of magnitude.

The index that measures the geomagnetic activity is called *Ap* Index, which is obtained from magnetic field variations measured at different locations for a given day. It is given in nanoTesla (nT).

1.1.3. Empirical density models

At orbital altitudes, the atmospheric composition varies with altitude, as show in Fig 1.7. This composition fluctuates as the atmosphere expands and contracts under the influence of the solar cycle or geomagnetic activity.

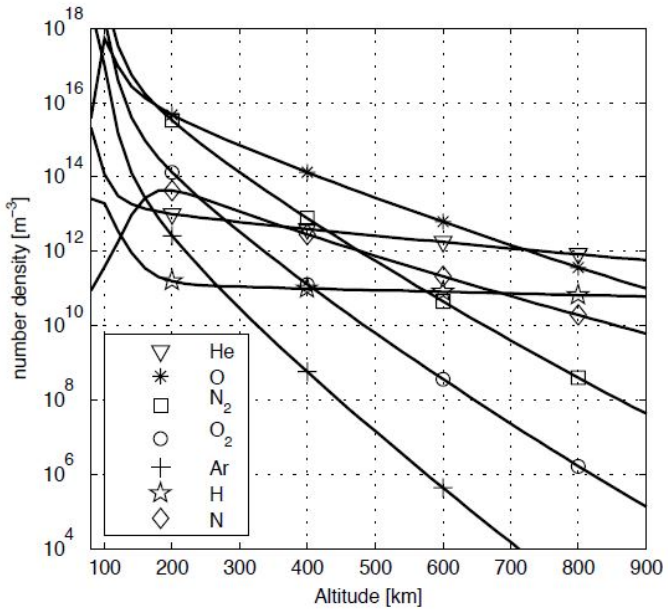

Figure 1.4: Variation of the Earth's atmospheric composition with altitude as defined by NRLM-SISE00 model.

There exists a wide variety of models which can be used to predict thermospheric characteristics which provide both neutral density and temperature, as functions of the spacecraft position, solar radiation and geomagnetic activity. Two of the most recent models are the NRLMSISE-00 and the JB2006.

The **NRLMSISE-00** model, developed by the US Naval Research Laboratory, provides, among other parameters, temperature, total mass density, and gas composition (in number density of each element or molecule). The required inputs are altitude, latitude, longitude and the two indexes $F_{10.7}$ and Ap. It covers all the range from sea level to the exosphere.

The **JB2006** model provides neutral density and temperature from 120 km to the exosphere. The inputs are again the $F_{10.7}$ and Ap indexes, but this model incorporates two new indexes for solar radiation, called S10 and Mg10, in order to obtain improved accuracy in density variation calculations.

The ECSS standard on Space environment estates that NRLMSISE-00 model should be used for calculating neutral temperature, gas composition and density below 120 km, while the JB2006 model should be used for computing the total density above 120 km.

1.2. Gas dynamics

The range of variation of atmospheric density values is huge. Density varies between values close to 1 kg/m^3 near the Earth's surface, and down to 10^{-15} kg/m^3 at the outermost layers of the thermosphere. These density variations have important consequences with respect to the behaviour of matter, which can be safely interpreted as a continuous flow at lower altitudes, but requires to be understood as a rarefied medium at altitudes $\gtrsim$ 100 km. We now describe the main parameters which determine the atmospheric fluid regimes.

1.2.1. Mean free path

The ideal gas model assumes that gas molecules only have collisions with the walls of the container, which produce the gas pressure, and not between each other. However, there are phenomena that are occasioned due to the collisions between molecules, such as diffusion. That's why it is important to know the distance travelled between collisions.

The mean free path of a gas is an important fundamental concept of the kinetic theory of gases. It is defined as the average distance traveled by a gas molecule between two consecutive collisions (see Figure 1.5). Gas mean free path may be estimated from kinetic theory too (10).

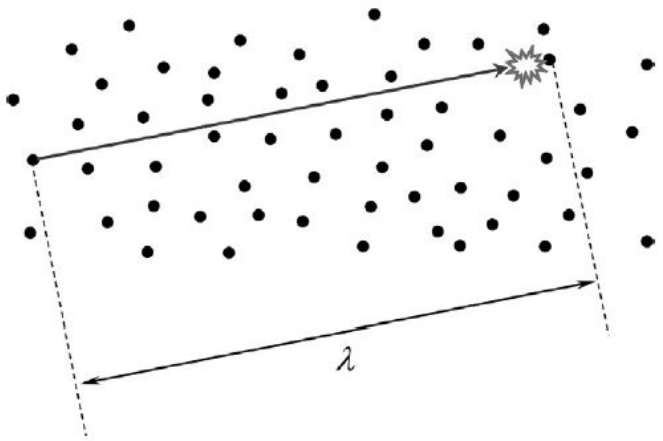

Figure 1.5: Mean free path (λ). Credit (2)

1.2.2. Knudsen number

Whether a gas flow can be interpreted as a continuum or a rarefied medium depends on the relation between the molecular free path (λ) and the characteristic dimensions of the flow field (L). If the free path is much shorter than the dimensions of the flow field, an arbitrary molecule has a high chance of colliding with another, that is, the medium is dense and can be understood as a continuum. On the other hand, if λ is comparable to L, the flow is rarefied. The Knudsen number

$$Kn = \frac{\lambda}{L} \tag{1.2}$$

is a measure of how rarefied a fluid is. Non-negligible Kn values correspond to rarefied fluids. Besides, Kn is related to the Reynolds number Re and the Mach number M through the expression:

$$Kn = 1.26\sqrt{\gamma}\frac{M}{Re} \tag{1.3}$$

where γ is the isentropic exponent, Re is the Reynolds number, that is, a quotient between inertial and viscous forces in the fluid. A low Re is associated to a laminar fluid regime, and a high Re is associated to a turbulent regime. Finally M is the Mach number, that is, the quotient between the local fluid speed and the sound speed in the fluid.

1.2.3. Division of flow regimes

According to the range of the Knudsen number Kn, the flow regimes are:

$Kn < 0.01$	Continuum flow regime
$0.01 < Kn < 0.1$	Slip flow regime
$0.1 < Kn < 10$	Transitional regime
$Kn > 10$	Free molecular regime

Table 1.1: The regimes of gas dynamics in terms of Kn. Credit (7)

In the *slip flow regime*, some phenomena appear in the gas flow different from ordinary flows, such as velocity slip or temperature jump. Ordinary gas dynamics equations are still valid but it is necessary to introduce some modifications into the boundary conditions. The layer of gas immediately adjacent to the fluid surface cannot be assumed at rest, but moving with a non-negligible tangential velocity.

In the *transitional regime*, between the slip flow and the free molecular flow, the collisions with the surface and between molecules have the same importance, so the analysis of this type of flow becomes difficult and molecular gas dynamics methods must be applied.

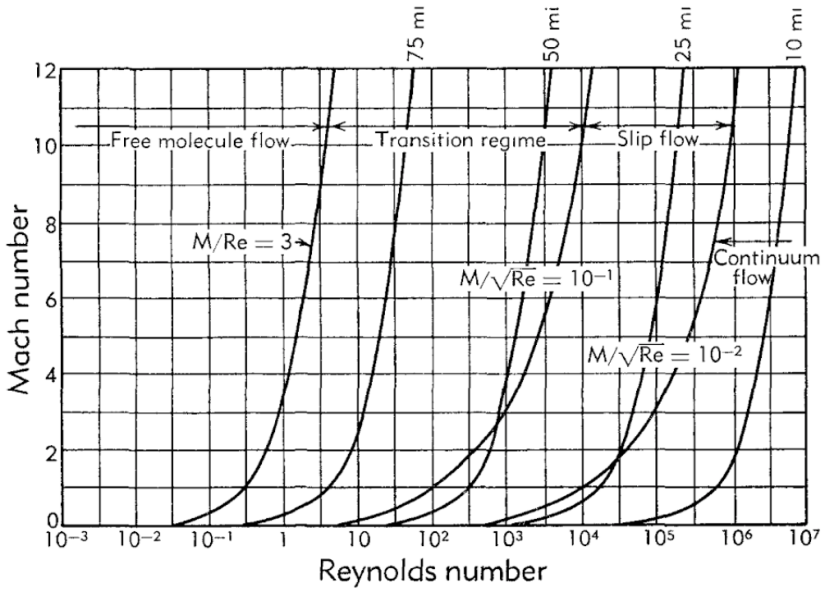

Figure 1.6: Different dynamic flow regimes in the Re-M diagram. Credit (3).

At large Knudsen numbers, where the gas is very rarefied, collisions of the gas molecules with the surface of the body prevail. When λ is much larger than L, the molecules reflected from the surface of the body collide with other molecules only after a large distance. Momentum and energy of the incoming flow can be easily calculated as the velocity distribution function is not influenced by the presence of the body. This regime is called the *free molecular flow*, and is the regime of interest in the study of spacecraft drag (see Figure 1.7).

The behaviour of flows, either in the continuum regime, in the rarefied regime, or in the intermediate cases (the slip flow, or the transition regime), is determined by the characteristic Mach number and Reynolds number of the flow (11; 3). Figure 1.6 shows the boundaries for the different regimes of fluid dynamics.

1.3. Free Molecular Flow

The relevant regime when studying gas dynamics at the characteristic heights of the thermosphere corresponds to the free molecular flow, that is, to very high Knudsen number Kn. The relation between Kn and density implies a variation of Kn as function of the solar activity. In Figure 1.7 we can see that high solar activity and thus increasing density leads Kn values almost one order of magnitude lower for typical heights of the lower thermosphere.

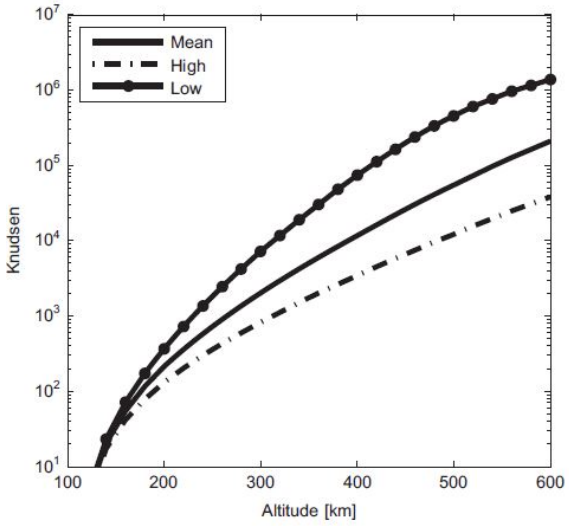

Figure 1.7: Variation of the Knudsen number versus height in the Earth's atmosphere. Credit (2).

Note that the safe approximation to the free molecular flow has an important consequence in terms of the interaction flow-spacecraft and, ultimately, on the calculation of drag coefficients which we will consider in the following chapters. The low number density of fluid particles allows the molecules which hit the body and are re-emitted to travel very far before they interact with other molecules. Thus the fluxes of incident and re-emitted particles can be treated separately, and only their interactions with the spacecraft are to be considered.

Besides, typical spacecraft velocities at the thermosphere are high enough that the relative velocity of the surrounding gas with respect to the spacecraft, v_{rel}, correspond to the hyperthermal case. In this case the random motion of gas particles can be neglected, because the associated velocities are much lower than v_{rel}

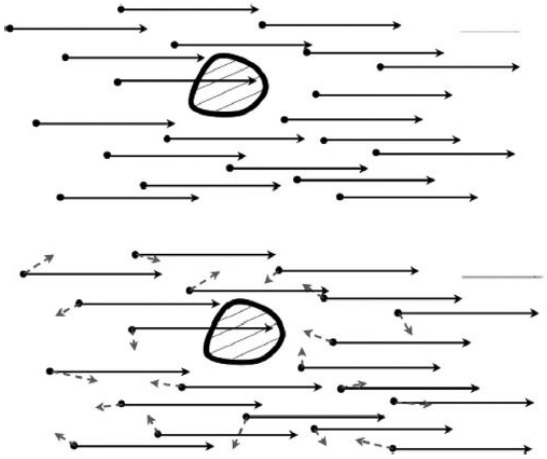

Figure 1.8: Sketch depicting a hyperthermal (upper panel) and a normal velocity fluid (lower panel). Credit (2).

1.4. Gas-Surface Interactions

As previously mentioned, under conditions of free molecular flow, collisions between molecules are extremely rare, even between incident and reflected particles. Then, reflected particles do not have a relevant effect on incident flow.

Assuming only gas-surface interaction, the force on the surface is related to the incident (subindex 'i') and reflected momentum (subindex 'r') as follows:

$$\frac{d\vec{f}}{dA} = (p_i + p_r)\vec{n} + (\tau_i - \tau_r)\vec{t} \tag{1.4}$$

Normal momentum flux is represented by p and tangential momentum flux by τ (see Figure 1.9). Normal and tangential incident fluxes (p_i, τ_i) depend on the incident velocity and the mass flux.

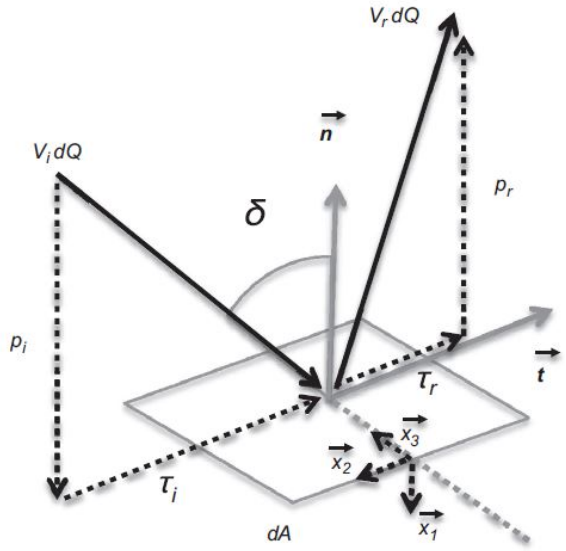

Figure 1.9: Incident and reflected fluxes on a convex body. Credit (2).

The incident fluxes are described by the following equations:

$$p_i = \frac{\rho V_i^2}{2s^2}\Gamma_1(s\cos\delta) \tag{1.5}$$

$$\tau_i = \frac{\rho V_i^2}{2s}\sin\delta\,\Gamma_2(s\cos\delta) \tag{1.6}$$

where

$$\Gamma_1(x) = \frac{1}{\sqrt{\pi}}\{x\exp(-x^2) + \frac{\sqrt{\pi}}{2}(1+2x^2)[1+erf(x))]\} \quad (1.7)$$

$$\Gamma_2(x) = \frac{1}{\sqrt{\pi}}\{x\exp(-x^2) + \sqrt{\pi}x[1+erf(x)]\} \quad (1.8)$$

$$erf(x) = \frac{2}{\sqrt{\pi}}\int_0^x e^{-t^2} \quad dt \quad (1.9)$$

Regarding Eqs.1.5 and 1.6, ρ corresponds to the neutral density of the gas, V_i is the velocity of the incident molecules computed as the sum of the gas velocity and the orbital velocity, and s is the velocity ratio, which is calculated as the ratio between the orbital velocity and the gas velocity.

Figure 1.10 shows the normal and tangential momentum versus angle of attack for some specific data extracted from an NRL-MSISE00 online calculator. Having described the incident fluxes, the next key point is the determination of the reflected fluxes, which is a difficult and complex problem.

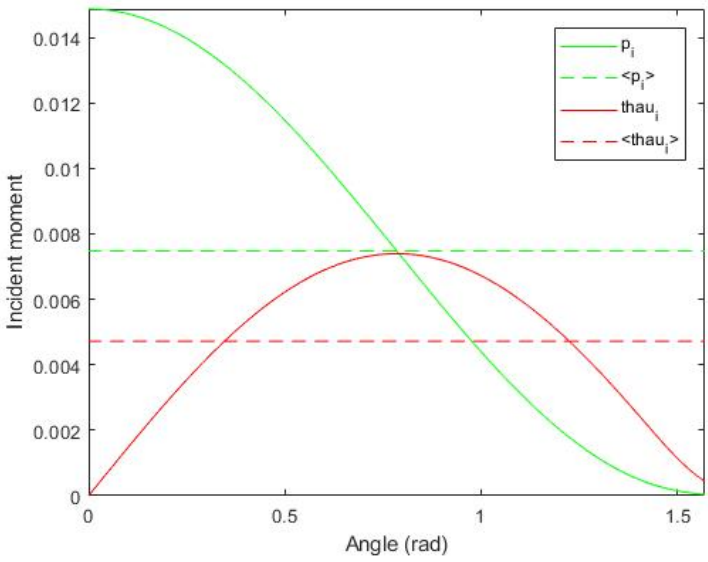

Figure 1.10: Incident normal and tangential momentum versus angle of attack.

CHAPTER 2. SCHAAF AND CHAMBRE MODEL FOR DRAG COEFFICIENTS

2.1. Model description

Schaaf and Chambre (1958) model (3) for the calculation of the drag coefficient contemplates the calculation of incident and reflected (or re-emitted) fluxes of momentum, and of the energies of atmospheric particles incident on the spacecraft and reflected by it. It is based on the following assumptions:

i) This model is restricted to the case of free molecular flow, convenient for the study of the dynamics of the thermosphere. Let us briefly recall that a free molecular flow is characterised by long mean free paths, and thus by the low probability of particle collisions. This allows to make the safe assumption that the flows of incident and reflected particles from the spacecraft will not interfere, and thus can be treated separately.

ii) Only selected average parameters are necessary in order to characterise the interaction flow-spacecraft. No complete determination of the velocity distributions of reflected (or re-emitted) particles as a function of incident velocities is required.

2.1.1. Energy considerations

The energy accommodation coefficient α was defined by Smoluchowski (1898) and Knudsen (1911), in terms of the incident and re-emitted energy flux (dE_i and dE_r respectively), and the energy flux which would be carried away if all incident molecules were re-emitted following a Maxwellian distribution corresponding to a surface temperature T_w:

$$\alpha = \frac{dE_i - dE_r}{dE_i - dE_w} \tag{2.1}$$

α close to zero corresponds to the case of negligible energy transfer between incident molecules and surface. α values close to 1 correspond to cases in which $dE_i \sim dE_w$, and thus to a case in which reemitted particles have 'accommodated' their energies to the Maxwellian case.

2.1.2. Flux of momentum considerations

A proper account of the effects of linear momentum exchange requires to consider separately the normal (p) and tangential (τ) components. Following the same nomenclature for subindexes as in the former subsection, (3) defined the following phenomenological coefficients [1]:

$$\sigma = \frac{\tau_i - \tau_r}{\tau_i - \tau_w} \qquad \sigma' = \frac{p_i - p_r}{p_i - p_w} \tag{2.2}$$

[1] Note that all the coefficients described in this subsection are phenomenological averages. They may, and probably depend on other parameters, such as gas and surface temperatures, gas pressure, gas characteristics, and direction of the mean flow with respect to the spacecraft surface.

Perfect specular reflection ($p_r = p_i$, $\tau_r = \tau_i$) would correspond to $\sigma = \sigma' = 0$. If, additionally, accommodation were complete, then $\alpha = 0$. The opposite limit case, that is, complete diffuse reflection ($p_r = p_w$, $\tau_r = \tau_w$), would correspond to $\sigma = \sigma' = \alpha = 1$.

At the time in which the work by Schaaf and Chambre was presented, only experimental values of α and σ at low velocities could be obtained. Such values were close to 1 (see Table A.1 from Appendix A), and thus supported the assumption of almost completely diffuse re-emission.

At this point we have the expressions for p_i (Equation 1.5) and τ_i (Equation 1.6) obtained in Chapter 1. From Equation 2.2, p_r, τ_r can be expressed as functions of σ, σ' and p_w (note that τ_w=0 for a Maxwellian distribution):

$$p_r = (1-\sigma')p_i + \sigma' p_w \tag{2.3}$$
$$\tau_r = (1-\sigma)\tau_i \tag{2.4}$$

Thus the net normal momentum flux (p) and tangential momentum flux (τ) are:

$$p = p_i + p_r = (2-\sigma')p_i + \sigma' p_w \tag{2.5}$$
$$\tau = \tau_i - \tau_r = \sigma\tau_i \tag{2.6}$$

We know the relation between force per unit area:

$$\frac{d\vec{F}}{dA} = (p_i + p_r)\vec{n} + (\tau_i - \tau_r)\vec{\tau} \tag{2.7}$$

and finally, from the expression for the drag coefficient as function of the drag acceleration (immediate from equation 1.1), we can obtain the geometry-dependant drag coefficient expression either for the flat plate or for the sphere, which are going to be analyzed in the following sections.

Along the next subsections we analyze the variation of C_D as a function of spacecraft wall temperature, T_w, σ and angle of attack of the incident molecules, θ, for two basic spacecraft geometries: spherical and flat plate.

2.2. Flat plate

For a flat plate at an angle of attack θ and one side exposed to the flow has for specular reflection

$$C_{D,spec} = \frac{4\sin\theta}{\sqrt{\pi}S^2}\left[(S\sin\theta)e^{-(S\sin\theta)^2} + \sqrt{\pi}\left[\frac{1}{2} + (S\sin\theta)^2\right]erf(S\sin\theta)\right] \tag{2.8}$$

and for diffuse reflection

$$C_{D,diff} = \frac{2}{\sqrt{\pi}S}\left[e^{-(S\sin\theta)^2} + \sqrt{\pi}S\sin\theta\left(1 + \frac{1}{2S^2}\right)erf(S\sin\theta) + \frac{\pi S}{S_w}\sin^2\theta\right] \tag{2.9}$$

where:

$$S_w = \frac{U}{\sqrt{2RT_w}} \tag{2.10}$$

All models studied in this section have the following nomenclature for and easier identification: $M - F - T_w T_w T_w - \sigma - \theta\theta$

2.2.1. Completely specular reflection

In this model, the study will consider completely specular reflection, which means that $\sigma = 0$. We will only consider the case in which the angle of attack is varied (from 0^o to 90^o). Note that the equation corresponding to the specular case (Equation 2.8) does not include T_w, and thus we will disregard its effect at this point of the project.

Table 2.1 shows the values of the parameters for each case. The five cases are plotted in the same figure in order to facilitate analysis and comparison (see Figure 2.1).

Model	$T_w(^oC)$	σ	$\theta(^o)$
M-F-ANY-0-var	Any	0	[0,90]

Table 2.1: Analyzed Schaaf and Chambre model for flat plate and specular reflection. $\theta = [0, 90]^o$ and $\sigma = 0$.

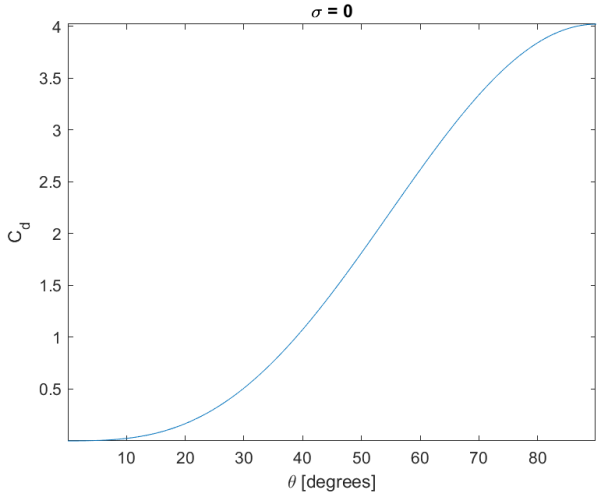

Figure 2.1: Analyzed Schaaf and Chambre models for flat plate and specular reflection. $\theta = [0, 90]^o$ and $\sigma = 0$.

Figure 2.1 shows that C_D increases significantly with the angle of attack as its value goes from almost 0 to around 4.

2.2.2. Completely diffuse reflection

We now present results for the completely diffuse case, in which $\sigma = 1$. Two studies will be performed, one with constant T_w, and another with constant θ.

2.2.2.1. Constant T_w

In this case, T_w will be kept constant along each calculation, while the angle of attack will be varied from 0^o to 90^o. The drag coefficient will be computed for several temperatures. Table 2.2 shows the values of the parameters for each case.

Model	$T_w(^oC)$	σ	θ(°)
M-F-000-0-var	0	1	[0,90]
M-F-025-0-var	25	1	[0,90]
M-F-050-0-var	50	1	[0,90]
M-F-075-0-var	75	1	[0,90]
M-F-100-0-var	100	1	[0,90]

Table 2.2: Analyzed Schaaf and Chambre models for flat plate and diffuse reflection. $\theta = [0,90]^o$, $\sigma = 1$ and $T_w = [0\ 25\ 50\ 75\ 90]^oC$.

Figure 2.2 shows the effects of the angle of attack at different temperatures. In the diffuse cases, there is a slight variation with T_w that increases with θ. Despite existing an increase in C_D as temperature increases, the variation is practically negligible.

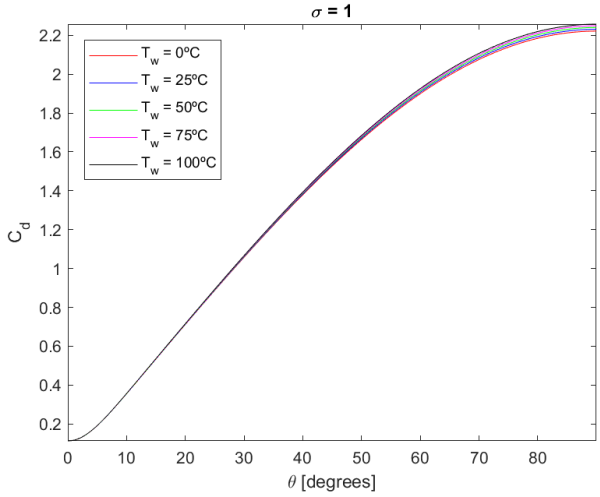

Figure 2.2: Analyzed Schaaf and Chambre models for flat plate and diffuse reflection. $\theta = [0,90]^o$, $\sigma = 1$ and $T_w = [0\ 25\ 50\ 75\ 90]^oC$.

2.2.2.2. Constant θ

In this case, θ will be kept constant along each calculation, while the temperature of the wall will be varied from 0^oC to 100^oC. The drag coefficient will be computed for several angles of attack. Table 2.3 shows the values of the parameters for each case.

Model	$T_w(^oC)$	σ	θ(°)
M-F-var-0-00	[0,100]	1	0
M-F-var-0-15	[0,100]	1	15
M-F-var-0-30	[0,100]	1	30
M-F-var-0-45	[0,100]	1	45
M-F-var-0-60	[0,100]	1	60
M-F-var-0-75	[0,100]	1	75
M-F-var-0-90	[0,100]	1	90

Table 2.3: Analyzed Schaaf and Chambre models for flat plate and diffuse reflection. $\theta = [0\ 15\ 30\ 45\ 60\ 75\ 90]^o$, $\sigma = 1$ and $T_w = [0,100]^oC$.

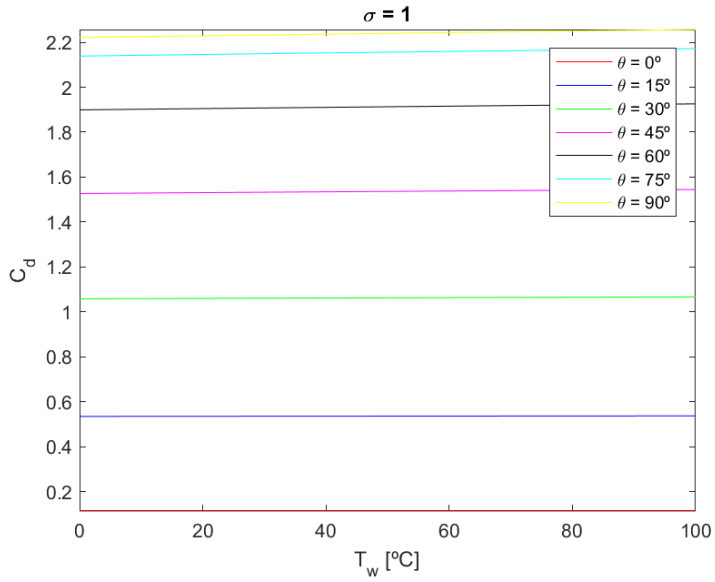

Figure 2.3: Analyzed Schaaf and Chambre models for flat plate and diffuse reflection. $\theta =$ [0 15 30 45 60 75 90]º, $\sigma = 1$ and $T_w = [0, 100]^oC$.

Figure 2.3 is consistent with Figure 2.2, that is, there's not a significant variation in C_D with temperature. It is reasonable to assume that T_w is not relevant when computing the drag coefficient, whereas the angle of attack must definitely be taken into consideration.

2.2.3. Specular - Diffuse reflection

In this case, the analysis intends to show the difference in C_D as σ varies from specular reflection to diffuse reflection. This study will be performed fixing $T_w = 50^oC$ and varying the angle of attack. We fix T_w because, as seen previously, it does not play a relevant role in C_D calculation. Table 2.4 shows the values of the parameters for each model.

Figure 2.4 shows that there is an important variation of C_D for different angles of attack. It can also be seen that the larger the angle of attack, the greater the variation of C_D from specular to diffuse reflection.

Model	$T_w(^oC)$	σ	$\theta(^o)$
M-F-050-var-00	50	[0,1]	0
M-F-050-var-15	50	[0,1]	15
M-F-050-var-30	50	[0,1]	30
M-F-050-var-45	50	[0,1]	45
M-F-050-var-60	50	[0,1]	60
M-F-050-var-75	50	[0,1]	75
M-F-050-var-90	50	[0,1]	90

Table 2.4: Analyzed Schaaf and Chambre models for flat plate and transition from specular to diffuse reflection. $\theta =$ [0 15 30 45 60 75 90]º, $\sigma = [0, 1]$ and $T_w = 50^oC$.

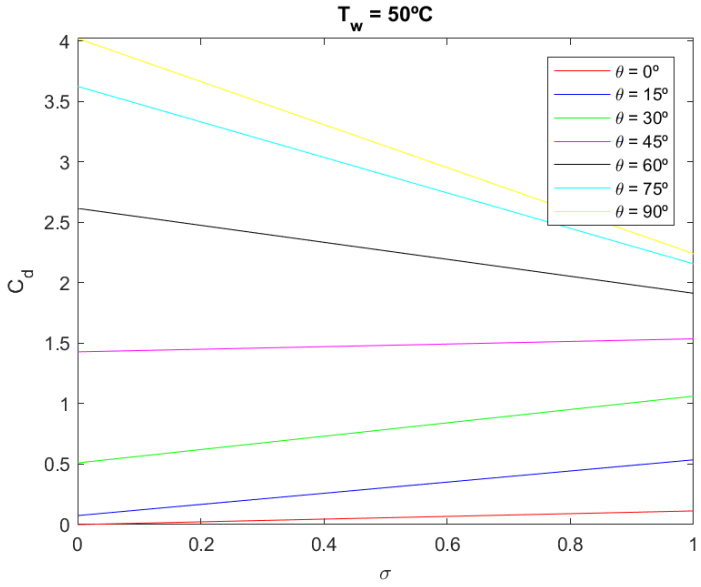

Figure 2.4: Analyzed Schaaf and Chambre models for flat plate and transition from specular to diffuse reflection. $\theta = [0\ 15\ 30\ 45\ 60\ 75\ 90]^o$, $\sigma = [0,1]$ and $T_w = 50^oC$.

2.3. Sphere

Spherical geometry implies a reduction of input parameters, as angles of attack will not be considered. The analysis structure of the different cases is the same as for the flat plate. A sphere with projected area A has the following drag coefficient for diffuse reflection:

$$C_{D,diff} = \frac{e^{-S^2/2}}{\sqrt{\pi}S^2}(1+2S^2) + \frac{4S^4+4S^2-1}{2S^4}erf(S) + \frac{2\sqrt{\pi}}{3S_w} \tag{2.11}$$

and for specular reflection:

$$C_{D,spec} = C_{D,diff} - \frac{2\sqrt{\pi}}{3S_w} \tag{2.12}$$

where:

$$S_w = \frac{U}{\sqrt{2RT_w}} \tag{2.13}$$

All models studied in this section have the following nomenclature for an easier identification: $M-S-T_wT_wT_w-\sigma$

2.3.1. Completely specular reflection

In this case, the only difference with respect to the flat plate is that there's no need to take into account the angles of attack. Table 2.5 shows the values of T_w and σ for this model.

Model	$T_w(^oC)$	σ
M-S-var-0	[0,100]	0

Table 2.5: Analyzed Schaaf and Chambre models for sphere and specular reflection. $\sigma = 0$ and $T_w = [0, 100]^oC$.

For this model, we only have one calculation, as the only parameter that varies is the temperature. In this case, C_D adopts a constant value equal to 2.02, see Figure B.1 from Appendix B, as C_D (Equation 2.12) does not depend on T_w when reflection is specular. This happens due to the fact that, in this case, molecules do no exchange temperature with the surface so re-emission is independent of T_w.

2.3.2. Completely diffuse reflection

Again, the only relevant parameter is T_w (from 0^oC to 100^oC), and the difference is that $\sigma = 1$. Table 2.6 shows the values of the parameters for this model.

Model	$T_w(^oC)$	σ
M-S-var-1	[0,100]	1

Table 2.6: Schaaf and Chambre models for sphere. Diffuse reflection. $T_w = [0, 100]^oC$.

In this case, it can be observed from Figure 2.5 that when diffuse reflection occurs, T_w plays a role in C_D calculation. However, it can be seen that the variation of C_D due to temperature changes is smaller than 0.1, so T_w would not be a determining factor.

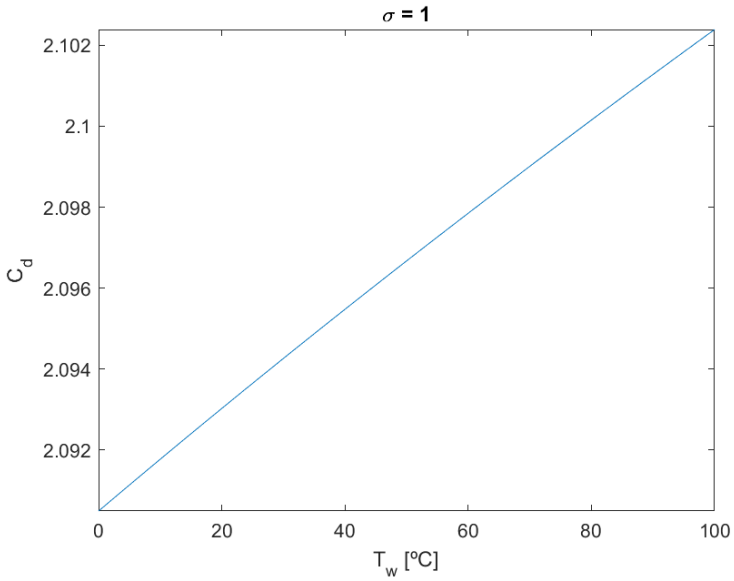

Figure 2.5: Schaaf and Chambre models for sphere. Diffuse reflection. $T_w = [0, 100]^oC$.

2.3.3. Transition Specular - Diffuse reflection

In this case the value of σ will vary from 0 to 1 and different values of T_w will be analyzed. Table 2.7 shows the values of the parameters for each model.

Model	$T_w(^oC)$	σ
M-S-000-var	0	[0,1]
M-S-025-var	25	[0,1]
M-S-050-var	50	[0,1]
M-S-075-var	75	[0,1]
M-S-100-var	100	[0,1]

Table 2.7: Schaaf and Chambre models for sphere. Transition specular-diffuse reflection. $T_w = [0\ 25\ 50\ 75\ 100]^oC$.

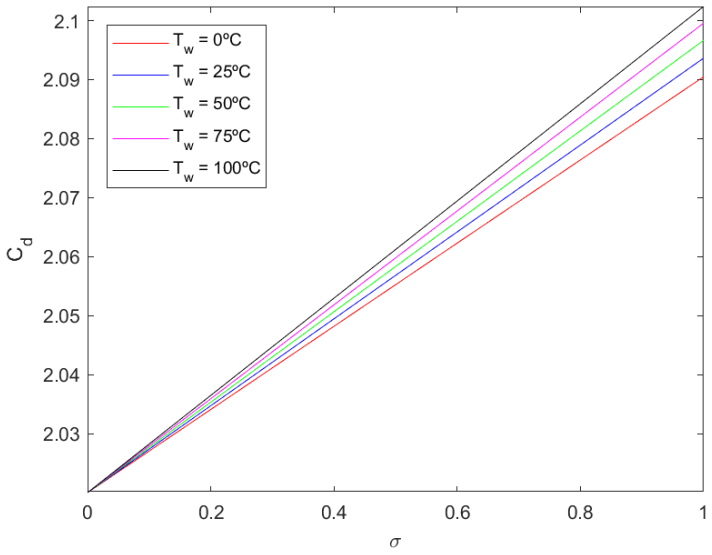

Figure 2.6: Schaaf and Chambre models for sphere. Transition specular-diffuse reflection. $T_w = [0\ 25\ 50\ 75\ 100]^oC$.

Figure 2.6 ratifies what we have seen in the specular and diffuse cases. For specular reflection, T_w does not affect when computing the C_D, but as σ approaches to the diffuse reflection value, variation of T_w implies a variation of C_D. Again, the variation of C_D is too low to be relevant.

CHAPTER 3. SCHAMBERG MODEL FOR DRAG COEFFICIENTS

3.1. Model description

An alternative model for surface interactions was proposed by Schamberg (5) in 1958 and is used to calculate force coefficient of flat plate and convex bodies in "hyperthermal" free-molecule flow, in which the random thermal motion of molecules is negligible relative to the speed of the body. We are going to use formulae to estimate the effects of uncertainty in the surface interaction on the drag of satellites for flat plate and spherical geometries.

Mean free path of molecules in the gas is so great that the frequency of collisions between gas molecules is entirely negligible relative to the frequency of collisions between gas molecules and the surface of the body analyzed. However, these interaction effects are not understood in detail and there's no sufficient empirical information available.

The analytic formulation of an hypothesis for the gas-surface interaction in a rarefied gas goes back to Maxwell who postulated that a certain fraction, σ, of the incident molecules are temporarily absorbed by the surface and, after a certain time, re-emitted diffusely with a mean temperature equal to the temperature of the wall, while the rest of molecules are assumed to be reflected specularly with $\theta_r = \theta_i$ and $V_r = V_i$.

Von Smoluchowski introduced the concept of "accommodation" to account for his experiments on heat transfer, which showed the re-emission velocity of gas molecules is determined by a temperature of re-emission, T_r, which takes an intermediate value between the incident temperature and the surface temperature, that is

$$T_r = T_i + \alpha(T_w - T_i) \tag{3.1}$$

where α is a positive number called the "accommodation coefficient" and its value varies between 0 and 1.

The forces on and heat transfer to simple bodies in free-molecule flow have been calculated by several scientists using the empirical "constants" σ and α as arbitrary parameters to describe the interaction between the gas and the surface, and these results are summarized in the Schaaf and Chambre model (3). As σ and α denote the exchange of tangential momentum and energy, a third coefficient was introduced later, σ', to parametrize the normal momentum exchange. The fact is that there's no empirical information to justify that these coefficients are "constants" which do not depend on the angle of incidence. The alternative model for describing gas-surface interaction proposed by Schamberg intends an improvement about the aspect by choosing different parameters which are expected to be more independent of the local angle of attack of the body.

Even using simple coefficients like σ and α, the interaction model leads to lengthy expressions that are hard to solve, but fortunately, for calculating the drag of earth satellites, a simplification is possible. This can be done because at altitudes lower than 1000 miles, where the atmosphere is sufficiently dense to produce appreciable neutral-particle drag, the satellite speed is, at least, 6 times bigger than the thermal speed of the molecules, so the drag can be approximated by its asymptotic values for infinite speed ratio and can be

calculated with much simpler equations. For example, for a flat plate at a speed ratio of 6 and at 45^o angle of attack, the drag coefficient differs from that for infinite speed ratio by only a 6%, and this accuracy, apparently, is more than adequate.

3.1.1. Analytic representation of surface interaction

We consider a uniform, parallel stream of molecules colliding with a flat surface at an angle of incidence θ_i and incident velocity V_i. After hitting the surface, the molecules are expected to be re-emitted or reflected in a conical or wedge-shaped beam having a half-angular width denoted by ϕ_0. The direction of re-emission is denoted as θ_r.

There's a need to make some phenomenological assumptions concerning three questions(5):

- How does the angles of reflection θ_r vary with the angles of incidence θ_i, the incident speed V_i, type of gas and surface, etc?
- What is the distribution of the number and speed of re-emitted molecules within the reflected beam?
- How does the speed V_r of the reflected molecules vary with the incident speed V_i, and with the temperature and nature of the surface?

First of all we need to parametrize the relation between the angles of reflection and incidence somehow including the limiting cases of specular reflections, in which $\theta_i = \theta_r$, and diffuse reflection, in which $\theta_r = 90^o$ for any value of θ_i. It looks like $\theta_r \geq \theta_i$. The following form is chosen as being both simple and convenient for easier manipulation:

$$\cos\theta_r = (\cos\theta_i)^\nu, \qquad \nu \geq 1 \tag{3.2}$$

Then for specular reflection

$$\nu = 1, \qquad \cos\theta_r = \cos\theta_i \tag{3.3}$$

and for diffuse reflection

$$\nu \to \infty, \qquad \theta_r = \frac{\pi}{2} \tag{3.4}$$

There is evidence that the distribution of molecules is symmetric about the axis of the beam and can be approximated by a cosine distribution:

$$n_r(\phi) = K\cos\left(\frac{\phi}{\phi_0}\cdot\frac{\pi}{2}\right) \tag{3.5}$$

where n_r is the number of re-emitted molecules per unit time whose direction of re-emission lies between ϕ and $\phi + d\phi$ and K is a constant of proportionality that depends on the total number of molecules re-emitted per unit time and on whether the re-emitted beam is wedge-shaped or conical.

Little is known about the distribution of speeds, so it will be assumed that re-emission speed V_r is constant independent of re-emission angles θ_r.

The magnitude of the speed V_r can be related to the incident velocity V_i and the temperature of the surface, T_w, by using the coefficient α,

$$\frac{V_r}{V_i} = \sqrt{\frac{T_r}{T_i}} = \sqrt{1+\alpha\left(\frac{T_w}{T_i}-1\right)} \tag{3.6}$$

3.1.2. Drag coefficient of flat plates and convex bodies

The drag coefficient is defined in the conventional manner as

$$C_D = \frac{D}{\frac{1}{2}\rho_i V_i^2 A} \tag{3.7}$$

It turns out that the hyperthermal drag coefficients for all geometries can be expressed in this simple form:

$$C_D = 2\left[1+\phi(\phi_0)\frac{V_r}{V_i} f(\nu, shape)\right] \tag{3.8}$$

The first term inside the bracket, unity, represents the drag that the incident molecules would produce if all of them stuck to the body ($V_r = 0$), that takes the value 2 and it's independent of the body shape.

The second term represents the contribution to the drag of the momentum of the molecules which are re-emitted from the surface of the body. It can be positive or negative depending on the direction of re-emission.

The factor $\phi(\phi_0)$ is defined as:

$$\phi(\phi_0) = \frac{1-(2\phi_0/\pi)^2}{1-4(2\phi_0/\pi)} \cdot \frac{\frac{1}{2}\sin 2\phi_0 - (2\phi_0/\pi)}{\sin\phi_0 - (2\phi_0/\pi)} \tag{3.9}$$

The term ϕ_0 is shown in Figure 3.1. The values for the limiting cases are for specular reflection $\phi(0) = 1$ and for diffuse reflection $\phi(\frac{\pi}{2}) = \frac{2}{3}$.

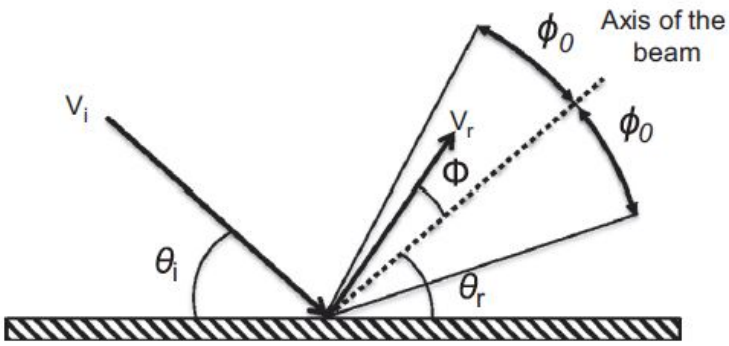

Figure 3.1: Schamberg's GSIM. Credit (2)

The factor $f(\nu, shape)$ accounts for the combined effect of the reflection law of Eq.(3.2) and the shape of the body.

It is defined for flat plate at an angle of attack θ_i as

$$f(\nu,\theta_i) = [\sin\theta_i\sqrt{1-\cos^{2\nu}\theta_i} - (\cos\theta_i)^{\nu+1}] \tag{3.10}$$

and for sphere as

$$f(\nu) = 2\left[I_1(\nu) - \frac{1}{\nu+3}\right] \tag{3.11}$$

where

$$I_1(\nu) = \int_0^1 x\sqrt{(1-x^{2\nu})(1-x^2)}\quad dx \tag{3.12}$$

the limiting values of this definite integral are

$$I_1(\nu=1) = \frac{1}{4}; \qquad I_1(\nu\to\infty) = \frac{1}{3} \tag{3.13}$$

3.2. Flat plate

All models studied in this section have the following nomenclature for an easier identification: $M-F-T_wT_wT_w-\alpha\alpha-\theta\theta-\phi-\frac{1}{\nu}$

3.2.1. Completely specular reflection

In this model, the study will consider completely specular reflection (that is, $\phi_0 = 0^\circ$), which means that $\phi = 1$ and $\frac{1}{\nu} = 1$. Two different cases will be studied, one in which T_w and α will be kept constant, and the other in which T_w and θ will be kept constant.

3.2.1.1. Constant T_w and α

In this case, the study will represent the drag coefficient for a flat plate and specular reflection. To do so, the different models have been structured keeping α constant among each computation and for each accommodation factor, several T_w values have been used [0 50 100] ^oC. Table 3.1 shows the parameter values for each model. Some other intermediate values have also been computed.

Model	$T_w(^oC)$	α	$\theta(^o)$	ϕ	$\frac{1}{\nu}$
M-F-000-00-var-1-1	0	0	[0,90]	1	1
M-F-050-00-var-1-1	50	0	[0,90]	1	1
M-F-100-00-var-1-1	100	0	[0,90]	1	1
M-F-000-05-var-1-1	0	0.5	[0,90]	1	1
M-F-050-05-var-1-1	50	0.5	[0,90]	1	1
M-F-100-05-var-1-1	100	0.5	[0,90]	1	1
M-F-000-10-var-1-1	0	1	[0,90]	1	1
M-F-050-10-var-1-1	50	1	[0,90]	1	1
M-F-100-10-var-1-1	100	1	[0,90]	1	1

Table 3.1: Analyzed Schamberg models for flat plate and specular reflection. T_w = [0 50 100]^oC, α = [0 0.5 1], $\theta = [0,90]^o$, $\phi = 1$ and $\frac{1}{\nu} = 1$.

After structuring the different models, it's time for calculation. When designing the plots, two different combinations have been computed. Figure 3.2 is representing C_D vs. θ and each colored line corresponds to a constant value of α, while each line style corresponds to a different value of T_w. To validate the information shown in the first plot, Figure 3.3 shows C_D vs. θ, but in this case, each colored line represents a constant value of T_w while each line style corresponds to a different value of α.

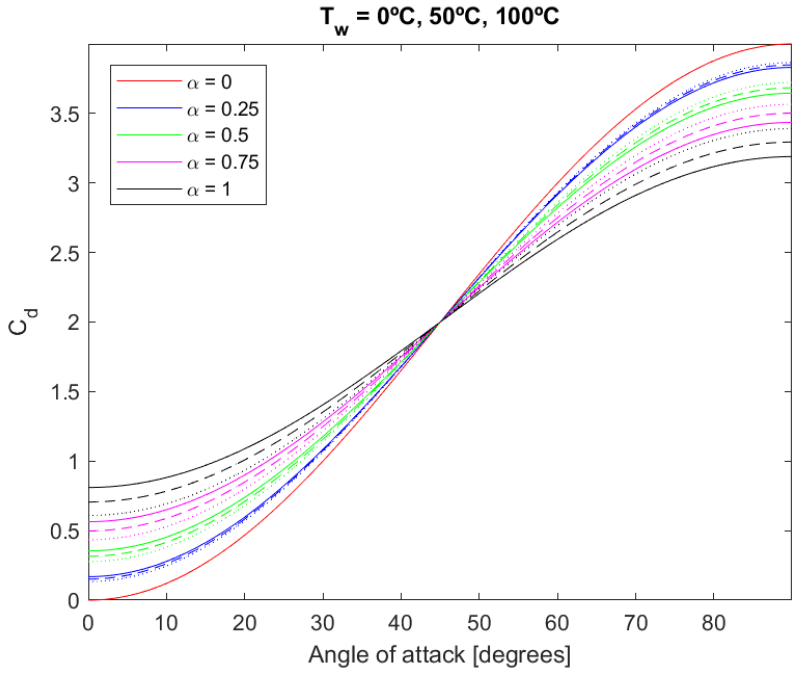

Figure 3.2: Analyzed Schamberg models for flat plate and specular reflection. T_w = [0 50 100]^oC, α = [0 0.5 1], $\theta = [0,90]^o$, $\phi = 1$ and $\frac{1}{\nu} = 1$. Note that solid lines correspond to $T_w = 0^oC$, dashed lines correspond to $T_w = 50^oC$ and dotted lines correspond to $T_w = 100^oC$.

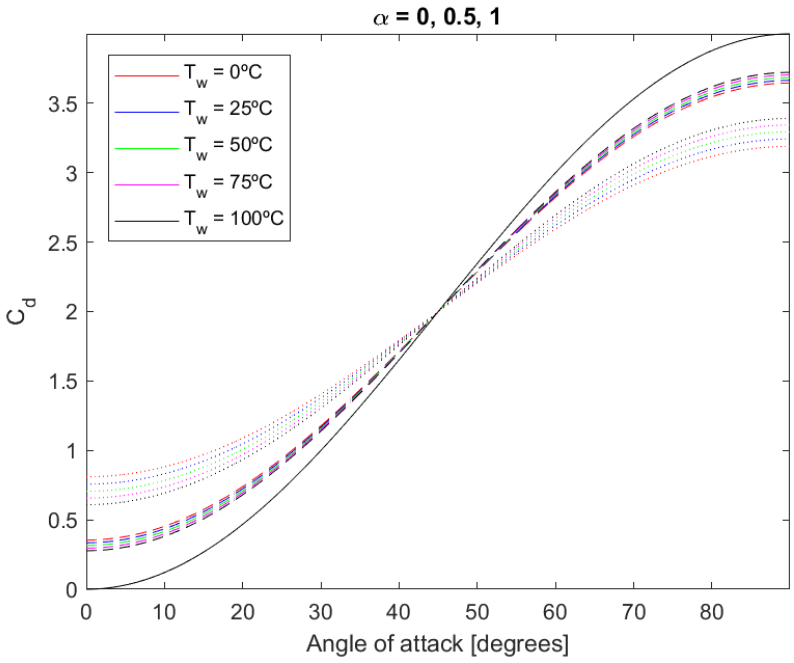

Figure 3.3: Analyzed Schamberg models for flat plate and specular reflection. $T_w = [0\ 25\ 50\ 75\ 100]^oC$, $\alpha = [0\ 0.5\ 1]$, $\theta = [0, 90]^o$, $\phi = 1$ and $\frac{1}{v} = 1$. Note that solid lines correspond to $\alpha = 0$, dashed lines correspond to $\alpha = 0.5$ and dotted lines correspond to $\alpha = 1$.

From both Figure 3.2 and Figure 3.3 it can be seen that the angle of attack plays a very important role when computing the drag coefficient as the variation of C_D is very big. Regarding the accommodation coefficient and the different values of T_w, it can be affirmed, as expected, that the greater the accommodation coefficient, the greater C_D variation with temperature. This makes perfect sense due to the fact that, for $\alpha = 0$ there is no accommodation of the molecule with the surface so the temperature of the surface is not playing any role there, but when accommodation appears, T_w starts to take center stage due to the heat exchange between the molecule and the surface, so this involves an energy exchange then the value of C_D varies depending on the amount of energy transferred.

3.2.1.2. Constant T_w and θ

In this case, the study will be almost the same as the previous case but the varying parameters. Now, T_w and θ will be kepts constant and α will vary from 0 to 1. Table 3.2 shows the structure of the different models studied.

Model	$T_w(^oC)$	α	$\theta(^\circ)$	ϕ	$\frac{1}{\nu}$	Model	$T_w(^oC)$	α	$\theta(^\circ)$	ϕ	$\frac{1}{\nu}$
M-F-000-var-00-1-1	0	[0,1]	0	1	1	M-F-075-var-45-1-1	75	[0,1]	45	1	1
M-F-025-var-00-1-1	25	[0,1]	0	1	1	M-F-100-var-45-1-1	100	[0,1]	45	1	1
M-F-050-var-00-1-1	50	[0,1]	0	1	1	M-F-000-var-60-1-1	0	[0,1]	60	1	1
M-F-075-var-00-1-1	75	[0,1]	0	1	1	M-F-025-var-60-1-1	25	[0,1]	60	1	1
M-F-100-var-00-1-1	100	[0,1]	0	1	1	M-F-050-var-60-1-1	50	[0,1]	60	1	1
M-F-000-var-15-1-1	0	[0,1]	15	1	1	M-F-075-var-60-1-1	75	[0,1]	60	1	1
M-F-025-var-15-1-1	25	[0,1]	15	1	1	M-F-100-var-60-1-1	100	[0,1]	60	1	1
M-F-050-var-15-1-1	50	[0,1]	15	1	1	M-F-000-var-75-1-1	0	[0,1]	75	1	1
M-F-075-var-15-1-1	75	[0,1]	15	1	1	M-F-025-var-75-1-1	25	[0,1]	75	1	1
M-F-100-var-15-1-1	100	[0,1]	15	1	1	M-F-050-var-75-1-1	50	[0,1]	75	1	1
M-F-000-var-30-1-1	0	[0,1]	30	1	1	M-F-075-var-75-1-1	75	[0,1]	75	1	1
M-F-025-var-30-1-1	25	[0,1]	30	1	1	M-F-100-var-75-1-1	100	[0,1]	75	1	1
M-F-050-var-30-1-1	50	[0,1]	30	1	1	M-F-000-var-90-1-1	0	[0,1]	90	1	1
M-F-075-var-30-1-1	75	[0,1]	30	1	1	M-F-025-var-90-1-1	25	[0,1]	90	1	1
M-F-100-var-30-1-1	100	[0,1]	30	1	1	M-F-050-var-90-1-1	50	[0,1]	90	1	1
M-F-000-var-45-1-1	0	[0,1]	45	1	1	M-F-075-var-90-1-1	75	[0,1]	90	1	1
M-F-025-var-45-1-1	25	[0,1]	45	1	1	M-F-100-var-90-1-1	100	[0,1]	90	1	1
M-F-050-var-45-1-1	50	[0,1]	45	1	1						

Table 3.2: Analyzed Schamberg models for flat plate and specular reflection. T_w = [0 25 50 75 100]^oC, α = [0,1], θ =[0 15 30 45 60 75 90]^o, $\phi = 1$ and $\frac{1}{\nu} = 1$.

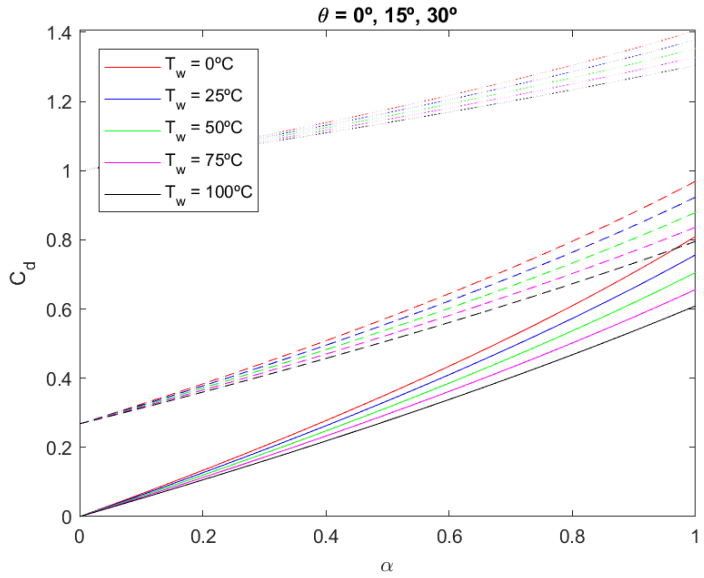

Figure 3.4: Analyzed Schamberg models for flat plate and specular reflection. T_w = [0 25 50 75 100]^oC, α = [0,1], θ =[0 15 30]^o, $\phi = 1$ and $\frac{1}{\nu} = 1$. Note that solid lines correspond to $\theta = 0^o$, dashed lines correspond to $\theta = 15^o$ and dotted lines correspond to $\theta = 30^o$.

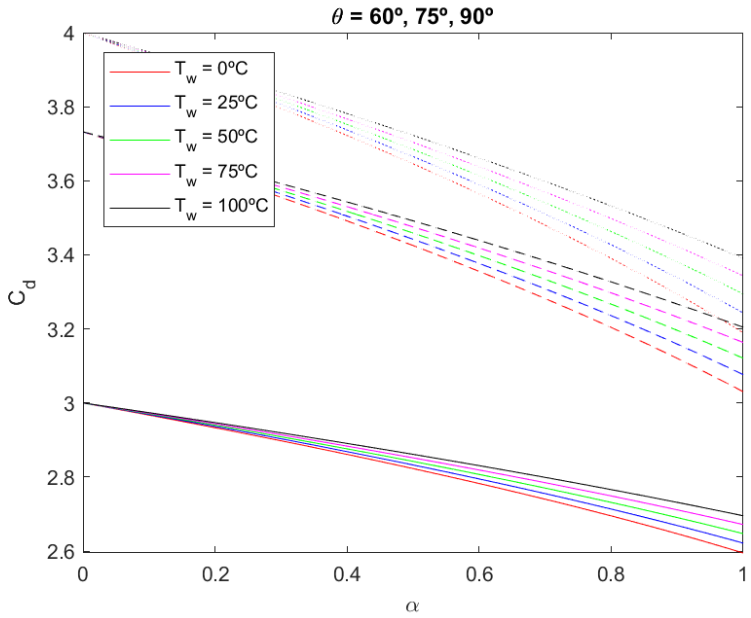

Figure 3.5: Analyzed Schamberg models for flat plate and specular reflection. T_w = [0 25 50 75 100]^oC, α = [0,1], θ =[60 75 90]^o, $\phi = 1$ and $\frac{1}{v} = 1$. Note that solid lines correspond to $\theta = 60^o$, dashed lines correspond to $\theta = 75^o$ and dotted lines correspond to $\theta = 90^o$.

As it can be seen from the two plots, variation of C_D is highly related with the angle of attack. Figure 3.4 and Figure 3.5 show again that when there's no accommodation, T_w does not cause a variation in C_D, but for $\alpha = 1$ it does. Note that the difference in C_D caused by the temperature of the surface is greater for the extreme cases than for the ones close to $\theta = 45^o$, in which T_w does not affect even if accommodation occurs. In the case in which $\theta = 45^o$, see Figure B.2 from Appendix B, it can be seen that there's no variation in C_D.

3.2.2. Completely diffuse reflection

In this model, the study will consider completely diffuse reflection, which means that $\phi = \frac{2}{3}$ and $\frac{1}{v} = 0$. Two different cases will be studied, one in which T_w and α will be kept constant, and the other in which T_w and θ will be kept constant.

3.2.2.1. Constant T_w and α

In this case, the study will represent the drag coefficient for a flat plate and diffuse reflection. To do so, the different models have been structured keeping α constant among each computation and for each accommodation factor, several T_w values have been used [0 50 100] ^oC. Table 3.3 shows the parameter values for each model. Some other intermediate values have also been computed.

Model	$T_w(^oC)$	α	$\theta(^\circ)$	ϕ	$\frac{1}{\nu}$
M-F-000-00-var-2/3-0	0	0	[0,90]	$\frac{2}{3}$	0
M-F-050-00-var-2/3-0	50	0	[0,90]	$\frac{2}{3}$	0
M-F-100-00-var-2/3-0	100	0	[0,90]	$\frac{2}{3}$	0
M-F-000-05-var-2/3-0	0	0.5	[0,90]	$\frac{2}{3}$	0
M-F-050-05-var-2/3-0	50	0.5	[0,90]	$\frac{2}{3}$	0
M-F-100-05-var-2/3-0	100	0.5	[0,90]	$\frac{2}{3}$	0
M-F-000-10-var-2/3-0	0	1	[0,90]	$\frac{2}{3}$	0
M-F-050-10-var-2/3-0	50	1	[0,90]	$\frac{2}{3}$	0
M-F-100-10-var-2/3-0	100	1	[0,90]	$\frac{2}{3}$	0

Table 3.3: Analyzed Schamberg models for flat plate and diffuse reflection. T_w = [0 50 100]^oC, α = [0 0.5 1], θ =[0,90]^o, $\phi = \frac{2}{3}$ and $\frac{1}{\nu} = 0$.

The following two plots show C_D *vs*. θ. In Figure 3.6 colored lines correspond to different values of α and each line style correspond to different values of T_w, while in Figure 3.7 colored lines correspond to different T_w values and each line style corresponds to different values of α.

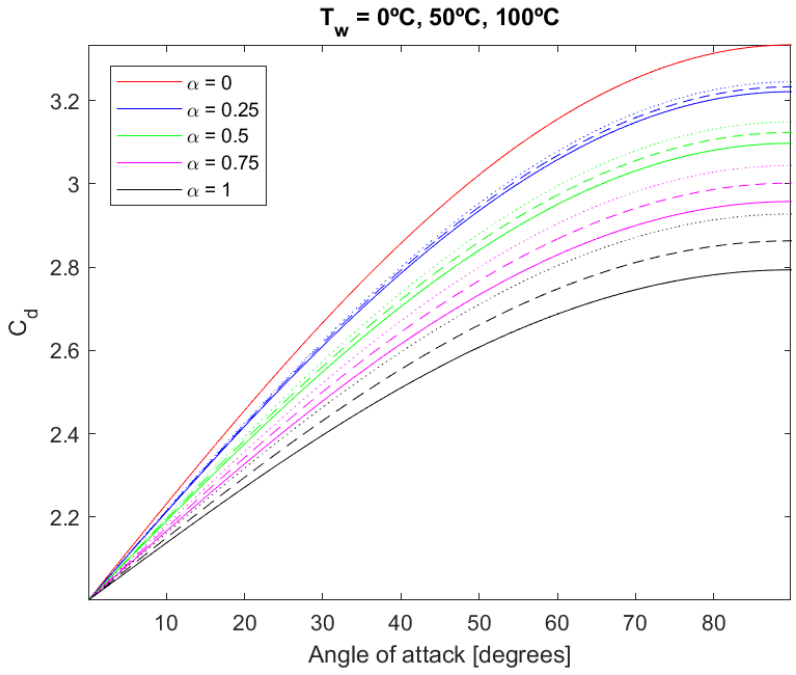

Figure 3.6: Analyzed Schamberg models for flat plate and diffuse reflection. T_w = [0 50 100]^oC, α = [0 0.25 0.5 0.75 1], θ =[0,90]^o, $\phi = \frac{2}{3}$ and $\frac{1}{\nu} = 0$. Note that solid lines correspond to $T_w = 0^oC$, dashed lines correspond to $T_w = 50^oC$ and dotted lines correspond to $T_w = 100^oC$.

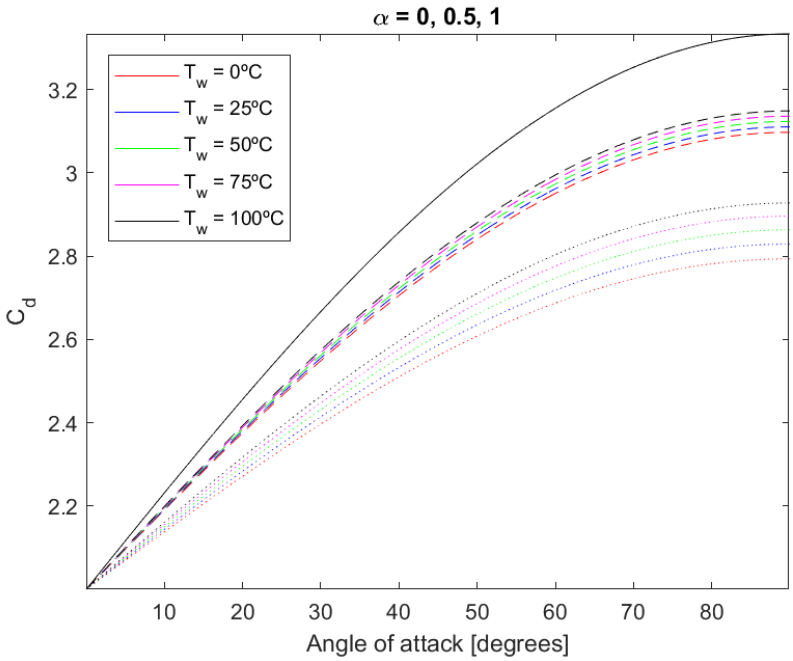

Figure 3.7: Analyzed Schamberg models for flat plate and diffuse reflection. T_w = [0 25 50 75 100]^oC, α = [0 0.5 1], θ =[0,90]^o, $\phi = \frac{2}{3}$ and $\frac{1}{v} = 0$. Note that solid lines correspond to $\alpha = 0$, dashed lines correspond to $\alpha = 0.5$ and dotted lines correspond to $\alpha = 1$.

From both Figure 3.6 and Figure 3.7 it can be seen that the behaviour of C_D is similar to the specular reflection case, but for diffuse reflection there are no values of C_D lower than 2 and for $\theta = 0^o$, the value of T_w or α does not cause a variation in C_D.

3.2.2.2. Constant T_w and θ

Table 3.4 shows the structure of the different models studied. As it can be seen from Figure 3.9 and Figure 3.10, variation of C_D decreases as θ increases (note that ΔC_D between 15^o and 30^o is much bigger than between 75^o and 90^o). There's a special case when $\theta = 0^o$, that can be seen in Figure 3.8, that differs a lot with the other values of θ. This could be due to the fact that maybe, this model is not taking into account the thermal speed of molecules and, as a result, the behaviour of C_D for $\theta = 0^o$ should not be taken into account.

Model	$T_w(^oC)$	α	$\theta(^o)$	ϕ	$\frac{1}{v}$	Model	$T_w(^oC)$	α	$\theta(^o)$	ϕ	$\frac{1}{v}$
M-F-000-var-00-2/3-0	0	[0,1]	0	$\frac{2}{3}$	0	M-F-075-var-45-2/3-0	75	[0,1]	45	$\frac{2}{3}$	0
M-F-025-var-00-2/3-0	25	[0,1]	0	$\frac{2}{3}$	0	M-F-100-var-45-2/3-0	100	[0,1]	45	$\frac{2}{3}$	0
M-F-050-var-00-2/3-0	50	[0,1]	0	$\frac{2}{3}$	0	M-F-000-var-60-2/3-0	0	[0,1]	60	$\frac{2}{3}$	0
M-F-075-var-00-2/3-0	75	[0,1]	0	$\frac{2}{3}$	0	M-F-025-var-60-2/3-0	25	[0,1]	60	$\frac{2}{3}$	0
M-F-100-var-00-2/3-0	100	[0,1]	0	$\frac{2}{3}$	0	M-F-050-var-60-2/3-0	50	[0,1]	60	$\frac{2}{3}$	0
M-F-000-var-15-2/3-0	0	[0,1]	15	$\frac{2}{3}$	0	M-F-075-var-60-2/3-0	75	[0,1]	60	$\frac{2}{3}$	0
M-F-025-var-15-2/3-0	25	[0,1]	15	$\frac{2}{3}$	0	M-F-100-var-60-2/3-0	100	[0,1]	60	$\frac{2}{3}$	0
M-F-050-var-15-2/3-0	50	[0,1]	15	$\frac{2}{3}$	0	M-F-000-var-75-2/3-0	0	[0,1]	75	$\frac{2}{3}$	0
M-F-075-var-15-2/3-0	75	[0,1]	15	$\frac{2}{3}$	0	M-F-025-var-75-2/3-0	25	[0,1]	75	$\frac{2}{3}$	0
M-F-100-var-15-2/3-0	100	[0,1]	15	$\frac{2}{3}$	0	M-F-050-var-75-2/3-0	50	[0,1]	75	$\frac{2}{3}$	0
M-F-000-var-30-2/3-0	0	[0,1]	30	$\frac{2}{3}$	0	M-F-075-var-75-2/3-0	75	[0,1]	75	$\frac{2}{3}$	0
M-F-025-var-30-2/3-0	25	[0,1]	30	$\frac{2}{3}$	0	M-F-100-var-75-2/3-0	100	[0,1]	75	$\frac{2}{3}$	0
M-F-050-var-30-2/3-0	50	[0,1]	30	$\frac{2}{3}$	0	M-F-000-var-90-2/3-0	0	[0,1]	90	$\frac{2}{3}$	0
M-F-075-var-30-2/3-0	75	[0,1]	30	$\frac{2}{3}$	0	M-F-025-var-90-2/3-0	25	[0,1]	90	$\frac{2}{3}$	0
M-F-100-var-30-2/3-0	100	[0,1]	30	$\frac{2}{3}$	0	M-F-050-var-90-2/3-0	50	[0,1]	90	$\frac{2}{3}$	0
M-F-000-var-45-2/3-0	0	[0,1]	45	$\frac{2}{3}$	0	M-F-075-var-90-2/3-0	75	[0,1]	90	$\frac{2}{3}$	0
M-F-025-var-45-2/3-0	25	[0,1]	45	$\frac{2}{3}$	0	M-F-100-var-90-2/3-0	100	[0,1]	90	$\frac{2}{3}$	0
M-F-050-var-45-2/3-0	50	[0,1]	45	$\frac{2}{3}$	0						

Table 3.4: Analyzed Schamberg models for flat plate and diffuse reflection. T_w = [0 25 50 75 100]^oC, α = [0,1], θ =[0 15 30 45 60 75 90]^o, $\phi = \frac{2}{3}$ and $\frac{1}{v} = 0$.

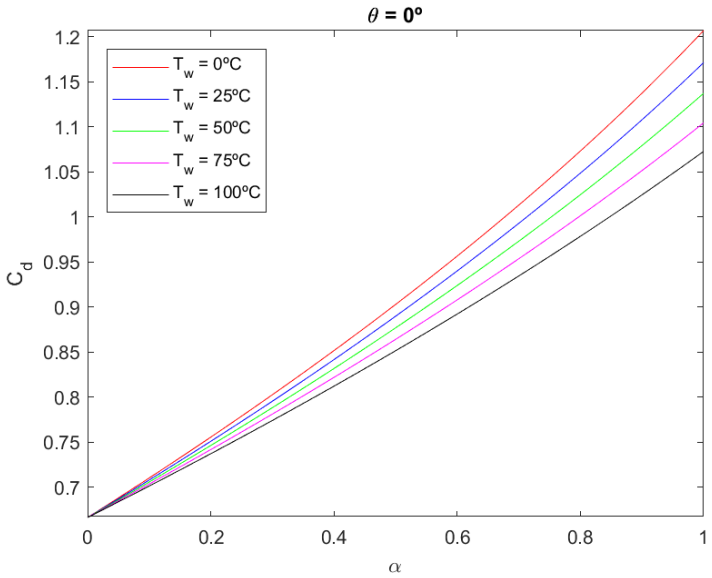

Figure 3.8: Analyzed Schamberg models for flat plate and diffuse reflection. T_w = [0 25 50 75 100]^oC, α = [0,1], $\theta = 0^o$, $\phi = \frac{2}{3}$ and $\frac{1}{v} = 0$.

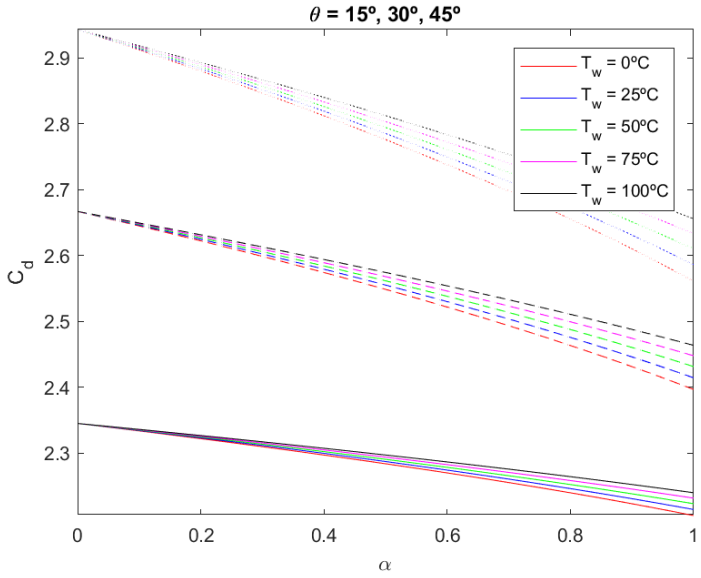

Figure 3.9: Analyzed Schamberg models for flat plate and diffuse reflection. $T_w = [0\ 25\ 50\ 75\ 100]^oC$, $\alpha = [0,1]$, $\theta = [15\ 30\ 45]^o$, $\phi = \frac{2}{3}$ and $\frac{1}{v} = 0$. Note that solid lines correspond to $\theta = 15^o$, dashed lines correspond to $\theta = 30^o$ and dotted lines correspond to $\theta = 45^o$.

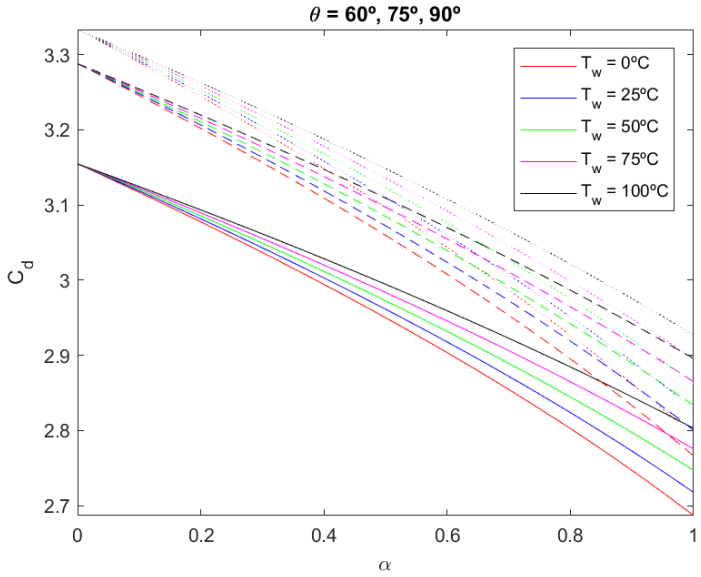

Figure 3.10: Analyzed Schamberg models for flat plate and diffuse reflection. $T_w = [0\ 25\ 50\ 75\ 100]^oC$, $\alpha = [0,1]$, $\theta = [60\ 75\ 90]^o$, $\phi = \frac{2}{3}$ and $\frac{1}{v} = 0$. Note that solid lines correspond to $\theta = 60^o$, dashed lines correspond to $\theta = 75^o$ and dotted lines correspond to $\theta = 90^o$.

3.2.3. Specular - Diffuse reflection

The study now will be focused on the transition from specular to diffuse reflection, so ϕ will vary from 1 to $\frac{2}{3}$ and $\frac{1}{v}$ will vary from 1 to 0. For easier identification, it will be structured in three different sections depending on the value of α. Each section will include

a parameters table and two plots, and they will be discussed all together at the end of Section 3.2.3.

3.2.3.1. $\alpha = 0$

Model	$T_w(^oC)$	α	$\theta(^\circ)$	ϕ	$\frac{1}{v}$	Model	$T_w(^oC)$	α	$\theta(^\circ)$	ϕ	$\frac{1}{v}$
M-F-000-00-00-var-var	0	0	0	$[1,\frac{2}{3}]$	[1,0]	M-F-100-00-45-var-var	100	0	45	$[1,\frac{2}{3}]$	[1,0]
M-F-050-00-00-var-var	50	0	0	$[1,\frac{2}{3}]$	[1,0]	M-F-000-00-60-var-var	0	0	60	$[1,\frac{2}{3}]$	[1,0]
M-F-100-00-00-var-var	100	0	0	$[1,\frac{2}{3}]$	[1,0]	M-F-050-00-60-var-var	50	0	60	$[1,\frac{2}{3}]$	[1,0]
M-F-000-00-15-var-var	0	0	15	$[1,\frac{2}{3}]$	[1,0]	M-F-100-00-60-var-var	100	0	60	$[1,\frac{2}{3}]$	[1,0]
M-F-050-00-15-var-var	50	0	15	$[1,\frac{2}{3}]$	[1,0]	M-F-000-00-75-var-var	0	0	75	$[1,\frac{2}{3}]$	[1,0]
M-F-100-00-15-var-var	100	0	15	$[1,\frac{2}{3}]$	[1,0]	M-F-050-00-75-var-var	50	0	75	$[1,\frac{2}{3}]$	[1,0]
M-F-000-00-30-var-var	0	0	30	$[1,\frac{2}{3}]$	[1,0]	M-F-100-00-75-var-var	100	0	75	$[1,\frac{2}{3}]$	[1,0]
M-F-050-00-30-var-var	50	0	30	$[1,\frac{2}{3}]$	[1,0]	M-F-000-00-90-var-var	0	0	90	$[1,\frac{2}{3}]$	[1,0]
M-F-100-00-30-var-var	100	0	30	$[1,\frac{2}{3}]$	[1,0]	M-F-050-00-90-var-var	50	0	90	$[1,\frac{2}{3}]$	[1,0]
M-F-000-00-45-var-var	0	0	45	$[1,\frac{2}{3}]$	[1,0]	M-F-100-00-90-var-var	100	0	90	$[1,\frac{2}{3}]$	[1,0]
M-F-050-00-45-var-var	50	0	45	$[1,\frac{2}{3}]$	[1,0]						

Table 3.5: Analyzed Schamberg models for flat plate and transition from specular to diffuse reflection. $T_w = [0\ 50\ 100]^oC$, $\alpha = 0$, $\theta = [0\ 15\ 30\ 45\ 60\ 75\ 90]^o$, $\phi = [1, \frac{2}{3}]$ and $\frac{1}{v} = [1,0]$.

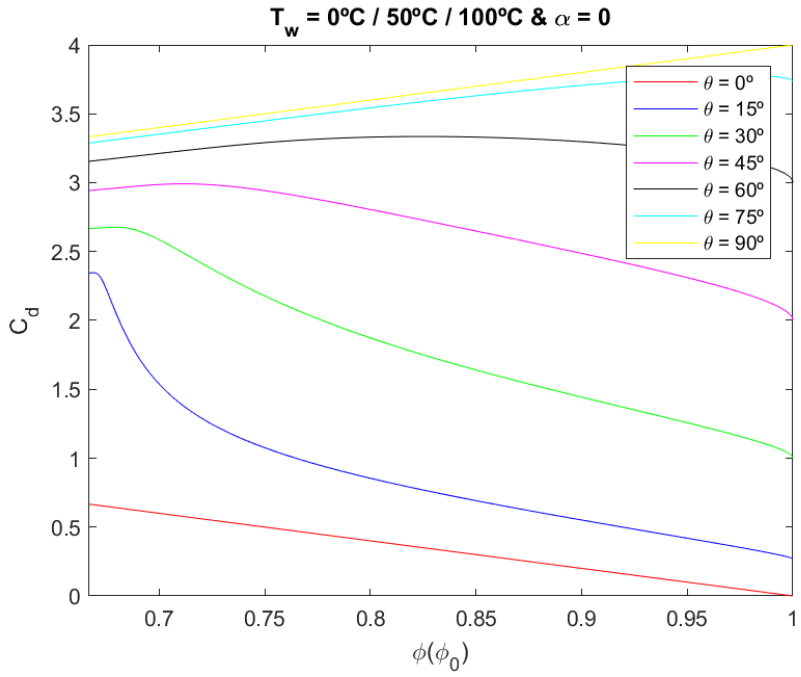

Figure 3.11: (C_D *vs.* $\phi(\phi_0)$) - Analyzed Schamberg models for flat plate and transition from specular to diffuse reflection. $T_w = [0\ 50\ 100]^oC$, $\alpha = 0$, $\theta = [0\ 15\ 30\ 45\ 60\ 75\ 90]^o$, $\phi = [1, \frac{2}{3}]$ and $\frac{1}{v} = [1,0]$.

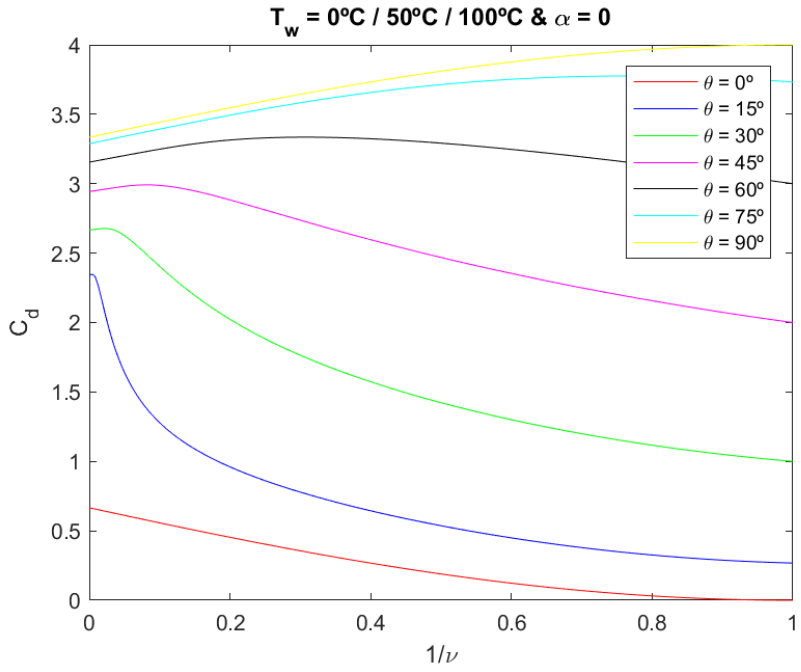

Figure 3.12: (C_D *vs.* $\frac{1}{\nu}$) - Analyzed Schamberg models for flat plate and transition from specular to diffuse reflection. T_w = [0 50 100]^oC, $\alpha = 0$, θ =[0 15 30 45 60 75 90]^o, $\phi = [1, \frac{2}{3}]$ and $\frac{1}{\nu} = [1, 0]$.

3.2.3.2. $\alpha = 0.5$

Model	$T_w(^oC)$	α	$\theta(^\circ)$	ϕ	$\frac{1}{\nu}$	Model	$T_w(^oC)$	α	$\theta(^\circ)$	ϕ	$\frac{1}{\nu}$
M-F-000-05-00-var-var	0	0.5	0	$[1,\frac{2}{3}]$	[1,0]	M-F-100-05-45-var-var	100	0.5	45	$[1,\frac{2}{3}]$	[1,0]
M-F-050-05-00-var-var	50	0.5	0	$[1,\frac{2}{3}]$	[1,0]	M-F-000-05-60-var-var	0	0.5	60	$[1,\frac{2}{3}]$	[1,0]
M-F-100-05-00-var-var	100	0.5	0	$[1,\frac{2}{3}]$	[1,0]	M-F-050-05-60-var-var	50	0.5	60	$[1,\frac{2}{3}]$	[1,0]
M-F-000-05-15-var-var	0	0.5	15	$[1,\frac{2}{3}]$	[1,0]	M-F-100-05-60-var-var	100	0.5	60	$[1,\frac{2}{3}]$	[1,0]
M-F-050-05-15-var-var	50	0.5	15	$[1,\frac{2}{3}]$	[1,0]	M-F-000-05-75-var-var	0	0.5	75	$[1,\frac{2}{3}]$	[1,0]
M-F-100-05-15-var-var	100	0.5	15	$[1,\frac{2}{3}]$	[1,0]	M-F-050-05-75-var-var	50	0.5	75	$[1,\frac{2}{3}]$	[1,0]
M-F-000-05-30-var-var	0	0.5	30	$[1,\frac{2}{3}]$	[1,0]	M-F-100-05-75-var-var	100	0.5	75	$[1,\frac{2}{3}]$	[1,0]
M-F-050-05-30-var-var	50	0.5	30	$[1,\frac{2}{3}]$	[1,0]	M-F-000-05-90-var-var	0	0.5	90	$[1,\frac{2}{3}]$	[1,0]
M-F-100-05-30-var-var	100	0.5	30	$[1,\frac{2}{3}]$	[1,0]	M-F-050-05-90-var-var	50	0.5	90	$[1,\frac{2}{3}]$	[1,0]
M-F-000-05-45-var-var	0	0.5	45	$[1,\frac{2}{3}]$	[1,0]	M-F-100-05-90-var-var	100	0.5	90	$[1,\frac{2}{3}]$	[1,0]
M-F-050-05-45-var-var	50	0.5	45	$[1,\frac{2}{3}]$	[1,0]						

Table 3.6: Analyzed Schamberg models for flat plate and transition from specular to diffuse reflection. T_w = [0 50 100]^oC, $\alpha = 0.5$, θ =[0 15 30 45 60 75 90]^o, $\phi = [1, \frac{2}{3}]$ and $\frac{1}{\nu} = [1, 0]$.

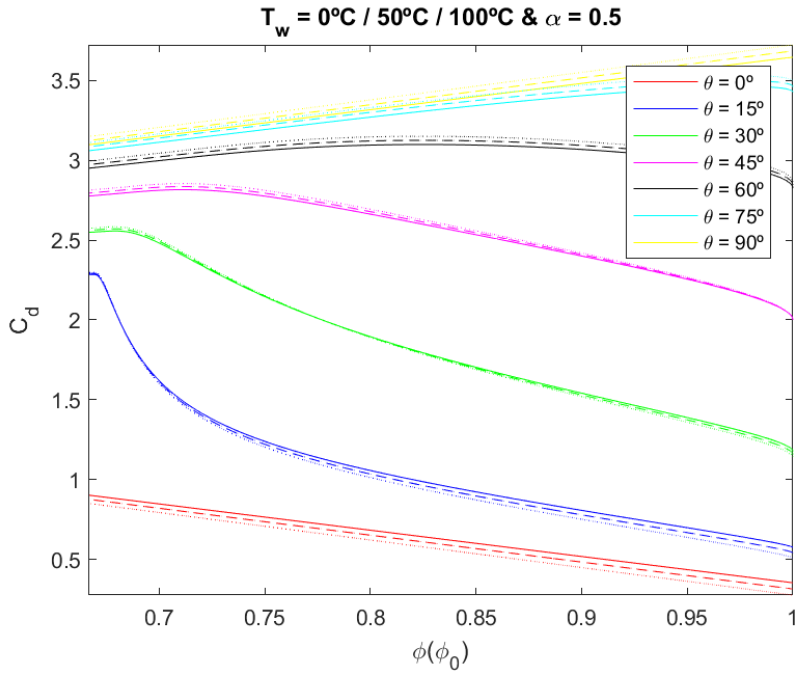

Figure 3.13: (C_D *vs.* $\phi(\phi_0)$) - Analyzed Schamberg models for flat plate and transition from specular to diffuse reflection. T_w = [0 50 100]^oC, $\alpha = 0.5$, θ =[0 15 30 45 60 75 90]^o, $\phi = [1, \frac{2}{3}]$ and $\frac{1}{\nu} = [1, 0]$. Note that solid lines correspond to $T_w = 0^oC$, dashed lines correspond to $T_w = 50^oC$ and dotted lines correspond to $T_w = 100^oC$.

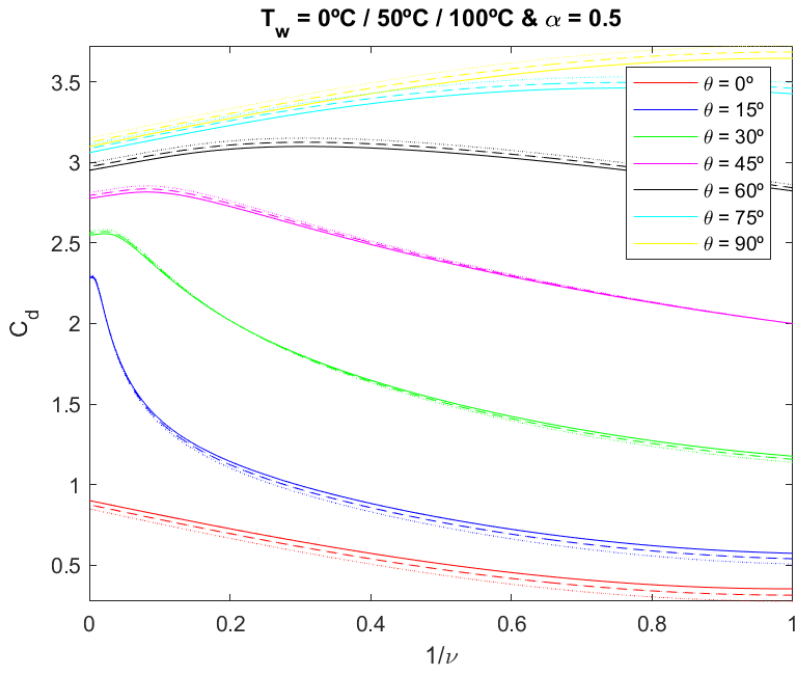

Figure 3.14: (C_D *vs.* $\frac{1}{\nu}$) - Analyzed Schamberg models for flat plate and transition from specular to diffuse reflection. T_w = [0 50 100]^oC, $\alpha = 0.5$, θ =[0 15 30 45 60 75 90]^o, $\phi = [1, \frac{2}{3}]$ and $\frac{1}{\nu} = [1, 0]$. Note that solid lines correspond to $T_w = 0^oC$, dashed lines correspond to $T_w = 50^oC$ and dotted lines correspond to $T_w = 100^oC$.

3.2.3.3. $\alpha = 1$

Model	$T_w(^oC)$	α	$\theta(^\circ)$	ϕ	$\frac{1}{v}$	Model	$T_w(^oC)$	α	$\theta(^\circ)$	ϕ	$\frac{1}{v}$
M-F-000-10-00-var-var	0	1	0	$[1,\frac{2}{3}]$	[1,0]	M-F-100-10-45-var-var	100	1	45	$[1,\frac{2}{3}]$	[1,0]
M-F-050-10-00-var-var	50	1	0	$[1,\frac{2}{3}]$	[1,0]	M-F-000-10-60-var-var	0	1	60	$[1,\frac{2}{3}]$	[1,0]
M-F-100-10-00-var-var	100	1	0	$[1,\frac{2}{3}]$	[1,0]	M-F-050-10-60-var-var	50	1	60	$[1,\frac{2}{3}]$	[1,0]
M-F-000-10-15-var-var	0	1	15	$[1,\frac{2}{3}]$	[1,0]	M-F-100-10-60-var-var	100	1	60	$[1,\frac{2}{3}]$	[1,0]
M-F-050-10-15-var-var	50	1	15	$[1,\frac{2}{3}]$	[1,0]	M-F-000-10-75-var-var	0	1	75	$[1,\frac{2}{3}]$	[1,0]
M-F-100-10-15-var-var	100	1	15	$[1,\frac{2}{3}]$	[1,0]	M-F-050-10-75-var-var	50	1	75	$[1,\frac{2}{3}]$	[1,0]
M-F-000-10-30-var-var	0	1	30	$[1,\frac{2}{3}]$	[1,0]	M-F-100-10-75-var-var	100	1	75	$[1,\frac{2}{3}]$	[1,0]
M-F-050-10-30-var-var	50	1	30	$[1,\frac{2}{3}]$	[1,0]	M-F-000-10-90-var-var	0	1	90	$[1,\frac{2}{3}]$	[1,0]
M-F-100-10-30-var-var	100	1	30	$[1,\frac{2}{3}]$	[1,0]	M-F-050-10-90-var-var	50	1	90	$[1,\frac{2}{3}]$	[1,0]
M-F-000-10-45-var-var	0	1	45	$[1,\frac{2}{3}]$	[1,0]	M-F-100-10-90-var-var	100	1	90	$[1,\frac{2}{3}]$	[1,0]
M-F-050-10-45-var-var	50	1	45	$[1,\frac{2}{3}]$	[1,0]						

Table 3.7: Analyzed Schamberg models for flat plate and transition from specular to diffuse reflection. T_w = [0 50 100]^oC, $\alpha = 1$, θ =[0 15 30 45 60 75 90]^o, $\phi = [1, \frac{2}{3}]$ and $\frac{1}{v} = [1,0]$.

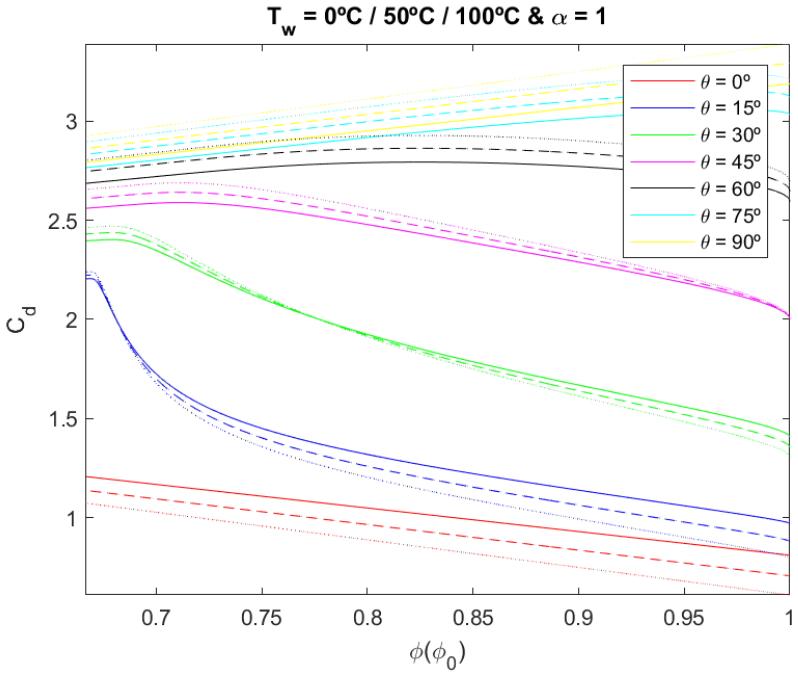

Figure 3.15: (C_D *vs.* $\phi(\phi_0)$) - Analyzed Schamberg models for flat plate and transition from specular to diffuse reflection. T_w = [0 50 100]^oC, $\alpha = 1$, θ =[0 15 30 45 60 75 90]^o, $\phi = [1, \frac{2}{3}]$ and $\frac{1}{v} = [1,0]$. Note that solid lines correspond to $T_w = 0^oC$, dashed lines correspond to $T_w = 50^oC$ and dotted lines correspond to $T_w = 100^oC$.

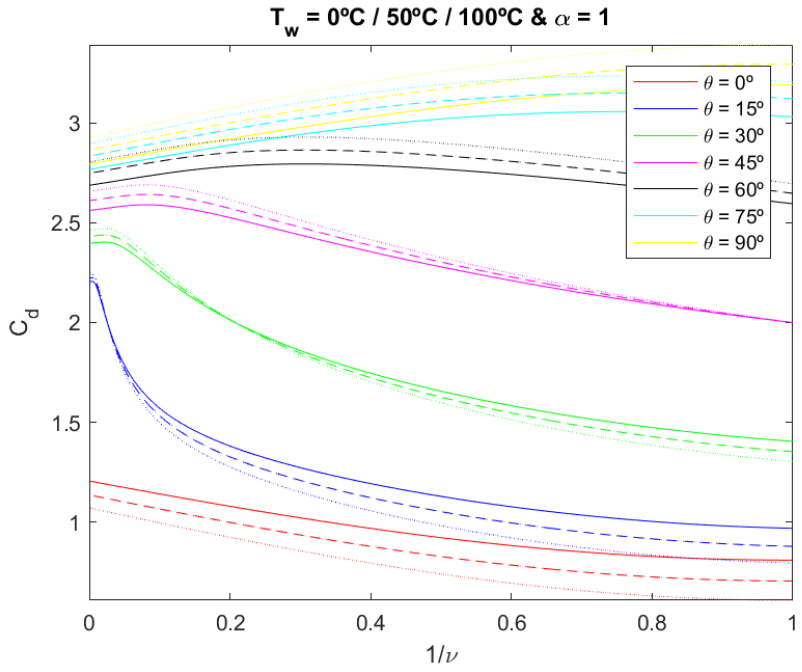

Figure 3.16: (C_D *vs.* $\frac{1}{\nu}$) - Analyzed Schamberg models for flat plate and transition from specular to diffuse reflection. T_w = [0 50 100]^oC, $\alpha = 1$, θ =[0 15 30 45 60 75 90]^o, $\phi = [1, \frac{2}{3}]$ and $\frac{1}{\nu} = [1, 0]$. Note that solid lines correspond to $T_w = 0^oC$, dashed lines correspond to $T_w = 50^oC$ and dotted lines correspond to $T_w = 100^oC$.

3.2.3.4. Comparison

In the previous figures it can be seen that the relation between α and T_w is the same either for specular or diffuse reflection. As α increases, different values of T_w cause more variation in C_D. Note that ΔC_D caused by T_w is greater for extreme values of θ than for intermediate ones, while ΔC_D between different values of θ becomes smaller for extreme values.

3.3. Sphere

All models studied in this section have the following nomenclature for an easier identification: $M - S - T_w T_w T_w - \alpha\alpha - \phi - \frac{1}{\nu}$

3.3.1. Completely specular reflection

This study is going to be focused on specular reflection, which implies $\phi = 1$ and $\frac{1}{\nu} = 1$. It will be divided into two cases; T_w is going to be kept constant for the first case and α for the second case.

3.3.1.1. Constant T_w and α

This case includes two different combinations. One in which T_w = [0 50 100] ^oC and $\alpha = [0,1]$, and the other one in which $T_w = [0,100]^oC$ and α = [0 0.5 1]. Table 3.8 shows the values of both cases.

Model	$T_w(^oC)$	α	ϕ	$\frac{1}{v}$	Model	$T_w(^oC)$	α	ϕ	$\frac{1}{v}$
M-S-000-var-1-1	0	[0,1]	1	1	M-S-var-00-1-1	[0,100]	0	1	1
M-S-050-var-1-1	50	[0,1]	1	1	M-S-var-05-1-1	[0,100]	0.5	1	1
M-S-100-var-1-1	100	[0,1]	1	1	M-S-var-10-1-1	[0,100]	1	1	1

Table 3.8: Analyzed Schamberg models for sphere and specular reflection. $T_w = [0,100]^oC$, $\alpha = [0,1]$, $\phi = 1$ and $\frac{1}{v} = 1$.

Specular reflection cases using Schamberg's model yield constant C_D values exactly equal to 2 (see Figure B.3 and Figure B.4 from Appendix B). No dependence either on wall temperature or accommodation coefficient is detected, which is consistent with equation for C_D in spherical case.

3.3.2. Completely diffuse reflection

In this section, the procedure to develop is computing C_D for diffuse reflection on a sphere, which involves $\phi = \frac{2}{3}$ and $\frac{1}{v} = 0$. The same structure of the previous section will be followed here.

3.3.2.1. Constant T_w and α

This case will be performed using the same procedure as for specular reflection. Table 3.9 shows the values of each parameter

Model	$T_w(^oC)$	α	ϕ	$\frac{1}{v}$	Model	$T_w(^oC)$	α	ϕ	$\frac{1}{v}$
M-S-000-var-2/3-0	0	[0,1]	$\frac{2}{3}$	0	M-S-var-00-2/3-0	[0,100]	0	$\frac{2}{3}$	0
M-S-050-var-2/3-0	50	[0,1]	$\frac{2}{3}$	0	M-S-var-05-2/3-0	[0,100]	0.5	$\frac{2}{3}$	0
M-S-100-var-2/3-0	100	[0,1]	$\frac{2}{3}$	0	M-S-var-10-2/3-0	[0,100]	1	$\frac{2}{3}$	0

Table 3.9: Analyzed Schamberg models for sphere and diffuse reflection. $T_w = [0,100]^oC$, $\alpha = [0,1]$, $\phi = \frac{2}{3}$ and $\frac{1}{v} = 0$.

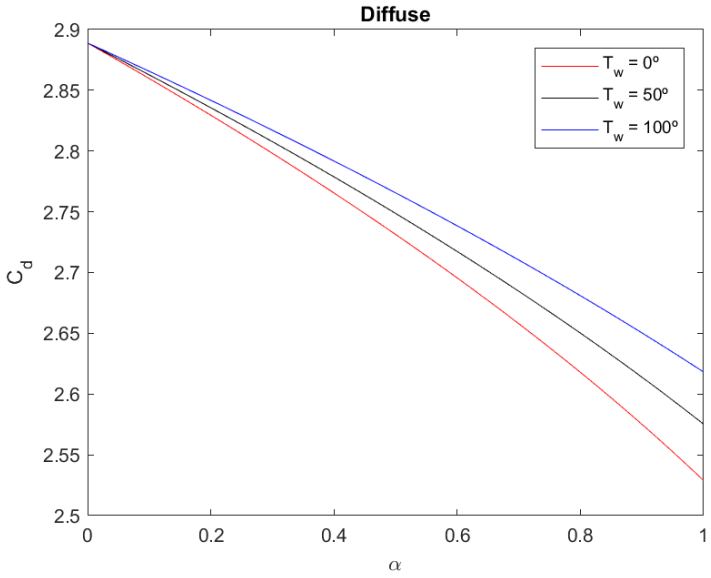

Figure 3.17: Analyzed Schamberg models for sphere and diffuse reflection. $T_w = [0\ 50\ 100]^oC$, $\alpha = [0, 1]$, $\phi = \frac{2}{3}$ and $\frac{1}{v} = 0$.

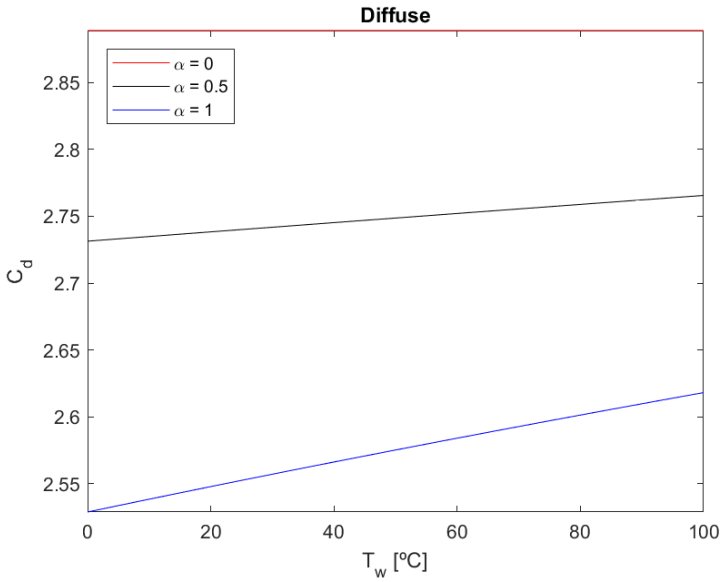

Figure 3.18: Analyzed Schamberg models for sphere and diffuse reflection. $T_w = [0, 100]^oC$, $\alpha = [0\ 0.5\ 1]$, $\phi = \frac{2}{3}$ and $\frac{1}{v} = 0$.

Regarding both Figure 3.17 and Figure 3.18, it can be seen that as α increases, the variation in C_D due to T_w increases too.

3.3.3. Specular - Diffuse reflection

Finally, the transition from specular to diffuse reflection is going to be studied. Now $\phi = [1, \frac{2}{3}]$ and $\frac{1}{v} = [1, 0]$. Table 3.9 shows the values of the parameters for each model.

Model	$T_w(^oC)$	α	ϕ	$\frac{1}{s}$	Model	$T_w(^oC)$	α	ϕ	$\frac{1}{s}$
M-S-000-00-var-var	0	0	$[\frac{2}{3},1]$	[0,1]	M-S-100-05-var-var	100	0.5	$[\frac{2}{3},1]$	[0,1]
M-S-050-00-var-var	50	0	$[\frac{2}{3},1]$	[0,1]	M-S-000-10-var-var	0	1	$[\frac{2}{3},1]$	[0,1]
M-S-100-00-var-var	100	0	$[\frac{2}{3},1]$	[0,1]	M-S-050-10-var-var	50	1	$[\frac{2}{3},1]$	[0,1]
M-S-000-05-var-var	0	0.5	$[\frac{2}{3},1]$	[0,1]	M-S-100-10-var-var	100	1	$[\frac{2}{3},1]$	[0,1]
M-S-050-05-var-var	50	0.5	$[\frac{2}{3},1]$	[0,1]					

Table 3.10: Analyzed Schamberg models for sphere and transition from specular to diffuse reflection. $T_w = [0\ 50\ 100]^oC$, $\alpha = [0\ 0.5\ 1]$, $\phi = [1, \frac{2}{3}]$ and $\frac{1}{s} = [1,0]$.

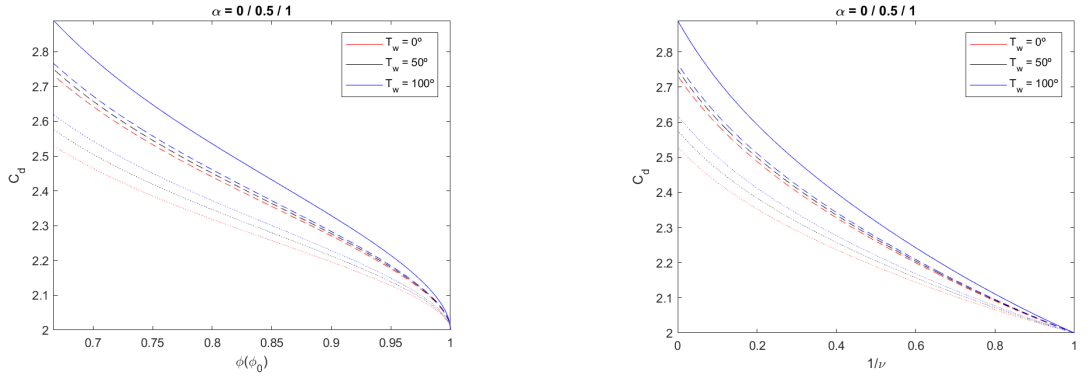

(a) C_D *vs.* $\phi(\phi_0)$ (b) C_D *vs.* $\frac{1}{s}$

Figure 3.19: Schamberg models for sphere. Specular-Diffuse reflection. $T_w = [0\ 50\ 100]^oC$, $\alpha = [0\ 0.5\ 1]$, $\phi = [1, \frac{2}{3}]$ and $\frac{1}{s} = [1,0]$. Note that solid lines correspond to $\alpha = 0$, dashed lines to $\alpha = 0.5$ and dotted lines to $\alpha = 1$.

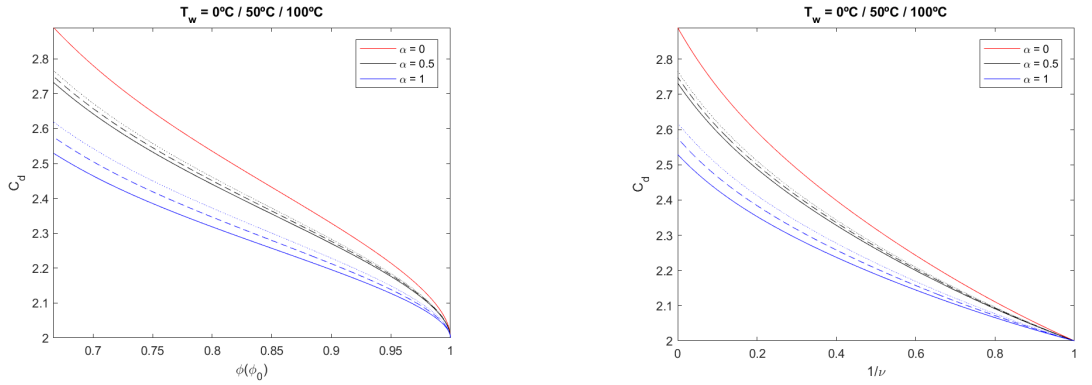

(a) C_D *vs.* $\phi(\phi_0)$ (b) C_D *vs.* $\frac{1}{s}$

Figure 3.20: Schamberg models for sphere. Specular-Diffuse reflection. $T_w = [0\ 50\ 100]^oC$, $\alpha = [0\ 0.5\ 1]$, $\phi = [1, \frac{2}{3}]$ and $\frac{1}{s} = [1,0]$. Note that solid lines correspond to $T_w = 0^oC$, dashed lines to $T_w = 50^oC$ and dotted lines to $T_w = 100^oC$.

As it can be seen in Figure 3.19 and Figure 3.20, the ΔC_D cause by T_w and α variations i greater as the reflection becomes more diffuse. It can also be observed that ΔC_D between different values of T_w is larger for high values of α.

CHAPTER 4. SENTMAN MODEL FOR DRAG COEFFICIENTS

In this chapter, we are going to expose Sentman model for drag coefficients that could fit when computing drag coefficient for diffuse reflection.

4.1. Model Description

The accommodation coefficient in this model is treated as an empirical parameter effective over the entire satellite surface. Momentum is highly sensitive to accommodation, as postulated in (12), and is strongly related to atomic oxygen absorption of the satellite's surface. So the variation of C_D with altitude is driven by changes in atomic oxygen absorption which indicates that density changes also produce variations in C_D. The accommodation coefficient is defined by (3) as:

$$\alpha = \frac{T_{k,in} - T_{k,out}}{T_{k,in} - T_w} \tag{4.1}$$

where $T_{k,in}$ is the kinetic temperature of incoming molecules, $T_{k,out}$ the distribution temperature of the reflected molecules and T_w the surface temperature and can be written as:

$$T_{k,in} = \frac{mV_r^2}{3k_b} \tag{4.2}$$

$$T_{k,out} = \frac{m}{3k_b} V_r^2(1-\alpha) + \alpha T_w \tag{4.3}$$

There are typically two types of reflection ascribed to the gas-surface interactions in low-earth orbit, as can be seen in Figure 4.1, that's why this combination of models intends to be useful for computing C_D for both types of reflection.

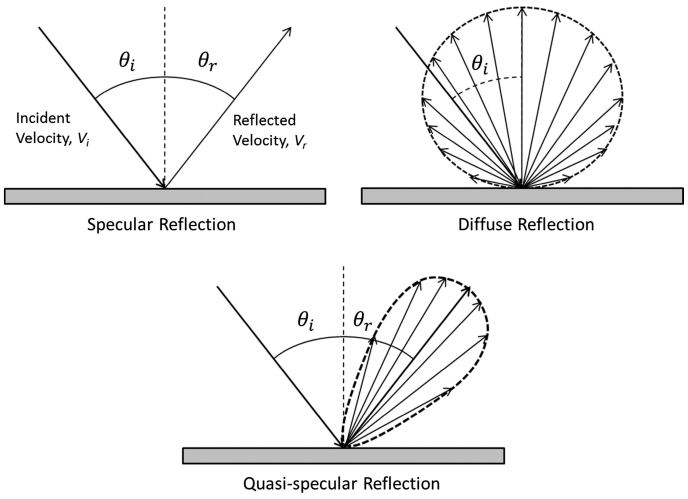

Figure 4.1: Different cases of particle reflection. Credit (4).

The majority of interactions below 500 km are diffuse in character with a scattering kernel that approximates the cosine (12). This happens when the velocities of reflected molecules are centered around the surface normal vector in a cosine distribution, as shown in the left panel of Figure 4.1. In the second model, the molecules are reflected in a narrow lobe centered around the specular direction.

A successful technique when computing C_D is to adapt the diffuse model developed by Sentman (6) and the quasi-specular model developed by Schamberg (5). Sentman's model adapts the diffuse energy distribution with a variable accommodation coefficient, which is a diffuse reflection with incomplete accommodation, while Schamberg's model reflects the majority of molecules around a direction such that the angle of reflection θ_r is smaller or equal than θ_i.

Once a set of incident and reflected velocity distribution is set, we can compute the drag coefficient for diffuse reflection on a flat plate and a sphere by using the following equations:

When computing the drag coefficients using this model, we will use Schamberg's approximation (5) for the temperature quotient defined as:

$$\sqrt{\frac{T_{k,out}}{T_a}} = \sqrt{1-\alpha} \tag{4.4}$$

So then

$$C_{D,plate} = \frac{2}{s\sqrt{\pi}}\exp\left[-s^2\sin^2(\theta_i)\right] + \frac{\sin(\theta_i)}{s^2}(1+2s^2)erf[s\sin(\theta_i)] + \frac{\sqrt{\pi}}{s}\sin^2(\theta_i)\sqrt{1-\alpha} \tag{4.5}$$

$$C_{D,sphere,diff} = \frac{2s^2+1}{\sqrt{\pi}s^3}\exp(-s^2) + \frac{4s^4+4s^2-1}{2s^4}erf(s) + \frac{2\sqrt{\pi}}{3s}\sqrt{1-\alpha} \tag{4.6}$$

Now, using Eqs.4.5 and 4.6 we can compute the drag coefficient fro a flat plate and a sphere. In the flat plate case we are going to consider the variation of the angle of attack, θ_i, and different values for the accommodation coefficient, α, [0 0.25 0.5 0.75 1].

It can be seen from Figure 4.2 that C_D goes from values close to zero for small angles of attack, where α does not have any influence, to values around 2 for high angles of attack, and then α plays an important role causing ΔC_D. From Figure 4.3, we can say that the variation of the accommodation coefficient does not cause a big change in C_D for a sphere.

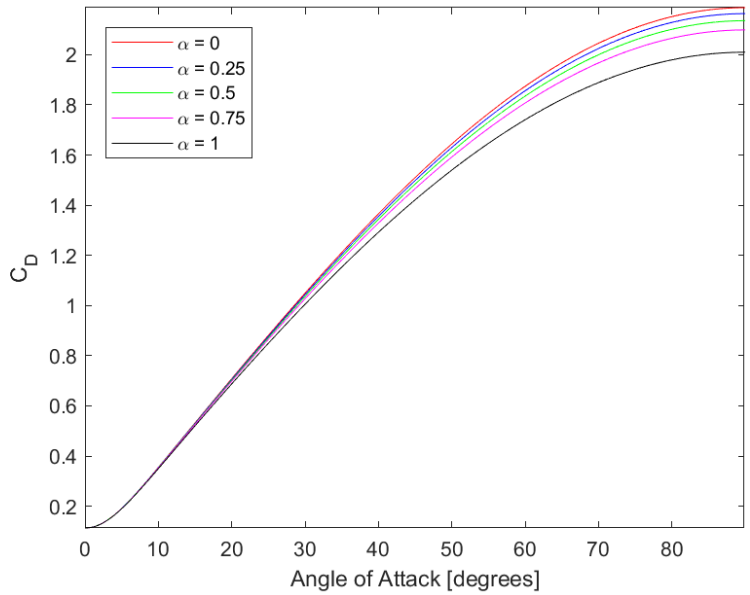

Figure 4.2: Analyzed Sentman model for flat plate and diffuse reflection. $\theta = [0, 90]^{o}$ and $\alpha =$ [0 0.25 0.5 0.75 1].

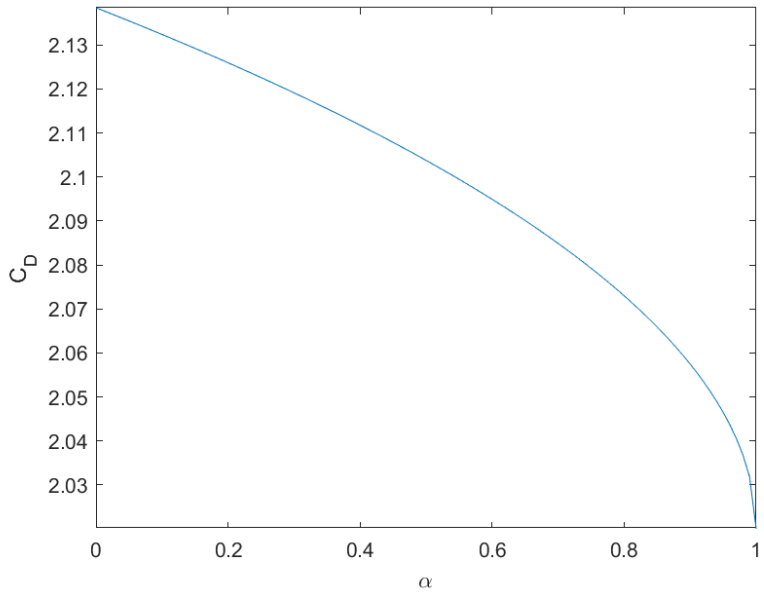

Figure 4.3: Analyzed Sentman model for sphere and diffuse reflection. $\alpha = [0, 1]$.

CHAPTER 5. CONCLUSIONS

A proper assessment of satellite C_D values is critical for the understanding of satellite dynamics and, in particular, for a more accurate determination of atmospheric density values. We have calculated and analyzed the C_D values in free molecular flow and hyperthermal velocity conditions, both for flat plate and spherical symmetries, using the models by Schaaf and Chambre, (3), SC58, and by Schamberg (5), S58.

In spite of being relatively old, these models (or slightly modified versions, like (6)) are still used nowadays, and remain important touchstones when checking the results of more sophisticated recent numerical models. The determination of the parameters on which they depend (see Chapters 2 and 3) can be achieved by performing experiments, both on Earth and in space (13). Improved determinations have been made in the last decades (14), and their influence on C_D, as well as the dependence of the latter coefficient on altitude and solar activity has been studied.

We have analyzed the limitations of both models, whose performance varies depending on the specific problem conditions. Frequent (and most successful) applications actually combine both models. S58 is usually applied in cases of quasi-specular reflection (see Figure 4.1), for moderate-to-high angles of attack. Its main advantage lays in the fact that it can consider re-emission of particles in a certain angular range. However, as we have seen, this model yields unrealistically low values at low grazing angles probably because it uses a rather simplistic approximation for the incident stream of particles. SC58 is applied in cases of diffuse reflection. It can describe more accurately momentum transfer at moderate to low grazing angles. In practice, we express the total C_D as:

$$C_D = f\, C_{D,spec} + (1-f)\, C_{D,diff} \tag{5.1}$$

where f is a parameter to be determined in each case.

The main conclusions derived from our calculations are:

i) Comparing both Schaaf and Chambre and Schamberg models, we can deduce that for the specular case, we obtain similar values of C_D when varying the angle of attack.

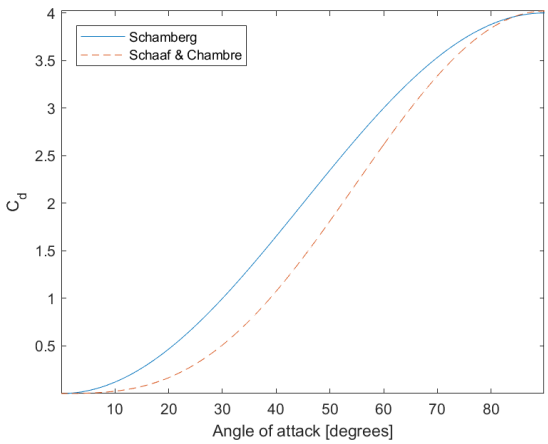

Figure 5.1: Comparison between Schaaf and Chambre (3) and Schamberg (5) for flat plate and specular reflection.

Figure 5.1 shows that both models return very similar values for a flat-plate when specular reflection occurs. For spherical geometries the result is also analogous and both models return a constant value. For SC58 we obtain $C_D = 2.02$, and for S58 we obtain $C_D = 2$. These constant values are due to the fact that perfect spherical symmetry the effect of the angle of attack is irrelevant. Neither there is a variation with T_w, because there no accommodation for these cases.

ii) If we analyze the diffuse cases, we realize that both SC58 and S58 models return different values for some particular conditions (see Figure 5.2).

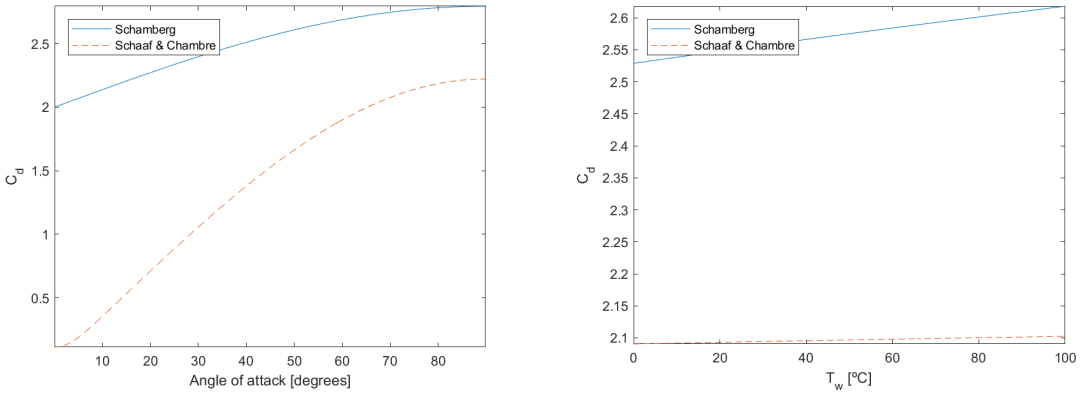

(a) Flat plate (b) Sphere

Figure 5.2: Comparison between Schaaf and Chambre (3) and Schamberg (5) for (a) Flat plate and (b) Sphere and diffuse reflection.

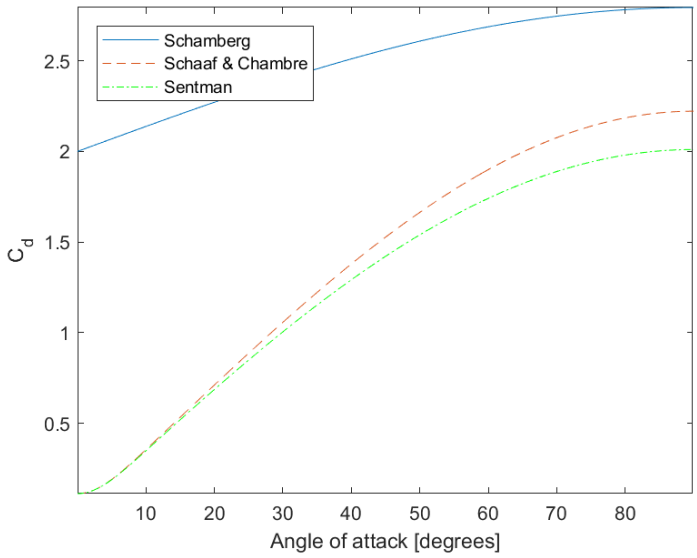

Figure 5.3: Comparison between Schaaf and Chambre (3), Schamberg (5) and Sentman (6) for flat plate and diffuse reflection.

Left panel of Figure 5.2 shows that there is a huge difference between both models, specially for low angles of attack, where Schamberg's values are about 20 times

greater than the ones obtained with Schaaf and Chambre model. Schamberg's values do not reproduce empirical values of C_D obtained from real satellites, for example CubeSats.

Actually, it is well known that S58 model is not accurate enough for diffuse reflection (and low grazing angles). Actually, an alternative popular C_D model, Sentman's model (6) yields values for diffuse reflection cases very similar to the ones by SC58, and widely different from the results with S58 (see Figure 5.3). A combination of both models (S58 for quasi-specular reflection and SC58 or Sentman's for diffuse reflection and low grazing angles) can handle almost any physical situation (14).

iii) We have checked the crucial role of the angle of attack when determining the value of C_D and flat-plate geometries, as it can cause variations of around 30 times between 0^o and 90^o. This is particularly important when specular reflection occurs. Given the problems for controlling satellite' attitude during the re-entry stage, any experiment designed for the assessment of C_D would be greatly simplified by using spherical symmetry.

iv) Regarding the accommodation coefficient, α, it is important to recall that it is a determining factor for C_D calculations both for Schamberg and Sentman models. Schaaf and Chambre equations for C_D calculations do not include the parameter α, but it is assumed to be $\alpha = 0$ for specular reflection and $\alpha = 1$ for diffuse reflection. Orbital velocity, as well as surface temperature, are the determining factor for different α values.

v) When analyzing the results from the different models, we can see that the surface temperature, T_w, must be taken into account for drag modelling. Variations in T_w do not cause wide C_D variations by themselves, as far as α is constant. However it is important to remind that in real cases, T_w changes imply variations in α, which themselves causes high variations in C_D.

vi) Finally, it should be recalled that flat-plate geometry is an oversimplification of real satellite geometries, such as CubeSats. In particular, considering a single angle of attack is not realistic for most satellite orientations. We have seen that spherical satellites are more useful for the assessment of C_D (and ultimately, of atmospheric density). However, they pose the technical problem of the adaptation to standard launchers, which are rather designed for the launch of CubeSats. Probably, the solution to allow both interfacing with launchers and good orbital performance would be to design a dispenser that, once in orbit, could open and release one (or several) spherical satellite(s) as the final geometry that is going to orbit around the Earth and, eventually, obtain experimental data.

BIBLIOGRAPHY

[1] Dr Eelco Doornbos. *Thermospheric Density and Wind Determination from Satellite Dynamics*. PhD thesis, Delft University of Technology, 2012.

[2] David Mostaza Prieto, Benjamin P. Graziano, and Peter C.E. Roberts. Spacecraft drag modelling. *Progress in Aerospace Sciences*, 64:56–65, January 2014. doi:10.1016/j.paerosci.2013.09.001.

[3] Samuel A. Schaaf & Paul L. Chambré. *Flow of Rarefied Gases*. Princeton Aeronautical Paperbacks, Princeton, New Jersey, 1958.

[4] Andrew Walker, Piyush Mehta, and Josef Koller. Different implementations of diffuse reflection with incomplete accommodation for drag coefficient modeling. *Journal of Spacecraft and Rockets*, 02 2014. doi:10.2514/1.A32668.

[5] R. Schamberg. *A new analytic representation of surface interaction for hyperthermal free-molecule flow, with application to satellite drag*. The Rand Corporation, Santa Monica, California., 1958.

[6] Lee H. Sentman. Free molecule flow theory and its application to the determination of aerodynamic forces. 10 1961.

[7] C. Shen. *Rarefied Gas Dynamics*. Springer, Berlin, 2005. doi:10.1007/b138784.

[8] J. M. Picone, A. E. Hedin, D. P. Drob, and A. C. Aikin. NRLMSISE-00 empirical model of the atmosphere: Statistical comparisons and scientific issues. *Journal of Geophysical Research (Space Physics)*, 107:1468, December 2002. doi:10.1029/2002JA009430.

[9] L. G. Jacchia, J. W. Slowey, and U. von Zahn. Temperature, density, and composition in the disturbed thermosphere from Esro 4 gas analyzer measurements - A global model. , 82:684–688, February 1977. doi:10.1029/JA082i004p00684.

[10] Zhongchao Tan. Basic properties of gases. In *Air Pollution and Greenhouse Gases*, chapter 2, pages 27–58. Springer, Singapore, 2014. doi:10.1007/978-981-287-212-8_2.

[11] S. Tsien, H. Similarity Laws of Hypersonic Flows. *Journal of Mathematics and Physics*, 25:247–251, April 1946. doi:10.1109/ICSEngT.2012.6339294.

[12] Kenneth Moe and Mildred M. Moe. The effect of adsorption on densities measured by orbiting pressure gauges. *Planetary and Space Science*, 15(8):1329 – 1332, 1967. URL: http://www.sciencedirect.com/science/article/pii/0032063367901869, doi:https://doi.org/10.1016/0032-0633(67)90186-9.

[13] M. D. Pilinski. Dynamic gas-surface interaction modeling for satellite aerodynamic computations. Master's thesis, University of Colorado Boulder, 2011.

[14] Kenneth Moe, Mildred M. Moe, and Steven D. Wallace. Improved satellite drag coefficient calculations from orbital measurements of energy accommodation. *Journal of Spacecraft and Rockets - J SPACECRAFT ROCKET*, 35:266–272, 05 1998. doi:10.2514/2.3350.

UNIVERSITAT POLITÈCNICA DE CATALUNYA
BARCELONATECH
Escola d'Enginyeria de Telecomunicació
i Aeroespacial de Castelldefels

APPENDICES

TFG TITLE: Determination of drag coefficients in a free molecular flow

DEGREE: Grau en Enginyeria d'Aeronavegació

AUTHOR: Bernat Minguell Montes

ADVISORS: Jordi Gutiérrez Cabello
Pilar Gil Pons

DATE: July 17, 2018

APPENDIX A. TYPICAL THERMAL ACCOMMODATION COEFFICIENT VALUES FOR AIR

Surface	α
Flat lacquer on bronze	$0.88 - 0.89$
Polished bronze	$0.91 - 0.94$
Machined bronze	$0.89 - 0.93$
Etched bronze	$0.93 - 0.95$
Polished cast iron	$0.87 - 0.93$
Machined cast iron	$0.87 - 0.88$
Etched cast iron	$0.89 - 0.96$
Polished aluminum	$0.89 - 0.95$
Machined aluminum	$0.95 - 0.97$
Etched aluminum	$0.89 - 0.97$

Table A.1: Thermal accommodation coefficient α for air depending on the surface.

APPENDIX B. EXTRA FIGURES

This appendix contains some extra figures related to the models studied that are intended to show some exceptional cases mentioned during the project.

B.1. Schaaf and Chambre model

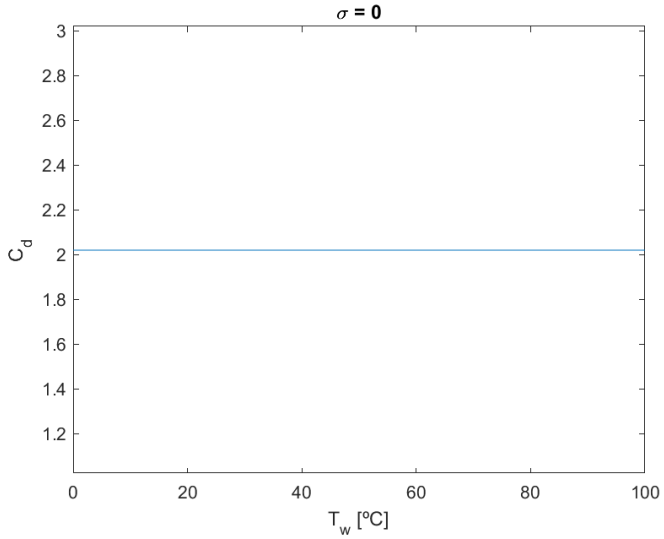

Figure B.1: Analyzed Schaaf and Chambre models for sphere and specular reflection. $\sigma = 0$ and $T_w = [0, 100]^{o}C$.

B.2. Schamberg model

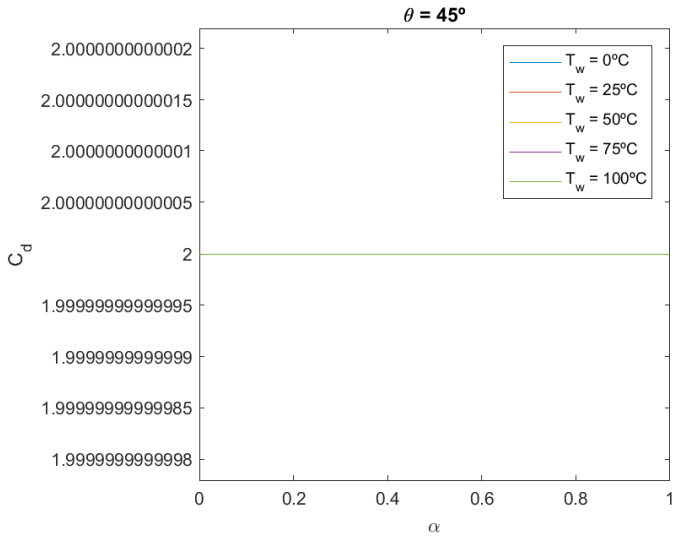

Figure B.2: Analyzed Schamberg models for flat plate and specular reflection. $T_w = [0\ 25\ 50\ 75\ 100]^{o}C$, $\alpha = [0,1]$, $\theta = 45^{o}$, $\phi = 1$ and $\frac{1}{v} = 1$.

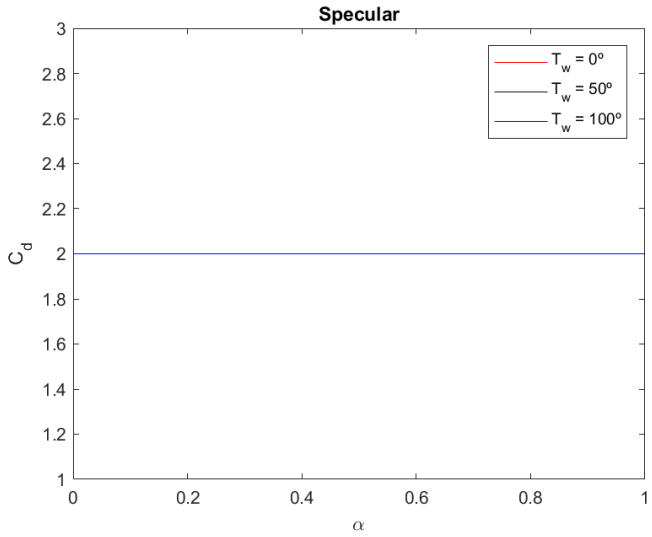

Figure B.3: Analyzed Schamberg models for sphere and specular reflection. $T_w = [0\ 50\ 100]^oC$ and $\alpha = [0, 1]$

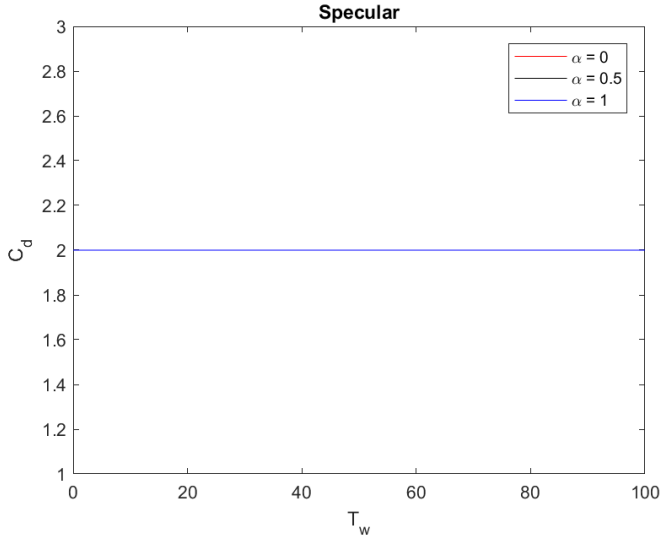

Figure B.4: Analyzed Schamberg models for sphere and specular reflection. $T_w = [0, 100]^oC$ and $\alpha = [0\ 0.5\ 1]$

APPENDIX C. MATLAB CODE

C.1. Schaaf and Chambre model

C.1.1. Flat plate

C.1.1.1. Main menu

```
clear all
close all

list = {'Specular','Diffuse','Variable'};
[indx,tf] = listdlg('PromptString','Select an option:','
    SelectionMode','single','ListSize',[400,200],'ListString',list
    );

if(indx == 1)
    list = {'Constant Temperature','Constant angle of attack'};
    [indx,tf] = listdlg('PromptString','Select an option:','
       SelectionMode','single','ListSize',[400,200],'ListString',
       list);
    if(indx == 1)
        T_w = [0 25 50 75 100] + 273;
        sigma=0;
        theta = 0.00001:0.00001:(pi/2);
        model=1;
        [C_d_SchaafChambre_flat] = SchaafChambre_plots_flat(T_w,
           sigma, theta, model);
        figure()
        plot(theta*180/pi,C_d_SchaafChambre_flat(:,1))
        xlabel('\theta [degrees]');
        ylabel('C_d');
        title('\sigma = 0');
        axis tight
        saveas(gcf,'Model_1_1.png')
    elseif(indx == 2)
        T_w = (0:1:100)+273;
        theta = 0:((pi/2)/(length(T_w)-1)):(pi/2);
        sigma=0;
        model=2;
        [C_d_SchaafChambre_flat] = SchaafChambre_plots_flat(T_w,
           sigma, theta, model);
        figure()
        plot(T_w,C_d_SchaafChambre_flat);
        xlabel('T_w');
        ylabel('C_d');
```

```
33          title('\sigma = 0');
34          axis tight
35          saveas(gcf,'Model_1_2.png')
36      end
37  end
38  if(indx == 2)
39      list = {'Constant Temperature','Constant angle of attack'};
40      [indx,tf] = listdlg('PromptString','Select an option:','
            SelectionMode','single','ListSize',[400,200],'ListString',
            list);
41      if(indx == 1)
42          T_w = [0 25 50 75 100] + 273;
43          sigma=0.5;
44          theta = 0:0.01:(pi/2);
45          model=3;
46          [C_d_SchaafChambre_flat] = SchaafChambre_plots_flat(T_w,
                sigma, theta, model);
47          figure()
48          plot(theta*180/pi,C_d_SchaafChambre_flat(:,1),'r');
49          hold on
50          plot(theta*180/pi,C_d_SchaafChambre_flat(:,2),'b');
51          plot(theta*180/pi,C_d_SchaafChambre_flat(:,3),'g');
52          plot(theta*180/pi,C_d_SchaafChambre_flat(:,4),'m');
53          plot(theta*180/pi,C_d_SchaafChambre_flat(:,5),'k');
54          hold off
55          legend('T_w = 0 C', 'T_w = 25 C', 'T_w = 50 C', 'T_w = 75
                C', 'T_w = 100 C', 'Location', 'northwest');
56          xlabel('\theta [degrees]');
57          ylabel('C_d');
58          title('\sigma = 1');
59          axis tight
60          saveas(gcf,'Model_2_1.png')
61      elseif(indx == 2)
62          T_w = (0:1:100)+273;
63          theta = [0 15 30 45 60 75 90]*pi/180;
64          sigma=1;
65          model=4;
66          [C_d_SchaafChambre_flat] = SchaafChambre_plots_flat(T_w,
                sigma, theta, model);
67          figure()
68          plot(T_w-273,C_d_SchaafChambre_flat(:,1),'r');
69          hold on
70          plot(T_w-273,C_d_SchaafChambre_flat(:,2),'b');
71          plot(T_w-273,C_d_SchaafChambre_flat(:,3),'g');
72          plot(T_w-273,C_d_SchaafChambre_flat(:,4),'m');
73          plot(T_w-273,C_d_SchaafChambre_flat(:,5),'k');
74          plot(T_w-273,C_d_SchaafChambre_flat(:,6),'c');
75          plot(T_w-273,C_d_SchaafChambre_flat(:,7),'y');
```

```
76          hold off
77          legend('\theta = 0 ', '\theta = 15 ', '\theta = 30 ', '\
                theta = 45 ', '\theta = 60 ', '\theta = 75 ', '\theta
                = 90 ');
78          xlabel('T_w [C]');
79          ylabel('C_d');
80          title('\sigma = 1');
81          axis tight
82          saveas(gcf,'Model_2_2.png')
83      end
84  end
85  if(indx == 3)
86      T_w = 50+273;
87      theta = [0 15 30 45 60 75 90]*pi/180;
88      sigma=0:0.001:1;
89      model=5;
90      [C_d_SchaafChambre_flat] = SchaafChambre_plots_flat(T_w,
            sigma, theta, model);
91      figure()
92      plot(sigma,C_d_SchaafChambre_flat(:,1),'r');
93      hold on
94      plot(sigma,C_d_SchaafChambre_flat(:,2),'b');
95      plot(sigma,C_d_SchaafChambre_flat(:,3),'g');
96      plot(sigma,C_d_SchaafChambre_flat(:,4),'m');
97      plot(sigma,C_d_SchaafChambre_flat(:,5),'k');
98      plot(sigma,C_d_SchaafChambre_flat(:,6),'c');
99      plot(sigma,C_d_SchaafChambre_flat(:,7),'y');
100     hold off
101     legend('\theta = 0 ', '\theta = 15 ', '\theta = 30 ', '\theta
            = 45 ', '\theta = 60 ', '\theta = 75 ', '\theta = 90 ');
102     xlabel('\sigma');
103     ylabel('C_d');
104     title('T_w = 50 C');
105     axis tight
106     saveas(gcf,'Model_3.png')
107 end
```

C.1.1.2. Function

```
1   function [C_d_SchaafChambre_flat] = SchaafChambre_plots_flat(T_w,
        sigma, theta, model)
2
3       M = xlsread("Datos1.xlsx"); % Read Excel
4       Elements = [M(:,2), M(:,3), M(:,4), M(:,8), M(:,9), M(:,10),
            M(:,11), M(:,12)]; % Atmospheric composition matrix
5       Height = M(:,1); % Height
6       Temp_neutral = M(:,6); % Neutral Temperature
7       Rt = 6.37E6; % Earth radius
8       Mt = 5.972E24; % Earth mass
```

```
9       G = 6.674E-11; % Gravitational constant
10      mu = []; % Empty mu vector
11      k = 1.3806488E-23; % Boltzmann constant
12      RIG = 8.314472; % Ideal gases constant
13
14      % Molar masses in g/mol
15      mass_O = 15.999; mass_N2 = 28.01340; mass_O2 = 31.99880;
            mass_He = 4.0026020;
16      mass_Ar = 39.9480; mass_H = 1.007940; mass_N = 14.00670;
            mass_AnomO = 15.999;
17
18      % Masses vector in Kg/mol
19      mass_total = [mass_O, mass_N2, mass_O2, mass_He, mass_Ar,
            mass_H, mass_N, mass_AnomO]/1000;
20
21      % Mu computation
22      for i=1:1:101
23          mu(i)=(Elements(i,:)*mass_total'/sum(Elements(i,:)));
24      end
25
26      R=RIG*ones(1,length(mu))./(mu);
27
28      V_a = sqrt(2*R'.*Temp_neutral);
29      V_orb = sqrt((G*Mt*ones(101,1))./(Height.*1000+Rt));
30
31      V_a_r = sqrt(2*R(21)*T_w);
32
33      s = (V_orb(21)/V_a(21));
34      s_w = (V_orb(21)*ones(1,length(V_a_r))./V_a_r);
35
36      if(model == 1)
37          for i=1:1:length(T_w)
38              C_d_SchaafChambre_flat_spec(:,i) = ((4*sin(theta))./(
                    sqrt(pi)*s^2)).*((s*sin(theta)).*exp(-((s*sin(
                    theta)).^2))+sqrt(pi)*(0.5+(s*sin(theta)).^2).*erf
                    (s*sin(theta)));
39          end
40          C_d_SchaafChambre_flat = C_d_SchaafChambre_flat_spec;
41      elseif(model == 2)
42          C_d_SchaafChambre_flat_spec = ((4*sin(theta))./(sqrt(pi)*
                s^2)).*((s*sin(theta)).*exp(-((s*sin(theta)).^2))+sqrt
                (pi)*(0.5+(s*sin(theta)).^2).*erf(s*sin(theta)));
43          C_d_SchaafChambre_flat = C_d_SchaafChambre_flat_spec;
44      elseif(model == 3)
45          for i=1:1:length(T_w)
46              C_d_SchaafChambre_flat_diff(:,i) = (2/(sqrt(pi)*s))
                    *((exp(-((s*sin(theta)).^2)))+sqrt(pi)*s*sin(theta
                    ).*(1+(1/(2*s^2))).*erf(s*sin(theta))+((pi*s)/s_w(
```

```
                i))*(sin(theta).^2));
47          end
48          C_d_SchaafChambre_flat = C_d_SchaafChambre_flat_diff;
49      elseif(model == 4)
50          for i=1:1:length(theta)
51              C_d_SchaafChambre_flat_diff(:,i) = (2/(sqrt(pi)*s))
                    *((exp(-((s*sin(theta(i)))^2)))+sqrt(pi)*s*sin(
                    theta(i))*(1+(1/(2*s^2)))*erf(s*sin(theta(i)))+((
                    pi*s)*ones(1,length(s_w))./s_w).*(sin(theta(i))^2)
                    );
52          end
53          C_d_SchaafChambre_flat = C_d_SchaafChambre_flat_diff;
54      elseif(model == 5)
55          for i=1:1:length(theta)
56              C_d_SchaafChambre_flat_diff(i) = (2/(sqrt(pi)*s))*((
                    exp(-((s*sin(theta(i)))^2)))+sqrt(pi)*s*sin(theta(
                    i))*(1+(1/(2*s^2)))*erf(s*sin(theta(i)))+((pi*s)/
                    s_w).*(sin(theta(i))^2));
57              C_d_SchaafChambre_flat_spec(i) = ((4*sin(theta(i)))/(
                    sqrt(pi)*s^2))*((s*sin(theta(i)))*exp(-((s*sin(
                    theta(i)))^2))+sqrt(pi)*(0.5+(s*sin(theta(i)))^2)*
                    erf(s*sin(theta(i))));
58              C_d_SchaafChambre_flat(:,i) =
                    C_d_SchaafChambre_flat_diff(i)*sigma +
                    C_d_SchaafChambre_flat_spec(i)*(1-sigma);
59          end
60      end
61  end
```

C.1.2. Sphere

C.1.2.1. Main menu

```
1  clear all
2  close all
3
4  list = {'Specular','Diffuse','Variable'};
5  [indx,tf] = listdlg('PromptString','Select an option:','
       SelectionMode','single','ListSize',[400,200],'ListString',list
       );
6
7  if(indx == 1)
8      T_w = (0:1:100)+273;
9      sigma=0;
10     model=1;
11     [C_d_SchaafChambre_sphere] = SchaafChambre_plots_sphere(T_w,
           sigma, model);
12     figure()
```

```
13      plot(T_w-273,C_d_SchaafChambre_sphere);
14      xlabel('T_w [C]');
15      ylabel('C_d');
16      title('\sigma = 0');
17      axis tight
18      saveas(gcf,'Model_1.png')
19  end
20  if(indx == 2)
21      T_w = (0:1:100)+273;
22      sigma=1;
23      model=2;
24      [C_d_SchaafChambre_sphere] = SchaafChambre_plots_sphere(T_w,
            sigma, model);
25      figure()
26      plot(T_w-273,C_d_SchaafChambre_sphere);
27      xlabel('T_w [C]');
28      ylabel('C_d');
29      title('\sigma = 1');
30      axis tight
31      saveas(gcf,'Model_2.png')
32  end
33  if(indx == 3)
34      T_w = [0 25 50 75 100] + 273;
35      sigma=0:0.01:1;
36      model=3;
37      [C_d_SchaafChambre_sphere] = SchaafChambre_plots_sphere(T_w,
            sigma, model);
38      figure()
39      plot(sigma,C_d_SchaafChambre_sphere(:,1),'r');
40      hold on
41      plot(sigma,C_d_SchaafChambre_sphere(:,2),'b');
42      plot(sigma,C_d_SchaafChambre_sphere(:,3),'g');
43      plot(sigma,C_d_SchaafChambre_sphere(:,4),'m');
44      plot(sigma,C_d_SchaafChambre_sphere(:,5),'k');
45      hold off
46      legend('T_w = 0 C', 'T_w = 25 C', 'T_w = 50 C', 'T_w = 75 C',
            'T_w = 100 C','Location','northwest');
47      xlabel('\sigma');
48      ylabel('C_d');
49      axis tight
50      saveas(gcf,'Model_3.png')
51  end
```

C.1.2.2. Function

```
1  function [C_d_SchaafChambre_sphere] = SchaafChambre_plots_sphere(
       T_w, sigma, model)
2
3      M = xlsread("Datos1.xlsx"); % Read Excel
```

```
4       Elements = [M(:,2), M(:,3), M(:,4), M(:,8), M(:,9), M(:,10),
            M(:,11), M(:,12)]; % Atmospheric composition matrix
5       Height = M(:,1); % Height
6       Temp_neutral = M(:,6); % Neutral Temperature
7       Rt = 6.37E6; % Earth radius
8       Mt = 5.972E24; % Earth mass
9       G = 6.674E-11; % Gravitational constant
10      mu = []; % Empty mu vector
11      k = 1.3806488E-23; % Boltzmann constant
12      RIG = 8.314472; % Ideal gases constant
13
14      % Molar masses in g/mol
15      mass_O = 15.999; mass_N2 = 28.01340; mass_O2 = 31.99880;
            mass_He = 4.0026020;
16      mass_Ar = 39.9480; mass_H = 1.007940; mass_N = 14.00670;
            mass_AnomO = 15.999;
17
18      % Masses vector in Kg/mol
19      mass_total = [mass_O, mass_N2, mass_O2, mass_He, mass_Ar,
            mass_H, mass_N, mass_AnomO]/1000;
20
21      % Mu computation
22      for i=1:1:101
23          mu(i)=(Elements(i,:)*mass_total'/sum(Elements(i,:)));
24      end
25
26      R=RIG*ones(1,length(mu))./(mu);
27
28      V_a = sqrt(2*R'.*Temp_neutral);
29      V_orb = sqrt((G*Mt*ones(101,1))./(Height.*1000+Rt));
30
31      V_a_r = sqrt(2*R(21)*T_w);
32
33      s = (V_orb(21)/V_a(21));
34      s_w = (V_orb(21)*ones(1,length(V_a_r))./V_a_r);
35
36      if(model == 1 || model == 2)
37          C_d_SchaafChambre_sphere = (exp(-(s^2)/2)/(sqrt(pi)*s^3))
                *(1+2*(s^2)) + ((4*(s^4)+4*(s^2)-1)/(2*(s^4)))*erf(s)
                + (2*sigma*sqrt(pi)*ones(1,length(s_w)))./(3*s_w);
38      elseif(model == 3)
39          for i=1:1:length(s_w)
40              C_d_SchaafChambre_sphere(:,i) = (exp(-(s^2)/2)/(sqrt(
                    pi)*s^3))*(1+2*(s^2)) + ((4*(s^4)+4*(s^2)-1)/(2*(s
                    ^4)))*erf(s) + (2*sigma.*sqrt(pi))./(3*s_w(i));
41          end
42      end
43  end
```

C.2. Schamberg model

C.2.1. Flat plate

C.2.1.1. Main menu

```
clear all
close all

list = {'Specular','Diffuse','Variable'};
[indx,tf] = listdlg('PromptString','Select an option:','
    SelectionMode','single','ListSize',[400,200],'ListString',list
    );

%% SPECULAR

if(indx == 1)
    list = {'Constant Temperature','Constant accomodation factor'
        , 'Constant angle of attack'};
    [indx,tf] = listdlg('PromptString','Select an option:','
        SelectionMode','single','ListSize',[400,200],'ListString',
        list);

    if(indx == 1)
        T_w1 = 0+273;
        T_w2 = 50+273;
        T_w3 = 100+273;
        alpha = [0 0.25 0.5 0.75 1];
        angle_of_attack = 0:0.01:(pi/2);
        phi = 1;
        nu_inv = 1;
        model = 1;
        [C_d_1, V_rel1, phi] = Schamberg_plots_flat(T_w1, alpha,
            angle_of_attack, phi, nu_inv, model);
        [C_d_2, V_rel2, phi] = Schamberg_plots_flat(T_w2, alpha,
            angle_of_attack, phi, nu_inv, model);
        [C_d_3, V_rel3, phi] = Schamberg_plots_flat(T_w3, alpha,
            angle_of_attack, phi, nu_inv, model);

        figure()
        p1 = plot(angle_of_attack*180/pi, C_d_1(:,1),'r');
        hold on
        p2 = plot(angle_of_attack*180/pi, C_d_1(:,2),'b');
        p3 = plot(angle_of_attack*180/pi, C_d_1(:,3),'g');
        p4 = plot(angle_of_attack*180/pi, C_d_1(:,4),'m');
        p5 = plot(angle_of_attack*180/pi, C_d_1(:,5),'k');
        p6 = plot(angle_of_attack*180/pi, C_d_2(:,1),'--r');
        p7 = plot(angle_of_attack*180/pi, C_d_2(:,2),'--b');
```

```
35          p8 = plot(angle_of_attack*180/pi, C_d_2(:,3),'--g');
36          p9 = plot(angle_of_attack*180/pi, C_d_2(:,4),'--m');
37          p10 = plot(angle_of_attack*180/pi, C_d_2(:,5),'--k');
38          p11 = plot(angle_of_attack*180/pi, C_d_3(:,1),':r');
39          p12 = plot(angle_of_attack*180/pi, C_d_3(:,2),':b');
40          p13 = plot(angle_of_attack*180/pi, C_d_3(:,3),':g');
41          p14 = plot(angle_of_attack*180/pi, C_d_3(:,4),':m');
42          p15= plot(angle_of_attack*180/pi, C_d_3(:,5),':k');
43          hold off
44          legend([p1 p2 p3 p4 p5],{'\alpha = 0', '\alpha = 0.25', '
               \alpha = 0.5', '\alpha = 0.75', '\alpha = 1'},'
               Location','northwest')
45          xlabel('Angle of attack [degrees]');
46          ylabel('C_d');
47          title('T_w = 0 C, 50 C, 100 C');
48          axis tight
49          saveas(gcf,'Model_1.png')
50      end
51      if(indx == 2)
52          alpha1 = 0;
53          alpha2 = 0.5;
54          alpha3 = 1;
55          T_w = [0 25 50 75 100] + 273;
56          angle_of_attack = 0:0.01:(pi/2);
57          phi = 1;
58          nu_inv = 1;
59          model = 2;
60          [C_d_1, V_rel1, phi] = Schamberg_plots_flat(T_w, alpha1,
               angle_of_attack, phi, nu_inv, model);
61          [C_d_2, V_rel2, phi] = Schamberg_plots_flat(T_w, alpha2,
               angle_of_attack, phi, nu_inv, model);
62          [C_d_3, V_rel3, phi] = Schamberg_plots_flat(T_w, alpha3,
               angle_of_attack, phi, nu_inv, model);
63
64          figure()
65          p1 = plot(angle_of_attack*180/pi, C_d_1(:,1),'r');
66          hold on
67          p2 = plot(angle_of_attack*180/pi, C_d_1(:,2),'b');
68          p3 = plot(angle_of_attack*180/pi, C_d_1(:,3),'g');
69          p4 = plot(angle_of_attack*180/pi, C_d_1(:,4),'m');
70          p5 = plot(angle_of_attack*180/pi, C_d_1(:,5),'k');
71          p6 = plot(angle_of_attack*180/pi, C_d_2(:,1),'--r');
72          p7 = plot(angle_of_attack*180/pi, C_d_2(:,2),'--b');
73          p8 = plot(angle_of_attack*180/pi, C_d_2(:,3),'--g');
74          p9 = plot(angle_of_attack*180/pi, C_d_2(:,4),'--m');
75          p10 = plot(angle_of_attack*180/pi, C_d_2(:,5),'--k');
76          p11 = plot(angle_of_attack*180/pi, C_d_3(:,1),':r');
77          p12 = plot(angle_of_attack*180/pi, C_d_3(:,2),':b');
```

```
78          p13 = plot(angle_of_attack*180/pi, C_d_3(:,3),':g');
79          p14 = plot(angle_of_attack*180/pi, C_d_3(:,4),':m');
80          p15 = plot(angle_of_attack*180/pi, C_d_3(:,5),':k');
81          hold off
82          legend([p1 p2 p3 p4 p5],{'T_w = 0 C', 'T_w = 25 C', 'T_w
                = 50 C', 'T_w = 75 C', 'T_w = 100 C'},'Location','
                northwest')
83          xlabel('Angle of attack [degrees]');
84          ylabel('C_d');
85          title('\alpha = 0, 0.5, 1');
86          axis tight
87          saveas(gcf,'Model_2.png')
88      end
89      if(indx == 3)
90          alpha = 0:0.001:1;
91          T_w = [0 25 50 75 100] + 273;
92          angle_of_attack = [0 15 30 45 60 75 90]*pi/180;
93          phi = 1;
94          nu_inv = 1;
95          model = 3;
96          [C_d_1, V_rel1, phi] = Schamberg_plots_flat(T_w, alpha,
                angle_of_attack(1), phi, nu_inv, model);
97          [C_d_2, V_rel2, phi] = Schamberg_plots_flat(T_w, alpha,
                angle_of_attack(2), phi, nu_inv, model);
98          [C_d_3, V_rel3, phi] = Schamberg_plots_flat(T_w, alpha,
                angle_of_attack(3), phi, nu_inv, model);
99          [C_d_4, V_rel4, phi] = Schamberg_plots_flat(T_w, alpha,
                angle_of_attack(4), phi, nu_inv, model);
100         [C_d_5, V_rel5, phi] = Schamberg_plots_flat(T_w, alpha,
                angle_of_attack(5), phi, nu_inv, model);
101         [C_d_6, V_rel6, phi] = Schamberg_plots_flat(T_w, alpha,
                angle_of_attack(6), phi, nu_inv, model);
102         [C_d_7, V_rel7, phi] = Schamberg_plots_flat(T_w, alpha,
                angle_of_attack(7), phi, nu_inv, model);
103
104         figure()
105         p1 = plot(alpha, C_d_1(:,1),'r');
106         hold on
107         p2 = plot(alpha, C_d_1(:,2),'b');
108         p3 = plot(alpha, C_d_1(:,3),'g');
109         p4 = plot(alpha, C_d_1(:,4),'m');
110         p5 = plot(alpha, C_d_1(:,5),'k');
111         p6 = plot(alpha, C_d_2(:,1),'--r');
112         p7 = plot(alpha, C_d_2(:,2),'--b');
113         p8 = plot(alpha, C_d_2(:,3),'--g');
114         p9 = plot(alpha, C_d_2(:,4),'--m');
115         p10 = plot(alpha, C_d_2(:,5),'--k');
116         p11 = plot(alpha, C_d_3(:,1),':r');
```

```
117         p12 = plot(alpha, C_d_3(:,2),':b');
118         p13 = plot(alpha, C_d_3(:,3),':g');
119         p14 = plot(alpha, C_d_3(:,4),':m');
120         p15= plot(alpha, C_d_3(:,5),':k');
121         hold off
122         legend([p1 p2 p3 p4 p5],{'T_w = 0 C', 'T_w = 25 C', 'T_w
               = 50 C', 'T_w = 75 C', 'T_w = 100 C'},'Location','
               northwest')
123         xlabel('\alpha');
124         ylabel('C_d');
125         title('\theta = 0 , 15 , 30 ');
126         axis tight
127         saveas(gcf,'Model_3_1.png')
128
129         figure()
130         plot(alpha,C_d_4);
131         legend('T_w = 0 C', 'T_w = 25 C', 'T_w = 50 C', 'T_w = 75
               C', 'T_w = 100 C')
132         xlabel('\alpha');
133         ylabel('C_d');
134         title('\theta = 45 ');
135         axis tight
136         saveas(gcf,'Model_3_2.png')
137
138         figure()
139         p1 = plot(alpha, C_d_5(:,1),'r');
140         hold on
141         p2 = plot(alpha, C_d_5(:,2),'b');
142         p3 = plot(alpha, C_d_5(:,3),'g');
143         p4 = plot(alpha, C_d_5(:,4),'m');
144         p5 = plot(alpha, C_d_5(:,5),'k');
145         p6 = plot(alpha, C_d_6(:,1),'--r');
146         p7 = plot(alpha, C_d_6(:,2),'--b');
147         p8 = plot(alpha, C_d_6(:,3),'--g');
148         p9 = plot(alpha, C_d_6(:,4),'--m');
149         p10 = plot(alpha, C_d_6(:,5),'--k');
150         p11 = plot(alpha, C_d_7(:,1),':r');
151         p12 = plot(alpha, C_d_7(:,2),':b');
152         p13 = plot(alpha, C_d_7(:,3),':g');
153         p14 = plot(alpha, C_d_7(:,4),':m');
154         p15 = plot(alpha, C_d_7(:,5),':k');
155         hold off
156         legend([p1 p2 p3 p4 p5],{'T_w = 0 C', 'T_w = 25 C', 'T_w
               = 50 C', 'T_w = 75 C', 'T_w = 100 C'},'Location','
               northwest')
157         xlabel('\alpha');
158         ylabel('C_d');
159         title('\theta = 60 , 75 , 90 ');
```

```
160             axis tight
161             saveas(gcf,'Model_3_3.png')
162         end
163     end
164
165     %% DIFFUSE
166
167     if(indx == 2)
168         list = {'Constant Temperature','Constant accomodation factor'
                , 'Constant angle of attack'};
169         [indx,tf] = listdlg('PromptString','Select an option:','
                SelectionMode','single','ListSize',[400,200],'ListString',
                list);
170
171         if(indx == 1)
172             T_w1 = 0+273;
173             T_w2 = 50+273;
174             T_w3 = 100+273;
175             alpha = [0 0.25 0.5 0.75 1];
176             angle_of_attack = 0.00001:0.00001:(pi/2);
177             phi = 2/3;
178             nu_inv = 0;
179             model = 4;
180             [C_d_1, V_rel1, phi] = Schamberg_plots_flat(T_w1, alpha,
                    angle_of_attack, phi, nu_inv, model);
181             [C_d_2, V_rel2, phi] = Schamberg_plots_flat(T_w2, alpha,
                    angle_of_attack, phi, nu_inv, model);
182             [C_d_3, V_rel3, phi] = Schamberg_plots_flat(T_w3, alpha,
                    angle_of_attack, phi, nu_inv, model);
183
184             figure()
185             p1 = plot(angle_of_attack*180/pi, C_d_1(:,1),'r');
186             hold on
187             p2 = plot(angle_of_attack*180/pi, C_d_1(:,2),'b');
188             p3 = plot(angle_of_attack*180/pi, C_d_1(:,3),'g');
189             p4 = plot(angle_of_attack*180/pi, C_d_1(:,4),'m');
190             p5 = plot(angle_of_attack*180/pi, C_d_1(:,5),'k');
191             p6 = plot(angle_of_attack*180/pi, C_d_2(:,1),'--r');
192             p7 = plot(angle_of_attack*180/pi, C_d_2(:,2),'--b');
193             p8 = plot(angle_of_attack*180/pi, C_d_2(:,3),'--g');
194             p9 = plot(angle_of_attack*180/pi, C_d_2(:,4),'--m');
195             p10 = plot(angle_of_attack*180/pi, C_d_2(:,5),'--k');
196             p11 = plot(angle_of_attack*180/pi, C_d_3(:,1),':r');
197             p12 = plot(angle_of_attack*180/pi, C_d_3(:,2),':b');
198             p13 = plot(angle_of_attack*180/pi, C_d_3(:,3),':g');
199             p14 = plot(angle_of_attack*180/pi, C_d_3(:,4),':m');
200             p15= plot(angle_of_attack*180/pi, C_d_3(:,5),':k');
201             hold off
```

```
202         legend([p1 p2 p3 p4 p5],{'\alpha = 0', '\alpha = 0.25', '
                \alpha = 0.5', '\alpha = 0.75', '\alpha = 1'},'
                Location','northwest')
203         xlabel('Angle of attack [degrees]');
204         ylabel('C_d');
205         title('T_w = 0 C, 50 C, 100 C');
206         axis tight
207         saveas(gcf,'Model_4.png')
208     end
209     if(indx == 2)
210         alpha1 = 0;
211         alpha2 = 0.5;
212         alpha3 = 1;
213         T_w = [0 25 50 75 100] + 273;
214         angle_of_attack = 0.00001:0.00001:(pi/2);
215         phi = 2/3;
216         nu_inv = 0;
217         model = 5;
218         [C_d_1, V_rel1, phi] = Schamberg_plots_flat(T_w, alpha1,
                angle_of_attack, phi, nu_inv, model);
219         [C_d_2, V_rel2, phi] = Schamberg_plots_flat(T_w, alpha2,
                angle_of_attack, phi, nu_inv, model);
220         [C_d_3, V_rel3, phi] = Schamberg_plots_flat(T_w, alpha3,
                angle_of_attack, phi, nu_inv, model);
221
222         figure()
223         p1 = plot(angle_of_attack*180/pi, C_d_1(:,1),'r');
224         hold on
225         p2 = plot(angle_of_attack*180/pi, C_d_1(:,2),'b');
226         p3 = plot(angle_of_attack*180/pi, C_d_1(:,3),'g');
227         p4 = plot(angle_of_attack*180/pi, C_d_1(:,4),'m');
228         p5 = plot(angle_of_attack*180/pi, C_d_1(:,5),'k');
229         p6 = plot(angle_of_attack*180/pi, C_d_2(:,1),'--r');
230         p7 = plot(angle_of_attack*180/pi, C_d_2(:,2),'--b');
231         p8 = plot(angle_of_attack*180/pi, C_d_2(:,3),'--g');
232         p9 = plot(angle_of_attack*180/pi, C_d_2(:,4),'--m');
233         p10 = plot(angle_of_attack*180/pi, C_d_2(:,5),'--k');
234         p11 = plot(angle_of_attack*180/pi, C_d_3(:,1),':r');
235         p12 = plot(angle_of_attack*180/pi, C_d_3(:,2),':b');
236         p13 = plot(angle_of_attack*180/pi, C_d_3(:,3),':g');
237         p14 = plot(angle_of_attack*180/pi, C_d_3(:,4),':m');
238         p15 = plot(angle_of_attack*180/pi, C_d_3(:,5),':k');
239         hold off
240         legend([p1 p2 p3 p4 p5],{'T_w = 0 C', 'T_w = 25 C', 'T_w
                = 50 C', 'T_w = 75 C', 'T_w = 100 C'},'Location','
                northwest')
241         xlabel('Angle of attack [degrees]');
242         ylabel('C_d');
```

```
243         title('\alpha = 0, 0.5, 1');
244         axis tight
245         saveas(gcf,'Model_5.png')
246     end
247     if(indx == 3)
248         alpha = 0:0.001:1;
249         T_w = [0 25 50 75 100] + 273;
250         angle_of_attack = [0 15 30 45 60 75 90]*pi/180;
251         phi = 2/3;
252         nu_inv = 0;
253         model = 6;
254         [C_d_1, V_rel1, phi] = Schamberg_plots_flat(T_w, alpha,
                angle_of_attack(1), phi, nu_inv, model);
255         [C_d_2, V_rel2, phi] = Schamberg_plots_flat(T_w, alpha,
                angle_of_attack(2), phi, nu_inv, model);
256         [C_d_3, V_rel3, phi] = Schamberg_plots_flat(T_w, alpha,
                angle_of_attack(3), phi, nu_inv, model);
257         [C_d_4, V_rel4, phi] = Schamberg_plots_flat(T_w, alpha,
                angle_of_attack(4), phi, nu_inv, model);
258         [C_d_5, V_rel5, phi] = Schamberg_plots_flat(T_w, alpha,
                angle_of_attack(5), phi, nu_inv, model);
259         [C_d_6, V_rel6, phi] = Schamberg_plots_flat(T_w, alpha,
                angle_of_attack(6), phi, nu_inv, model);
260         [C_d_7, V_rel7, phi] = Schamberg_plots_flat(T_w, alpha,
                angle_of_attack(7), phi, nu_inv, model);
261
262         figure()
263         plot(alpha,C_d_1);
264         legend('T_w = 0 C', 'T_w = 25 C', 'T_w = 50 C', 'T_w = 75
                C', 'T_w = 100 C','Location','northwest')
265         xlabel('\alpha');
266         ylabel('C_d');
267         title('\theta = 0 ');
268         axis tight
269         saveas(gcf,'Model_6_1.png')
270
271         figure()
272         p1 = plot(alpha, C_d_2(:,1),'r');
273         hold on
274         p2 = plot(alpha, C_d_2(:,2),'b');
275         p3 = plot(alpha, C_d_2(:,3),'g');
276         p4 = plot(alpha, C_d_2(:,4),'m');
277         p5 = plot(alpha, C_d_2(:,5),'k');
278         p6 = plot(alpha, C_d_3(:,1),'--r');
279         p7 = plot(alpha, C_d_3(:,2),'--b');
280         p8 = plot(alpha, C_d_3(:,3),'--g');
281         p9 = plot(alpha, C_d_3(:,4),'--m');
282         p10 = plot(alpha, C_d_3(:,5),'--k');
```

```
283         p11 = plot(alpha, C_d_4(:,1),':r');
284         p12 = plot(alpha, C_d_4(:,2),':b');
285         p13 = plot(alpha, C_d_4(:,3),':g');
286         p14 = plot(alpha, C_d_4(:,4),':m');
287         p15 = plot(alpha, C_d_4(:,5),':k');
288         hold off
289         legend([p1 p2 p3 p4 p5],{'T_w = 0 C', 'T_w = 25 C', 'T_w
                = 50 C', 'T_w = 75 C', 'T_w = 100 C'},'Location','
                northeast')
290         xlabel('\alpha');
291         ylabel('C_d');
292         title('\theta = 15 , 30 , 45 ');
293         axis tight
294         saveas(gcf,'Model_6_2.png')
295
296         figure()
297         p1 = plot(alpha, C_d_5(:,1),'r');
298         hold on
299         p2 = plot(alpha, C_d_5(:,2),'b');
300         p3 = plot(alpha, C_d_5(:,3),'g');
301         p4 = plot(alpha, C_d_5(:,4),'m');
302         p5 = plot(alpha, C_d_5(:,5),'k');
303         p6 = plot(alpha, C_d_6(:,1),'--r');
304         p7 = plot(alpha, C_d_6(:,2),'--b');
305         p8 = plot(alpha, C_d_6(:,3),'--g');
306         p9 = plot(alpha, C_d_6(:,4),'--m');
307         p10 = plot(alpha, C_d_6(:,5),'--k');
308         p11 = plot(alpha, C_d_7(:,1),':r');
309         p12 = plot(alpha, C_d_7(:,2),':b');
310         p13 = plot(alpha, C_d_7(:,3),':g');
311         p14 = plot(alpha, C_d_7(:,4),':m');
312         p15 = plot(alpha, C_d_7(:,5),':k');
313         hold off
314         legend([p1 p2 p3 p4 p5],{'T_w = 0 C', 'T_w = 25 C', 'T_w
                = 50 C', 'T_w = 75 C', 'T_w = 100 C'},'Location','
                northeast')
315         xlabel('\alpha');
316         ylabel('C_d');
317         title('\theta = 60 , 75 , 90 ');
318         axis tight
319         saveas(gcf,'Model_6_3.png')
320     end
321 end
322
323 %% VARIABLE
324
325 if(indx == 3)
326     list = {'Alpha = 0 & T_w = 0 C / 50 C / 100 C','Alpha = 0.5 &
```

```
        T_w = 0 C / 50 C / 100 C','Alpha = 1 & T_w = 0 C / 50 C /
        100 C'};
327     [indx,tf] = listdlg('PromptString','Select an option:','
           SelectionMode','single','ListSize',[400,200],'ListString',
           list);
328
329     if(indx == 1)
330         alpha = 0;
331         T_w1 = 0+273;
332         T_w2 = 50+273;
333         T_w3 = 100+273;
334         angle_of_attack = [0 15 30 45 60 75 90]*pi/180;
335         phi_0 = 0:0.001:(pi/2);
336         nu_inv = 1:-(1/(length(phi_0)-1)):0;
337         model = 7;
338         [C_d_1, V_rel, phi] = Schamberg_plots_flat(T_w1, alpha,
               angle_of_attack(1), phi_0, nu_inv, model);
339         [C_d_2, V_rel, phi] = Schamberg_plots_flat(T_w1, alpha,
               angle_of_attack(2), phi_0, nu_inv, model);
340         [C_d_3, V_rel, phi] = Schamberg_plots_flat(T_w1, alpha,
               angle_of_attack(3), phi_0, nu_inv, model);
341         [C_d_4, V_rel, phi] = Schamberg_plots_flat(T_w1, alpha,
               angle_of_attack(4), phi_0, nu_inv, model);
342         [C_d_5, V_rel, phi] = Schamberg_plots_flat(T_w1, alpha,
               angle_of_attack(5), phi_0, nu_inv, model);
343         [C_d_6, V_rel, phi] = Schamberg_plots_flat(T_w1, alpha,
               angle_of_attack(6), phi_0, nu_inv, model);
344         [C_d_7, V_rel, phi] = Schamberg_plots_flat(T_w1, alpha,
               angle_of_attack(7), phi_0, nu_inv, model);
345         [C_d_8, V_rel, phi] = Schamberg_plots_flat(T_w2, alpha,
               angle_of_attack(1), phi_0, nu_inv, model);
346         [C_d_9, V_rel, phi] = Schamberg_plots_flat(T_w2, alpha,
               angle_of_attack(2), phi_0, nu_inv, model);
347         [C_d_10, V_rel, phi] = Schamberg_plots_flat(T_w2, alpha,
               angle_of_attack(3), phi_0, nu_inv, model);
348         [C_d_11, V_rel, phi] = Schamberg_plots_flat(T_w2, alpha,
               angle_of_attack(4), phi_0, nu_inv, model);
349         [C_d_12, V_rel, phi] = Schamberg_plots_flat(T_w2, alpha,
               angle_of_attack(5), phi_0, nu_inv, model);
350         [C_d_13, V_rel, phi] = Schamberg_plots_flat(T_w2, alpha,
               angle_of_attack(6), phi_0, nu_inv, model);
351         [C_d_14, V_rel, phi] = Schamberg_plots_flat(T_w2, alpha,
               angle_of_attack(7), phi_0, nu_inv, model);
352         [C_d_15, V_rel, phi] = Schamberg_plots_flat(T_w3, alpha,
               angle_of_attack(1), phi_0, nu_inv, model);
353         [C_d_16, V_rel, phi] = Schamberg_plots_flat(T_w3, alpha,
               angle_of_attack(2), phi_0, nu_inv, model);
354         [C_d_17, V_rel, phi] = Schamberg_plots_flat(T_w3, alpha,
```

```
    angle_of_attack(3), phi_0, nu_inv, model);
[C_d_18, V_rel, phi] = Schamberg_plots_flat(T_w3, alpha,
    angle_of_attack(4), phi_0, nu_inv, model);
[C_d_19, V_rel, phi] = Schamberg_plots_flat(T_w3, alpha,
    angle_of_attack(5), phi_0, nu_inv, model);
[C_d_20, V_rel, phi] = Schamberg_plots_flat(T_w3, alpha,
    angle_of_attack(6), phi_0, nu_inv, model);
[C_d_21, V_rel, phi] = Schamberg_plots_flat(T_w3, alpha,
    angle_of_attack(7), phi_0, nu_inv, model);

figure()
p1 = plot(phi,C_d_1,'r');
hold on
p2 = plot(phi,C_d_2,'b');
p3 = plot(phi,C_d_3,'g');
p4 = plot(phi,C_d_4,'m');
p5 = plot(phi,C_d_5,'k');
p6 = plot(phi,C_d_6,'c');
p7 = plot(phi,C_d_7,'y');

p8 = plot(phi,C_d_8,'--r');
p9 = plot(phi,C_d_9,'--b');
p10 = plot(phi,C_d_10,'--g');
p11 = plot(phi,C_d_11,'--m');
p12 = plot(phi,C_d_12,'--k');
p13 = plot(phi,C_d_13,'--c');
p14 = plot(phi,C_d_14,'--y');

p15 = plot(phi,C_d_15,':r');
p16 = plot(phi,C_d_16,':b');
p17 = plot(phi,C_d_17,':g');
p18 = plot(phi,C_d_18,':m');
p19 = plot(phi,C_d_19,':k');
p20 = plot(phi,C_d_20,':c');
p21 = plot(phi,C_d_21,':y');
hold off
legend([p1 p2 p3 p4 p5 p6 p7],{'\theta = 0 ', '\theta =
    15 ', '\theta = 30 ', '\theta = 45 ', '\theta = 60 ',
    '\theta = 75 ', '\theta = 90 '});
xlabel('\phi(\phi_0)');
ylabel('C_d');
title('T_w = 0 C / 50 C / 100 C & \alpha = 0');
axis tight
saveas(gcf,'Model_7_1.png')

figure()
p1 = plot(nu_inv,C_d_1,'r');
hold on
```

```
396         p2 = plot(nu_inv,C_d_2,'b');
397         p3 = plot(nu_inv,C_d_3,'g');
398         p4 = plot(nu_inv,C_d_4,'m');
399         p5 = plot(nu_inv,C_d_5,'k');
400         p6 = plot(nu_inv,C_d_6,'c');
401         p7 = plot(nu_inv,C_d_7,'y');
402 
403         p8 = plot(nu_inv,C_d_8,'--r');
404         p9 = plot(nu_inv,C_d_9,'--b');
405         p10 = plot(nu_inv,C_d_10,'--g');
406         p11 = plot(nu_inv,C_d_11,'--m');
407         p12 = plot(nu_inv,C_d_12,'--k');
408         p13 = plot(nu_inv,C_d_13,'--c');
409         p14 = plot(nu_inv,C_d_14,'--y');
410 
411         p15 = plot(nu_inv,C_d_15,':r');
412         p16 = plot(nu_inv,C_d_16,':b');
413         p17 = plot(nu_inv,C_d_17,':g');
414         p18 = plot(nu_inv,C_d_18,':m');
415         p19 = plot(nu_inv,C_d_19,':k');
416         p20 = plot(nu_inv,C_d_20,':c');
417         p21 = plot(nu_inv,C_d_21,':y');
418         hold off
419         legend([p1 p2 p3 p4 p5 p6 p7],{'\theta = 0 ', '\theta =
              15 ', '\theta = 30 ', '\theta = 45 ', '\theta = 60 ',
              '\theta = 75 ', '\theta = 90 '});
420         xlabel('1/\nu');
421         ylabel('C_d');
422         title('T_w = 0 C / 50 C / 100 C & \alpha = 0');
423         axis tight
424         saveas(gcf,'Model_7_2.png')
425     end
426     if(indx == 2)
427         alpha = 0.5;
428         T_w1 = 0+273;
429         T_w2 = 50+273;
430         T_w3 = 100+273;
431         angle_of_attack = [0 15 30 45 60 75 90]*pi/180;
432         phi_0 = 0:0.001:(pi/2);
433         nu_inv = 1:-(1/(length(phi_0)-1)):0;
434         model = 7;
435         [C_d_1, V_rel, phi] = Schamberg_plots_flat(T_w1, alpha,
              angle_of_attack(1), phi_0, nu_inv, model);
436         [C_d_2, V_rel, phi] = Schamberg_plots_flat(T_w1, alpha,
              angle_of_attack(2), phi_0, nu_inv, model);
437         [C_d_3, V_rel, phi] = Schamberg_plots_flat(T_w1, alpha,
              angle_of_attack(3), phi_0, nu_inv, model);
438         [C_d_4, V_rel, phi] = Schamberg_plots_flat(T_w1, alpha,
```

```
    angle_of_attack(4), phi_0, nu_inv, model);
[C_d_5, V_rel, phi] = Schamberg_plots_flat(T_w1, alpha,
    angle_of_attack(5), phi_0, nu_inv, model);
[C_d_6, V_rel, phi] = Schamberg_plots_flat(T_w1, alpha,
    angle_of_attack(6), phi_0, nu_inv, model);
[C_d_7, V_rel, phi] = Schamberg_plots_flat(T_w1, alpha,
    angle_of_attack(7), phi_0, nu_inv, model);
[C_d_8, V_rel, phi] = Schamberg_plots_flat(T_w2, alpha,
    angle_of_attack(1), phi_0, nu_inv, model);
[C_d_9, V_rel, phi] = Schamberg_plots_flat(T_w2, alpha,
    angle_of_attack(2), phi_0, nu_inv, model);
[C_d_10, V_rel, phi] = Schamberg_plots_flat(T_w2, alpha,
    angle_of_attack(3), phi_0, nu_inv, model);
[C_d_11, V_rel, phi] = Schamberg_plots_flat(T_w2, alpha,
    angle_of_attack(4), phi_0, nu_inv, model);
[C_d_12, V_rel, phi] = Schamberg_plots_flat(T_w2, alpha,
    angle_of_attack(5), phi_0, nu_inv, model);
[C_d_13, V_rel, phi] = Schamberg_plots_flat(T_w2, alpha,
    angle_of_attack(6), phi_0, nu_inv, model);
[C_d_14, V_rel, phi] = Schamberg_plots_flat(T_w2, alpha,
    angle_of_attack(7), phi_0, nu_inv, model);
[C_d_15, V_rel, phi] = Schamberg_plots_flat(T_w3, alpha,
    angle_of_attack(1), phi_0, nu_inv, model);
[C_d_16, V_rel, phi] = Schamberg_plots_flat(T_w3, alpha,
    angle_of_attack(2), phi_0, nu_inv, model);
[C_d_17, V_rel, phi] = Schamberg_plots_flat(T_w3, alpha,
    angle_of_attack(3), phi_0, nu_inv, model);
[C_d_18, V_rel, phi] = Schamberg_plots_flat(T_w3, alpha,
    angle_of_attack(4), phi_0, nu_inv, model);
[C_d_19, V_rel, phi] = Schamberg_plots_flat(T_w3, alpha,
    angle_of_attack(5), phi_0, nu_inv, model);
[C_d_20, V_rel, phi] = Schamberg_plots_flat(T_w3, alpha,
    angle_of_attack(6), phi_0, nu_inv, model);
[C_d_21, V_rel, phi] = Schamberg_plots_flat(T_w3, alpha,
    angle_of_attack(7), phi_0, nu_inv, model);

figure()
p1 = plot(phi,C_d_1,'r');
hold on
p2 = plot(phi,C_d_2,'b');
p3 = plot(phi,C_d_3,'g');
p4 = plot(phi,C_d_4,'m');
p5 = plot(phi,C_d_5,'k');
p6 = plot(phi,C_d_6,'c');
p7 = plot(phi,C_d_7,'y');

p8 = plot(phi,C_d_8,'--r');
p9 = plot(phi,C_d_9,'--b');
```

```
469         p10 = plot(phi,C_d_10,'--g');
470         p11 = plot(phi,C_d_11,'--m');
471         p12 = plot(phi,C_d_12,'--k');
472         p13 = plot(phi,C_d_13,'--c');
473         p14 = plot(phi,C_d_14,'--y');
474
475         p15 = plot(phi,C_d_15,':r');
476         p16 = plot(phi,C_d_16,':b');
477         p17 = plot(phi,C_d_17,':g');
478         p18 = plot(phi,C_d_18,':m');
479         p19 = plot(phi,C_d_19,':k');
480         p20 = plot(phi,C_d_20,':c');
481         p21 = plot(phi,C_d_21,':y');
482         hold off
483         legend([p1 p2 p3 p4 p5 p6 p7],{'\theta = 0 ', '\theta =
                15 ', '\theta = 30 ', '\theta = 45 ', '\theta = 60 ',
                '\theta = 75 ', '\theta = 90 '});
484         xlabel('\phi(\phi_0)');
485         ylabel('C_d');
486         title('T_w = 0 C / 50 C / 100 C & \alpha = 0.5');
487         axis tight
488         saveas(gcf,'Model_8_1.png')
489
490         figure()
491         %T_w = 0 C
492         p1 = plot(nu_inv,C_d_1,'r');
493         hold on
494         p2 = plot(nu_inv,C_d_2,'b');
495         p3 = plot(nu_inv,C_d_3,'g');
496         p4 = plot(nu_inv,C_d_4,'m');
497         p5 = plot(nu_inv,C_d_5,'k');
498         p6 = plot(nu_inv,C_d_6,'c');
499         p7 = plot(nu_inv,C_d_7,'y');
500         %T_w = 50 C
501         p8 = plot(nu_inv,C_d_8,'--r');
502         p9 = plot(nu_inv,C_d_9,'--b');
503         p10 = plot(nu_inv,C_d_10,'--g');
504         p11 = plot(nu_inv,C_d_11,'--m');
505         p12 = plot(nu_inv,C_d_12,'--k');
506         p13 = plot(nu_inv,C_d_13,'--c');
507         p14 = plot(nu_inv,C_d_14,'--y');
508         %T_w = 100 C
509         p15 = plot(nu_inv,C_d_15,':r');
510         p16 = plot(nu_inv,C_d_16,':b');
511         p17 = plot(nu_inv,C_d_17,':g');
512         p18 = plot(nu_inv,C_d_18,':m');
513         p19 = plot(nu_inv,C_d_19,':k');
514         p20 = plot(nu_inv,C_d_20,':c');
```

```
515         p21 = plot(nu_inv,C_d_21,':y');
516         hold off
517         legend([p1 p2 p3 p4 p5 p6 p7],{'\theta = 0 ', '\theta =
                15 ', '\theta = 30 ', '\theta = 45 ', '\theta = 60 ',
                '\theta = 75 ', '\theta = 90 '});
518         xlabel('1/\nu');
519         ylabel('C_d');
520         title('T_w = 0 C / 50 C / 100 C & \alpha = 0.5');
521         axis tight
522         saveas(gcf,'Model_8_2.png')
523     end
524     if(indx == 3)
525         alpha = 1;
526         T_w1 = 0+273;
527         T_w2 = 50+273;
528         T_w3 = 100+273;
529         angle_of_attack = [0 15 30 45 60 75 90]*pi/180;
530         phi_0 = 0:0.001:(pi/2);
531         nu_inv = 1:-(1/(length(phi_0)-1)):0;
532         model = 7;
533         [C_d_1, V_rel, phi] = Schamberg_plots_flat(T_w1, alpha,
                angle_of_attack(1), phi_0, nu_inv, model);
534         [C_d_2, V_rel, phi] = Schamberg_plots_flat(T_w1, alpha,
                angle_of_attack(2), phi_0, nu_inv, model);
535         [C_d_3, V_rel, phi] = Schamberg_plots_flat(T_w1, alpha,
                angle_of_attack(3), phi_0, nu_inv, model);
536         [C_d_4, V_rel, phi] = Schamberg_plots_flat(T_w1, alpha,
                angle_of_attack(4), phi_0, nu_inv, model);
537         [C_d_5, V_rel, phi] = Schamberg_plots_flat(T_w1, alpha,
                angle_of_attack(5), phi_0, nu_inv, model);
538         [C_d_6, V_rel, phi] = Schamberg_plots_flat(T_w1, alpha,
                angle_of_attack(6), phi_0, nu_inv, model);
539         [C_d_7, V_rel, phi] = Schamberg_plots_flat(T_w1, alpha,
                angle_of_attack(7), phi_0, nu_inv, model);
540         [C_d_8, V_rel, phi] = Schamberg_plots_flat(T_w2, alpha,
                angle_of_attack(1), phi_0, nu_inv, model);
541         [C_d_9, V_rel, phi] = Schamberg_plots_flat(T_w2, alpha,
                angle_of_attack(2), phi_0, nu_inv, model);
542         [C_d_10, V_rel, phi] = Schamberg_plots_flat(T_w2, alpha,
                angle_of_attack(3), phi_0, nu_inv, model);
543         [C_d_11, V_rel, phi] = Schamberg_plots_flat(T_w2, alpha,
                angle_of_attack(4), phi_0, nu_inv, model);
544         [C_d_12, V_rel, phi] = Schamberg_plots_flat(T_w2, alpha,
                angle_of_attack(5), phi_0, nu_inv, model);
545         [C_d_13, V_rel, phi] = Schamberg_plots_flat(T_w2, alpha,
                angle_of_attack(6), phi_0, nu_inv, model);
546         [C_d_14, V_rel, phi] = Schamberg_plots_flat(T_w2, alpha,
                angle_of_attack(7), phi_0, nu_inv, model);
```

```
547         [C_d_15, V_rel, phi] = Schamberg_plots_flat(T_w3, alpha,
                angle_of_attack(1), phi_0, nu_inv, model);
548         [C_d_16, V_rel, phi] = Schamberg_plots_flat(T_w3, alpha,
                angle_of_attack(2), phi_0, nu_inv, model);
549         [C_d_17, V_rel, phi] = Schamberg_plots_flat(T_w3, alpha,
                angle_of_attack(3), phi_0, nu_inv, model);
550         [C_d_18, V_rel, phi] = Schamberg_plots_flat(T_w3, alpha,
                angle_of_attack(4), phi_0, nu_inv, model);
551         [C_d_19, V_rel, phi] = Schamberg_plots_flat(T_w3, alpha,
                angle_of_attack(5), phi_0, nu_inv, model);
552         [C_d_20, V_rel, phi] = Schamberg_plots_flat(T_w3, alpha,
                angle_of_attack(6), phi_0, nu_inv, model);
553         [C_d_21, V_rel, phi] = Schamberg_plots_flat(T_w3, alpha,
                angle_of_attack(7), phi_0, nu_inv, model);
554
555         figure()
556         p1 = plot(phi,C_d_1,'r');
557         hold on
558         p2 = plot(phi,C_d_2,'b');
559         p3 = plot(phi,C_d_3,'g');
560         p4 = plot(phi,C_d_4,'m');
561         p5 = plot(phi,C_d_5,'k');
562         p6 = plot(phi,C_d_6,'c');
563         p7 = plot(phi,C_d_7,'y');
564
565         p8 = plot(phi,C_d_8,'--r');
566         p9 = plot(phi,C_d_9,'--b');
567         p10 = plot(phi,C_d_10,'--g');
568         p11 = plot(phi,C_d_11,'--m');
569         p12 = plot(phi,C_d_12,'--k');
570         p13 = plot(phi,C_d_13,'--c');
571         p14 = plot(phi,C_d_14,'--y');
572
573         p15 = plot(phi,C_d_15,':r');
574         p16 = plot(phi,C_d_16,':b');
575         p17 = plot(phi,C_d_17,':g');
576         p18 = plot(phi,C_d_18,':m');
577         p19 = plot(phi,C_d_19,':k');
578         p20 = plot(phi,C_d_20,':c');
579         p21 = plot(phi,C_d_21,':y');
580         hold off
581         legend([p1 p2 p3 p4 p5 p6 p7],{'\theta = 0 ', '\theta =
                15 ', '\theta = 30 ', '\theta = 45 ', '\theta = 60 ',
                '\theta = 75 ', '\theta = 90 '});
582         xlabel('\phi(\phi_0)');
583         ylabel('C_d');
584         title('T_w = 0 C / 50 C / 100 C & \alpha = 1');
585         axis tight
```

```
586         saveas(gcf,'Model_9_1.png')
587
588         figure()
589         %T_w = 0 C
590         p1 = plot(nu_inv,C_d_1,'r');
591         hold on
592         p2 = plot(nu_inv,C_d_2,'b');
593         p3 = plot(nu_inv,C_d_3,'g');
594         p4 = plot(nu_inv,C_d_4,'m');
595         p5 = plot(nu_inv,C_d_5,'k');
596         p6 = plot(nu_inv,C_d_6,'c');
597         p7 = plot(nu_inv,C_d_7,'y');
598         %T_w = 50 C
599         p8 = plot(nu_inv,C_d_8,'--r');
600         p9 = plot(nu_inv,C_d_9,'--b');
601         p10 = plot(nu_inv,C_d_10,'--g');
602         p11 = plot(nu_inv,C_d_11,'--m');
603         p12 = plot(nu_inv,C_d_12,'--k');
604         p13 = plot(nu_inv,C_d_13,'--c');
605         p14 = plot(nu_inv,C_d_14,'--y');
606         %T_w = 100 C
607         p15 = plot(nu_inv,C_d_15,':r');
608         p16 = plot(nu_inv,C_d_16,':b');
609         p17 = plot(nu_inv,C_d_17,':g');
610         p18 = plot(nu_inv,C_d_18,':m');
611         p19 = plot(nu_inv,C_d_19,':k');
612         p20 = plot(nu_inv,C_d_20,':c');
613         p21 = plot(nu_inv,C_d_21,':y');
614         hold off
615         legend([p1 p2 p3 p4 p5 p6 p7],{'\theta = 0 ', '\theta =
               15 ', '\theta = 30 ', '\theta = 45 ', '\theta = 60 ',
               '\theta = 75 ', '\theta = 90 '});
616         xlabel('1/\nu');
617         ylabel('C_d');
618         title('T_w = 0 C / 50 C / 100 C & \alpha = 1');
619         axis tight
620         saveas(gcf,'Model_9_2.png')
621     end
622 end
```

C.2.1.2. Function

```
1  function [C_d_Schamberg_flat,V_rel, phi] = Schamberg_plots_flat(
       T_w, alpha, angle_of_attack, phi, nu_inv, model)
2
3      M = xlsread("Datos1.xlsx"); % Read Excel
4      Elements = [M(:,2), M(:,3), M(:,4), M(:,8), M(:,9), M(:,10),
           M(:,11), M(:,12)]; % Atmospheric composition matrix
5      Height = M(:,1); % Height
```

```
6       Temp_neutral = M(:,6); % Neutral Temperature
7       Rt = 6.37E6; % Earth radius
8       Mt = 5.972E24; % Earth mass
9       G = 6.674E-11; % Gravitational constant
10      mu = []; % Empty mu vector
11      k = 1.3806488E-23; % Boltzmann constant
12      RIG = 8.314472; % Ideal gases constant
13
14      % Molar masses in g/mol
15      mass_O = 15.999; mass_N2 = 28.01340; mass_O2 = 31.99880;
            mass_He = 4.0026020;
16      mass_Ar = 39.9480; mass_H = 1.007940; mass_N = 14.00670;
            mass_AnomO = 15.999;
17
18      % Masses vector in Kg/mol
19      mass_total = [mass_O, mass_N2, mass_O2, mass_He, mass_Ar,
            mass_H, mass_N, mass_AnomO]/1000;
20
21      % Mu computation
22      for i=1:1:101
23          mu(i)=(Elements(i,:)*mass_total'/sum(Elements(i,:)));
24      end
25
26      R=RIG*ones(1,length(mu))./(mu);
27
28      V_a = sqrt(2*R'.*Temp_neutral);
29      V_orb = sqrt((G*Mt*ones(101,1))./(Height.*1000+Rt));
30
31      if(model == 1 || model == 4)
32          f_shape_flat = sin(angle_of_attack).*sqrt(1-cos(
                angle_of_attack).^(2/nu_inv)) - cos(angle_of_attack)
                .^(1+1/nu_inv);
33          V_rel = sqrt(1+alpha.*(T_w/Temp_neutral(21) -1));
34          for i=1:1:length(V_rel)
35              C_d_Schamberg_flat(:,i) = 2*(1+f_shape_flat.*phi*
                    V_rel(i));
36          end
37      elseif(model == 2 || model == 5)
38          f_shape_flat = sin(angle_of_attack).*sqrt(1-cos(
                angle_of_attack).^(2/nu_inv)) - cos(angle_of_attack)
                .^(1+1/nu_inv);
39          V_rel = sqrt(1+alpha*(T_w./Temp_neutral(21) -1));
40          for i=1:1:length(V_rel)
41              C_d_Schamberg_flat(:,i) = 2*(1+f_shape_flat.*phi*
                    V_rel(i));
42          end
43      elseif(model == 3 || model == 6)
44          f_shape_flat = sin(angle_of_attack)*sqrt(1-cos(
```

```
            angle_of_attack)^(2/nu_inv)) - cos(angle_of_attack)
            ^(1+1/nu_inv);
        for i=1:1:length(T_w)
        V_rel(:,i) = sqrt(1+alpha.*(T_w(i)/Temp_neutral(21) -1));
        end
        C_d_Schamberg_flat = 2*(1+V_rel.*phi*f_shape_flat);
    else
        phi_var = ((1-(2*phi./pi).^2)./(1-4*(2*phi./pi).^2))
            .*((0.5*sin(2*phi)-(2*phi./pi))./(sin(phi)-(2*phi./pi)
            ));
        phi_var(1) = 1;
        f_shape_flat = sin(angle_of_attack)*sqrt(1-cos(
            angle_of_attack).^(2*ones(1,length(nu_inv))./nu_inv))
            - cos(angle_of_attack).^(1+ones(1,length(nu_inv))./
            nu_inv);
        V_rel = sqrt(1+alpha*(T_w/Temp_neutral(21) -1));
        C_d_Schamberg_flat = 2*(1+V_rel*phi_var.*f_shape_flat);
        phi=phi_var;
    end
end
```

C.2.2. Sphere

C.2.2.1. Main menu

```
clear all
close all

list = {'Specular','Diffuse','Variable','Customize'};
[indx,tf] = listdlg('PromptString','Select an option:','
    SelectionMode','single','ListSize',[400,200],'ListString',list
    );

%% SPECULAR

if(indx == 1)
    list = {'Constant Temperature','Constant accomodation factor'
        };
    [indx,tf] = listdlg('PromptString','Select an option:','
        SelectionMode','single','ListSize',[400,200],'ListString',
        list);
    if(indx == 1)
        T_w1 = 0+273;
        T_w2 = 50+273;
        T_w3 = 100+273;
        alpha = 0:0.01:1;
        model = 1;
        [C_d_1, V_rel1, phi] = Schamberg_plots_sphere(T_w1, 0,
```

```
            alpha, 1, model);
19          [C_d_2, V_rel2, phi] = Schamberg_plots_sphere(T_w2, 0,
                alpha, 1, model);
20          [C_d_3, V_rel3, phi] = Schamberg_plots_sphere(T_w3, 0,
                alpha, 1, model);
21          figure()
22          plot(alpha,C_d_1,'r');
23          hold on
24          plot(alpha,C_d_2,'k');
25          plot(alpha,C_d_3,'b');
26          hold off
27          legend('T_w = 0 ', 'T_w = 50 ', 'T_w = 100 ')
28          xlabel('\alpha');
29          ylabel('C_d');
30          title('Specular')
31          saveas(gcf,'Model_1.png')
32      end
33      if(indx == 2)
34          alpha_1 = 0;
35          alpha_2 = 0.5;
36          alpha_3 = 1;
37          T_w = 0:1:100;
38          model = 2;
39          [C_d_1, V_rel1, phi] = Schamberg_plots_sphere(T_w, 0,
                alpha_1, 1, model);
40          [C_d_2, V_rel2, phi] = Schamberg_plots_sphere(T_w, 0,
                alpha_2, 1, model);
41          [C_d_3, V_rel3, phi] = Schamberg_plots_sphere(T_w, 0,
                alpha_3, 1, model);
42          figure()
43          plot(T_w,C_d_1,'r');
44          hold on
45          plot(T_w,C_d_2,'k');
46          plot(T_w,C_d_3,'b');
47          hold off
48          legend('\alpha = 0', '\alpha = 0.5', '\alpha = 1');
49          xlabel('T_w');
50          ylabel('C_d');
51          title('Specular');
52          saveas(gcf,'Model_2.png')
53      end
54  end
55
56  %% DIFFUSE
57
58  if(indx == 2)
59      list = {'Constant Temperature','Constant accomodation factor'
            };
```

```
60      [indx,tf] = listdlg('PromptString','Select an option:','
            SelectionMode','single','ListSize',[400,200],'ListString',
            list);
61      if(indx == 1)
62          T_w1 = 0+273;
63          T_w2 = 50+273;
64          T_w3 = 100+273;
65          alpha = 0:0.01:1;
66          model = 1;
67          [C_d_1, V_rel1, phi] = Schamberg_plots_sphere(T_w1, pi/2,
                alpha, 0, model);
68          [C_d_2, V_rel2, phi] = Schamberg_plots_sphere(T_w2, pi/2,
                alpha, 0, model);
69          [C_d_3, V_rel3, phi] = Schamberg_plots_sphere(T_w3, pi/2,
                alpha, 0, model);
70          figure()
71          plot(alpha,C_d_1,'r');
72          hold on
73          plot(alpha,C_d_2,'k');
74          plot(alpha,C_d_3,'b');
75          hold off
76          legend('T_w = 0 ', 'T_w = 50 ', 'T_w = 100 ')
77          xlabel('\alpha');
78          ylabel('C_d');
79          title('Diffuse');
80          axis tight
81          saveas(gcf,'Model_3.png')
82      end
83      if(indx == 2)
84          alpha_1 = 0;
85          alpha_2 = 0.5;
86          alpha_3 = 1;
87          T_w = (0:1:100) + 273;
88          model = 2;
89          [C_d_1, V_rel1, phi] = Schamberg_plots_sphere(T_w, pi/2,
                alpha_1, 0, model);
90          [C_d_2, V_rel2, phi] = Schamberg_plots_sphere(T_w, pi/2,
                alpha_2, 0, model);
91          [C_d_3, V_rel3, phi] = Schamberg_plots_sphere(T_w, pi/2,
                alpha_3, 0, model);
92          figure()
93          plot(T_w-273,C_d_1,'r');
94          hold on
95          plot(T_w-273,C_d_2,'k');
96          plot(T_w-273,C_d_3,'b');
97          hold off
98          legend('\alpha = 0', '\alpha = 0.5', '\alpha = 1','
                Location','northwest');
```

```
99          xlabel('T_w [C]');
100         ylabel('C_d');
101         title('Diffuse');
102         axis tight
103         saveas(gcf,'Model_4.png')
104     end
105 end
106 %% VARIABLE
107
108 if(indx == 3)
109     list = {'alpha = 0 / 0.5 / 1','T_w = 0  / 50 C / 100 C'};
110     [indx,tf] = listdlg('PromptString','Select an option:','
            SelectionMode','single','ListSize',[400,200],'ListString',
            list);
111     if(indx == 1)
112         T_w1 = 0+273;
113         T_w2 = 50+273;
114         T_w3 = 100+273;
115         alpha = 0;
116         alpha2 = 0.5;
117         alpha3 = 1;
118         phi_0 = 0:0.001:(pi/2);
119         nu_inv = 1:-(1/(length(phi_0)-1)):0;
120         model = 3;
121         [C_d_1, V_rel1, phi1] = Schamberg_plots_sphere(T_w1,
                phi_0, alpha, nu_inv, model);
122         [C_d_2, V_rel2, phi2] = Schamberg_plots_sphere(T_w2,
                phi_0, alpha, nu_inv, model);
123         [C_d_3, V_rel3, phi3] = Schamberg_plots_sphere(T_w3,
                phi_0, alpha, nu_inv, model);
124         [C_d_4, V_rel4, phi4] = Schamberg_plots_sphere(T_w1,
                phi_0, alpha2, nu_inv, model);
125         [C_d_5, V_rel5, phi5] = Schamberg_plots_sphere(T_w2,
                phi_0, alpha2, nu_inv, model);
126         [C_d_6, V_rel6, phi6] = Schamberg_plots_sphere(T_w3,
                phi_0, alpha2, nu_inv, model);
127         [C_d_7, V_rel7, phi7] = Schamberg_plots_sphere(T_w1,
                phi_0, alpha3, nu_inv, model);
128         [C_d_8, V_rel8, phi8] = Schamberg_plots_sphere(T_w2,
                phi_0, alpha3, nu_inv, model);
129         [C_d_9, V_rel9, phi9] = Schamberg_plots_sphere(T_w3,
                phi_0, alpha3, nu_inv, model);
130         figure()
131         p1 = plot(phi1,C_d_1,'r');
132         hold on
133         p2 = plot(phi2,C_d_2,'k');
134         p3 = plot(phi3,C_d_3,'b');
135         p4 = plot(phi4,C_d_4,'--r');
```

```
136         p5 = plot(phi5,C_d_5,'--k');
137         p6 = plot(phi6,C_d_6,'--b');
138         p7 = plot(phi7,C_d_7,':r');
139         p8 = plot(phi8,C_d_8,':k');
140         p9 = plot(phi9,C_d_9,':b');
141         hold off
142         legend([p1 p2 p3],{'T_w = 0 ', 'T_w = 50 ', 'T_w = 100 '
                });
143         xlabel('\phi(\phi_0)');
144         ylabel('C_d');
145         title('\alpha = 0 / 0.5 / 1');
146         axis tight
147         saveas(gcf,'Model_5_1.png')
148 
149         figure()
150         p1 = plot(nu_inv,C_d_1,'r');
151         hold on
152         p2 = plot(nu_inv,C_d_2,'k');
153         p3 = plot(nu_inv,C_d_3,'b');
154         p4 = plot(nu_inv,C_d_4,'--r');
155         p5 = plot(nu_inv,C_d_5,'--k');
156         p6 = plot(nu_inv,C_d_6,'--b');
157         p7 = plot(nu_inv,C_d_7,':r');
158         p8 = plot(nu_inv,C_d_8,':k');
159         p9 = plot(nu_inv,C_d_9,':b');
160         hold off
161         legend([p1 p2 p3],{'T_w = 0 ', 'T_w = 50 ', 'T_w = 100 '
                });
162         xlabel('1/\nu');
163         ylabel('C_d');
164         title('\alpha = 0 / 0.5 / 1');
165         axis tight
166         saveas(gcf,'Model_5_2.png')
167     end
168     if(indx == 2)
169         alpha1 = 0;
170         alpha2 = 0.5;
171         alpha3 = 1;
172         T_w = 0+273;
173         T_w2 = 50+273;
174         T_w3 = 100+273;
175         phi_0 = 0:0.001:(pi/2);
176         nu_inv = 1:-(1/(length(phi_0)-1)):0;
177         model = 3;
178         [C_d_1, V_rel1, phi1] = Schamberg_plots_sphere(T_w, phi_0
                , alpha1, nu_inv, model);
179         [C_d_2, V_rel2, phi2] = Schamberg_plots_sphere(T_w, phi_0
                , alpha2, nu_inv, model);
```

```
180         [C_d_3, V_rel3, phi3] = Schamberg_plots_sphere(T_w, phi_0
                , alpha3, nu_inv, model);
181         [C_d_4, V_rel4, phi4] = Schamberg_plots_sphere(T_w2,
                phi_0, alpha1, nu_inv, model);
182         [C_d_5, V_rel5, phi5] = Schamberg_plots_sphere(T_w2,
                phi_0, alpha2, nu_inv, model);
183         [C_d_6, V_rel6, phi6] = Schamberg_plots_sphere(T_w2,
                phi_0, alpha3, nu_inv, model);
184         [C_d_7, V_rel7, phi7] = Schamberg_plots_sphere(T_w3,
                phi_0, alpha1, nu_inv, model);
185         [C_d_8, V_rel8, phi8] = Schamberg_plots_sphere(T_w3,
                phi_0, alpha2, nu_inv, model);
186         [C_d_9, V_rel9, phi9] = Schamberg_plots_sphere(T_w3,
                phi_0, alpha3, nu_inv, model);
187         figure()
188         p1 = plot(phi1,C_d_1,'r');
189         hold on
190         p2 = plot(phi2,C_d_2,'k');
191         p3 = plot(phi3,C_d_3,'b');
192         p4 = plot(phi4,C_d_4,'--r');
193         p5 = plot(phi5,C_d_5,'--k');
194         p6 = plot(phi6,C_d_6,'--b');
195         p7 = plot(phi7,C_d_7,':r');
196         p8 = plot(phi8,C_d_8,':k');
197         p9 = plot(phi9,C_d_9,':b');
198         hold off
199         legend([p1 p2 p3],{'\alpha = 0', '\alpha = 0.5', '\alpha
                = 1'});
200         xlabel('\phi(\phi_0)');
201         ylabel('C_d');
202         title('T_w = 0 C / 50 C / 100 C');
203         axis tight
204         saveas(gcf,'Model_6_1.png')
205
206         figure()
207         p1 = plot(nu_inv,C_d_1,'r');
208         hold on
209         p2 = plot(nu_inv,C_d_2,'k');
210         p3 = plot(nu_inv,C_d_3,'b');
211         p4 = plot(nu_inv,C_d_4,'--r');
212         p5 = plot(nu_inv,C_d_5,'--k');
213         p6 = plot(nu_inv,C_d_6,'--b');
214         p7 = plot(nu_inv,C_d_7,':r');
215         p8 = plot(nu_inv,C_d_8,':k');
216         p9 = plot(nu_inv,C_d_9,':b');
217         hold off
218         legend([p1 p2 p3],{'\alpha = 0', '\alpha = 0.5', '\alpha
                = 1'});
```

```
219         xlabel('1/\nu');
220         ylabel('C_d');
221         title('T_w = 0 C  / 50 C  / 100 C ');
222         axis tight
223         saveas(gcf,'Model_6_2.png')
224     end
225 end
```

C.2.2.2. Function

```
1  function [C_d_Schamberg,V_rel,phi] = Schamberg_plots_sphere(T_w,
       phi_0, alpha, nu_inv, model)
2      M = xlsread("Datos1.xlsx"); % Read Excel
3      Elements = [M(:,2), M(:,3), M(:,4), M(:,8), M(:,9), M(:,10),
           M(:,11), M(:,12)]; % Atmospheric composition matrix
4      Height = M(:,1); % Height
5      Temp_neutral = M(:,6); % Neutral Temperature
6      Rt = 6.37E6; % Earth radius
7      Mt = 5.972E24; % Earth mass
8      G = 6.674E-11; % Gravitational constant
9      mu = []; % Empty mu vector
10     k = 1.3806488E-23; % Boltzmann constant
11     RIG = 8.314472; % Ideal gases constant
12
13     % Molar masses in g/mol
14     mass_O = 15.999; mass_N2 = 28.01340; mass_O2 = 31.99880;
           mass_He = 4.0026020;
15     mass_Ar = 39.9480; mass_H = 1.007940; mass_N = 14.00670;
           mass_AnomO = 15.999;
16
17     % Masses vector in Kg/mol
18     mass_total = [mass_O, mass_N2, mass_O2, mass_He, mass_Ar,
           mass_H, mass_N, mass_AnomO]/1000;
19
20     % Mu computation
21     for i=1:1:101
22         mu(i)=(Elements(i,:)*mass_total'/sum(Elements(i,:)));
23     end
24
25     R=RIG*ones(1,length(mu))./(mu);
26
27     V_a = sqrt(2*R'.*Temp_neutral);
28     V_orb = sqrt((G*Mt*ones(101,1))./(Height.*1000+Rt));
29
30     if(model==1)
31         phi = ((1-(2*phi_0/pi)^2)/(1-4*(2*phi_0/pi)^2))*((0.5*sin
               (2*phi_0)-(2*phi_0/pi))/(sin(phi_0)-(2*phi_0/pi)));
32         if(phi_0==pi/2)
33             phi=2/3;
```

```
34          elseif(phi_0 == 0)
35              phi = 1;
36          end
37          fun = @(x,nu) x.*sqrt((1-x.^(2/nu)).*(1-x.^2));
38          I_1 = integral(@(x)fun(x,nu_inv),0,1);
39          f_shape = 2*(I_1 - (1/(1/nu_inv + 3)));
40          V_rel = sqrt(1+alpha.*(T_w/Temp_neutral(21) -1));
41          C_d_Schamberg = 2*(1+phi*V_rel.*f_shape);
42      elseif(model==2)
43          phi = ((1-(2*phi_0/pi)^2)/(1-4*(2*phi_0/pi)^2))*((0.5*sin
                (2*phi_0)-(2*phi_0/pi))/(sin(phi_0)-(2*phi_0/pi)));
44          if(phi_0==pi/2)
45              phi=2/3;
46          elseif(phi_0 == 0)
47              phi = 1;
48          end
49          fun = @(x,nu) x.*sqrt((1-x.^(2/nu)).*(1-x.^2));
50          I_1 = integral(@(x)fun(x,nu_inv),0,1);
51          f_shape = 2*(I_1 - (1/(1/nu_inv + 3)));
52          V_rel = sqrt(1+alpha*(T_w./Temp_neutral(21) -1));
53          C_d_Schamberg = 2*(1+phi*V_rel.*f_shape);
54      elseif(model==3)
55          phi = ((1-(2*phi_0./pi).^2)./(1-4*(2*phi_0./pi).^2))
                .*((0.5*sin(2*phi_0)-(2*phi_0./pi))./(sin(phi_0)-(2*
                phi_0./pi)));
56          phi(1) = 1;
57          fun = @(x,nu) x.*sqrt((1-x.^(2/nu)).*(1-x.^2));
58          for i=1:1:length(nu_inv)
59          I_1(i) = integral(@(x)fun(x,nu_inv(i)),0,1);
60          end
61          f_shape = 2*(I_1 - (1*ones(1,length(I_1)))./((1*ones(1,
                length(I_1))./nu_inv)+3));
62          V_rel = sqrt(1+alpha*(T_w/Temp_neutral(21) -1));
63          C_d_Schamberg = 2*(1+V_rel*phi.*f_shape);
64      elseif(model==4)
65          phi = phi_0;
66          fun = @(x,nu) x.*sqrt((1-x.^(2/nu)).*(1-x.^2));
67          I_1 = integral(@(x)fun(x,nu_inv),0,1);
68          f_shape = 2*(I_1 - (1/(1/nu_inv + 3)));
69          V_rel = sqrt(1+alpha*(T_w./Temp_neutral(21) -1));
70          C_d_Schamberg = 2*(1+phi*V_rel.*f_shape);
71      end
72  end
```

C.3. Sentman model

```
1  clear all
2  close all
```

```
3
4  M = xlsread("Datos1.xlsx"); % Read Excel
5  Elements = [M(:,2), M(:,3), M(:,4), M(:,8), M(:,9), M(:,10), M
       (:,11), M(:,12)]; % Atmospheric composition matrix
6  Height = M(:,1); % Height
7  Temp_neutral = M(:,6); % Neutral Temperature
8  Rt = 6.37E6; % Earth radius
9  Mt = 5.972E24; % Earth mass
10 G = 6.674E-11; % Gravitational constant
11 mu = []; % Empty mu vector
12 k = 1.3806488E-23; % Boltzmann constant
13 RIG = 8.314472; % Ideal gases constant
14
15 % Molar masses in g/mol
16 mass_O = 15.999; mass_N2 = 28.01340; mass_O2 = 31.99880; mass_He
       = 4.0026020;
17 mass_Ar = 39.9480; mass_H = 1.007940; mass_N = 14.00670;
       mass_AnomO = 15.999;
18
19 % Masses vector in Kg/mol
20 mass_total = [mass_O, mass_N2, mass_O2, mass_He, mass_Ar, mass_H,
        mass_N, mass_AnomO]/1000;
21
22 % Mu computation
23 for i=1:1:101
24 mu(i)=(Elements(i,:)*mass_total'/sum(Elements(i,:)));
25 end
26
27 R=RIG*ones(1,length(mu))./(mu);
28 V_a = sqrt(2*R'.*Temp_neutral);
29 V_orb = sqrt((G*Mt*ones(101,1))./(Height.*1000+Rt));
30 s = (V_orb(21)/V_a(21));
31
32 angle_of_attack = 0:0.00001:(pi/2);
33 alpha = [0 0.25 0.5 0.75 1];
34 for i=1:1:length(alpha)
35      C_d_flat(:,i) = (2/(s*sqrt(pi)))*exp(-s^2*(sin(
           angle_of_attack).^2)) + (sin(angle_of_attack)./(s^2))
           .*(1+2*s^2).*erf(s*sin(angle_of_attack)) + (sqrt(pi)/s)*(
           sin(angle_of_attack).^2).*sqrt(1-alpha(i));
36 end
37 alpha=0:0.01:1;
38 C_d_sph = ((2*s^2+1)/(sqrt(pi)*s^3))*exp(-s^2) + ((4*s^4+4*s^2-1)
       /(2*s^4))*erf(s) + ((2*sqrt(pi))/(3*s))*sqrt(1-alpha);
39
40 figure()
41 plot(angle_of_attack*180/pi,C_d_flat(:,1),'r')
42 hold on
```

```
plot(angle_of_attack*180/pi,C_d_flat(:,2),'b')
plot(angle_of_attack*180/pi,C_d_flat(:,3),'g')
plot(angle_of_attack*180/pi,C_d_flat(:,4),'m')
plot(angle_of_attack*180/pi,C_d_flat(:,5),'k')
xlabel('Angle of Attack [rad]');
ylabel('C_D');
legend('\alpha = 0','\alpha = 0.25','\alpha = 0.5','\alpha = 0.75
    ','\alpha = 1','Location','northwest');
axis tight

figure()
plot(alpha,C_d_sph)
xlabel('\alpha');
ylabel('C_D');
axis tight
```